POLITECNICO DI MILANO
School of Civil, Environmental and Land Management Engineering
Master of Science in Civil Engineering

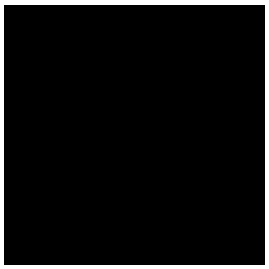

3D Seismic Isolation of the European – Extremely Large Telescope using Elastomeric Bearings

Supervisor: Prof. Luca Martinelli

Master's Thesis by:
Petar Ilkov, 10564598

Academic Year 2019-2020

Table of contents

List of Figures

List of Tables

Abstract

Seismic base isolation represents an innovative method for earthquake protection, that has been utilized with great success in reducing the danger from the horizontal ground motions. This thesis investigates the capability of an elastomeric bearing-based isolation system in terms of isolation in both the horizontal and the vertical direction. To this aim, the elastomeric bearings in question have been modelled with a low value of the shape factor ($S < 5$), which is expected to lower the vertical stiffness and provide sufficient isolation from the vertical earthquake-induced load. The design process is in accordance with the European Standards, with an exception in the defining of the design axial load, which is performed through a simplified approach that allows a relaxation of the strict requirements of the European Standards, at the cost of a reasonable reduction in the safety factor. The efficiency of the elastomeric bearings is tested through their implementation in a structure with considerable proportions and mass, in particular the European – Extremely Large Telescope, set to be the largest telescope in the world. This building is chosen, apart from its size, due to its sensitivity to high frequency vibrations. Validation of the bearings' design is performed through analyses in the OpenSees, using the *ElastomericX* element object by Kumar [2016], that models the bearing as a two-node, 12 degree-of-freedom element with six springs that represent the mechanical behavior in all directions. Analyses of the entire structure are performed using the recorded ground motions from the El Centro (1940) earthquake, which exhibited a similar horizontal elastic response spectrum as the one of El Cerro Armazones, where the structure is located. The analyses results produce useful insight concerning the bearings' behavior, such as the clear elastic response in the vertical direction. Moreover, the horizontal response exhibits strong similarities with the idealized bi-linear behavior. However, the results from the OpenSees analysis indicate the difficulty in accurately prediction the behavior of a 3D seismic isolation system, which will remain a field open for future studies and development.

Acknowledgements

I eternally thank my family for the restless love and support, for being my rock and for tolerating me on even my most unpleasant days.

I also extend my gratitude to Professor Martinelli for providing me with the much needed knowledge and guidance, as well as for putting up with all of the late night calls and emails.

Chapter 1

Introduction

Since the beginning of humankind, man has tried to tame the forces of nature. Learning about the environment and finding ways to adapt to diverse living conditions has been a constant quest over the ages. With the passing of time, knowledge of once inexplicable phenomena has grown, and with the sharp spike in technological advancements over the past few centuries, that knowledge has increased exponentially.

One such phenomenon is the earthquake – a shaking of the ground caused by a sudden release of immense energy beneath Earth's surface. These energy outbursts can cause anything between negligible vibrations and absolute chaos above ground. So far, powerful earthquakes have damaged or completely collapsed many structures and have taken countless lives, making them a hazard that cannot be overlooked. Nowadays, civil engineering considers earthquakes a priority concern for most types of structures.

A traditional type of design meant to lower the potential damage done to buildings by earthquakes includes intentionally creating a weak spot that would fail under the earthquake's force and absorb it, preventing damage to the rest of the rest of the structure. Such weak spots are called plastic hinges and are typically located somewhere at the bottom of the load-carrying construction. This method has been deemed efficient since it provides stability to the structure long enough for it to be evacuated, satisfying the most important safety condition which is saving human lives. However, the hinges themselves represent damage to the structure which is quite serious and often irreparable, which is obviously disastrous from a financial point of view. Considering the cost and importance of certain buildings, it is clear that a more sophisticated method of protection must be available.

The field of seismic protection has greatly evolved in the past century, with multiple different methods of securing a building during an earthquake and

enabling future use, at costs significantly lower than having to rebuild. One of those methods is via base isolation, using devices with an incredible deformation capacity that dissipate the energy from the earthquake before it reaches the structure. This idea is likely to have been born toward the end of the 19th century, with the emerging of many proposals for "devices which absorb or minimize shock to buildings arising from earthquakes, vibrations caused by heavy traffic or other disturbances of the earth's surface2" [de Montalk, 1932]. In 1906, Jacob Bechtold of Munich, Germany made an application for a U.S. patent for an "earthquake proof building consisting of a rigid base-plate to carry the building and a mass of spherical bodies of hard material to carry the said base-plate freely" [Bechtold, 1907] These are just a few of the many proposals made at the time, although as far as is determined, none of them were ever built, probably due to a lack of practicality or confidence in the possibility of success [Buckle and Mayes, 1990].

Going into the second half of the past century, seismic base isolation has seen widespread use, particularly by means of elastomeric bearings. These bearings are composed of layers of high quality vulcanized rubber, separated by layers of steel shims that increase the overall stiffness. They are placed in a plane so-called isolation gap, which divides the building into a *substructure* (foundations) and *superstructure* (the rest of the building above). When the ground begins to shake, the bearings develop considerable deformations between their top and bottom point, absorbing a significant amount of the energy before it reaches the superstructure. After the ground has settled, the bearings return to their initial configuration, or near enough. The key idea is to provide sufficient damping to the system to shift its period in the long range and evade any critical modes. With respect to the damping capacity that the bearings can provide, a categorization can be made dividing them into *high damping rubber* (HDR) and *low damping rubber* (LDR) bearings. As the name suggests, the former provide lower damping and usually need to be combined with additional damping devices. The latter have rubber infused with various additives, most commonly carbon black, and offer a much higher damping capacity. Another distinct type of bearing is *the lead-rubber* (LR) bearing, that in addition to the rubber layers and steel shims has a lead core whose plastic deformations govern the energy dissipation capacity.

In the past decades these devices have seen worldwide success in isolating various buildings of importance, such as skyscrapers or nuclear power plants. For seismic areas where the horizontal component of the earthquake is by far dominant, it is safe to say that the design of elastomeric bearings has been mastered and has shown to offer the required level of isolation for many structures. However, earthquakes with a more severe vertical component demand to be countered with a slightly different design that would offer a 3D base isolation to a structure. One proposition by [Kelly et al., 1989] suggests that this could be achieved with an additional criteria for the *shape factor* of

the elastomeric bearings, a ratio between the diameter and the rubber layer thickness. According to Kelly, bearings with a low shape factor are more adequate at isolating structures from vertical vibrations, which if strong can prove to be fatal.

The scope of this thesis is to analyze the behavior of an unorthodox building with an implemented 3D seismic base isolation system consisting of elastomeric bearings. The building in question is the European – Extremely Large Telescope (ELT), a structure of epic proportions funded by the European Southern Observatory. Set to be the largest telescope in the world, this building's size and importance make it a suitable choice for the project at hand. The elastomeric bearings chosen for the base isolation system are high damping rubber bearings with a low shape factor in order to assess their effect on the response in both the horizontal and the vertical direction. Their precise properties are obtained through a procedure defined by European Standards, followed by a verification process executed using an approach which simplifies the European Standards on the basis of a highly probable assumption. Finally, the designed bearings and the structure as a whole are analyzed using OpenSees (Open System for Earthquake Engineering Simulation).

This thesis is organized in seven chapters, the first being this introduction. The second is a brief overview of the literature on seismic protective systems and particularly seismic base isolation. The third chapter explains the mechanical behavior of elastomeric bearings through the mathematical model and introduces OpenSees as a framework. Chapter 4 elaborates the design and verification process, followed by Chapter 5 which implements them into the case study. Chapter 6 explains the analysis performed in OpenSees and the obtained results. The last chapter is the conclusion, obtained upon finishing the analyses and assessing the behavior of the E-ELT with an incorporated 3D seismic base isolation system.

Chapter 2

Seismic Isolation Knowledge Overview

The idea of isolating a structure from the seismic ground motions beneath it was first introduced well over a century ago. Notable practical applications however, took a long and steady road in the following decades. This unique concept is meant to offer, apart from efficiency in its purpose, necessary functioning (service) conditions for any type of structure built in this manner. Protection from earthquakes is a more vast field and in addition to isolation, it covers other protective strategies with essentially different concepts. Following is a brief overview of protective systems as a whole and then a closer look into the fundamental topics of seismic isolation and in particular, elastomeric bearings.

2.1 Earthquake Protective Systems Overview

Figure 2.1. shows the division of earthquake protective systems into active, passive and hybrid, as well as their sub-parts.

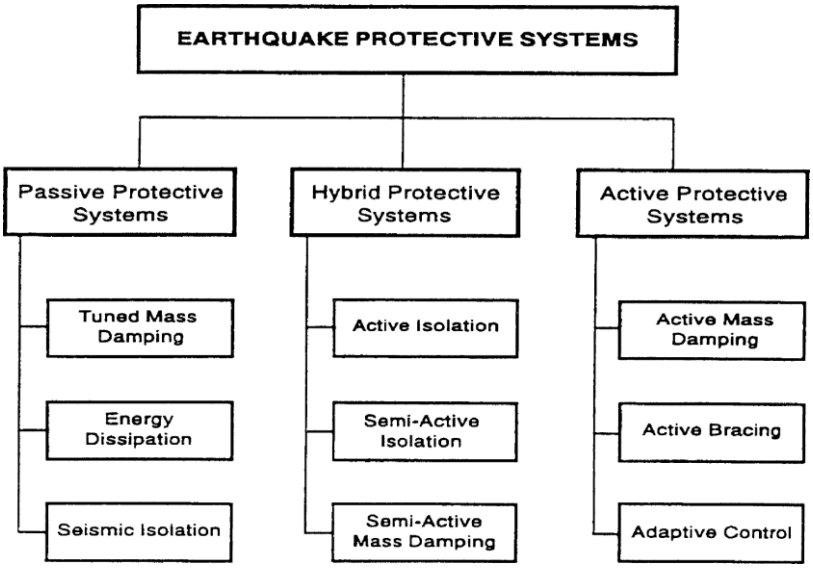

Figure 2.1: Family of earthquake protective systems (adapted from [Buckle, 2000]).

Active systems provide protection by imposing forces on the structure that act as counterbalance against the earthquake induced forces. They are considered active mainly in the sense that they rely on an energy source, but also they require motion sensors, computer control, feedback mechanisms and moving parts that need to be maintained. In the event of an earthquake, sensors positioned throughout the building assess the direction and intensity of its force, so the system can provide an equivalent and opposite force to counter it and provide equilibrium to the structure, thus avoiding structural damage.

Passive systems are called so since they do not require an additional energy source to operate, rather they are activated by the earthquake motion only. These systems include seismic (base) isolation and mechanical energy dissipation, where the former is perhaps the more developed with continuing novelties and applications. Seismic isolation is a design strategy that is based on the premise that it is both possible and feasible to uncouple a structure from the ground and thus protect it from damaging effects of earthquake ground motions. To achieve this result, the stiffness of the structural system is reduced by introducing flexible elements (isolators) near the base of a building, or on the pier cap, if a bridge. Additional damping may be provided in order to limit the isolator displacements to acceptable values [Buckle, 2000]. Common isolation systems include elastomeric and sliding bearings which may or may not have damping mechanisms (bearings with high damping rubber or bearings with a lead core).

The need to control isolator displacements gave rise to the development of energy dissipation systems, which in time became an adequate substitute for the isolation systems. Their main purpose is to reduce the load of the structural frame by dissipating the earthquake's energy, but also to increase the frame's

strength and stiffness. Passive energy dissipators may be simply classified as hysteretic or viscoelastic [Constantinou, Soong, and Dargush, 1998]. Hysteretic dissipators include the yielding of metals due to flexure, shear, torsion, or extrusion (metallic dampers) and sliding (friction dampers). They are all essentially displacement-dependent devices. Viscoelastic systems include viscoelastic solids, fluid orificing (fluid dampers), and viscoelastic fluids. They are essentially velocity-dependent devices (viscous in nature) and many are also frequency dependent. Some passive energy dissipators are modifications of the above set and may include elastic springs or pressurized cylinders to develop pre-load and re-centering capabilities [Buckle, 2000].

A notable subset of these dissipators are the tuned mass dampers (TMD) and tuned liquid dampers (TLD), used for transferring the kinetic energy between different modes of vibration. When tuned to a particular dominant mode, they can provide a comfortable level of damping. However, they are more suited for controlling wind-induced vibrations rather than ones from earthquakes, and are not of large importance to this topic.

Hybrid protective systems mainly refer to those systems that have active components, but are either more reliable, less expensive or less power demanding compared to fully active systems.

2.2 Seismic Base Isolation

Base isolation comprises of adding flexible elements to the structure that have a large capacity for lateral deformation and can increase the structure's natural period to a longer, safer range. These elements are located at the base, decoupling the superstructure from its substructure that is embedded in the ground. Once an earthquake occurs, its force travels through the substructure to the isolation elements, which deform sufficiently and in this manner greatly reduce the force that reaches the superstructure. This concept lowers the demands for the structural elements and allows them to remain in the elastic range, whereas conventional design would lead to plastic deformations and local structural damage that would later be quite costly to repair, if it is reparable at all.

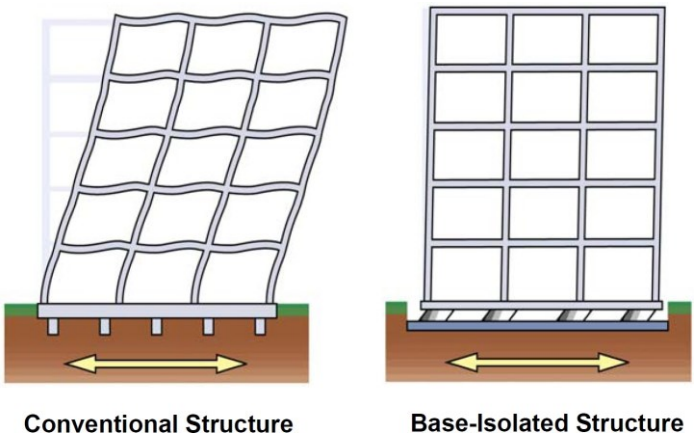

Figure 2.2: Conventional and base isolated structure deformations (adapted from [Symans, 2009]).

Seismic base isolation devices can be classified with respect to some major design differences as:

- **Elastomeric bearings**
  - Low-damping rubber bearings
  - High-damping rubber bearings
  - Lead rubber bearings
- **Sliding bearings**
  - Friction pendulum
  - Triple pendulum

Elastomeric bearings consist of stacked layers of elastomer and steel shims, usually both with a small thickness per layer. The elastomer layers have a very small horizontal stiffness, which allows large elastic deformations that dissipate the earthquake forces before they reach the superstructure. They are made from either natural or synthetic rubber that is pressurized under high temperatures in special molds along with the steel shims to achieve a bond. The steel shims provide vertical stiffness, restraining the rubber at the bond surface [Kelly et al., 1989]. It is very important to secure sufficient spacing between the bearings in order to avoid collision once they reach their maximum displacements.

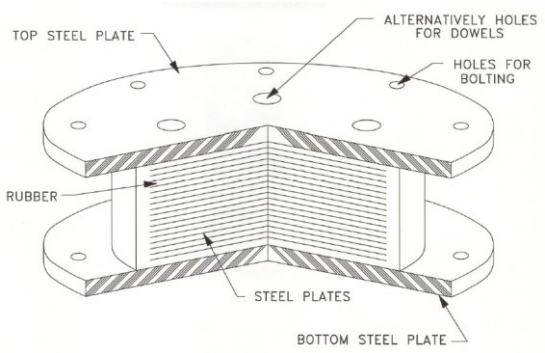

Figure 2.3: Cross section of an elastomeric bearing (adapted from Constantinou et al. [2006]).

A rubber cover is provided to protect the internal rubber layers and steel plates from environmental degradation due to ozone attack and corrosion, respectively [Symans, 2009].

Low damping rubber (LDR) inherently offer low damping values (usually about 2-3% equivalent damping ratios). They have very good linearity, a stable restoring force and excellent flexibility. However, these properties require that additional damping devices are incorporated in the base isolation solution.

High damping rubber (HDR) bearings have either natural or synthetic rubber layers infused with various materials (resins and other fillers) to increase the stiffness and provide higher damping values, so they exhibit both spring and damping characteristics. This way they meet the structure's energy dissipation without the need for additional dampers, which makes them particularly useful in situations with space constraints. The high stiffness lowers the risk of bearing instability in extreme scenarios, whereas in service conditions (low shear strains) it keeps the forces and deformations in the elastic range. Damping ratios generally range between 10% and 20% of the critical one at 100% shear strain [Grant et al., 2005]. High damping rubber bearings have relatively smooth hysteresis curves and the seismic isolation can be extended to the equipment inside the building. Certain loading conditions can cause a discontinuity in their properties in the initial motion cycles (scragging) affecting their dissipation ability and stiffness, although the values return to normal as the number of cycles increases. The behavior under virgin conditions could be strongly different from that under scragged conditions. After a sufficient amount of time, the initial properties are recovered [Warn and Ryan, 2012].

Lead rubber (LR) bearings have layers of laminated natural rubber (and steel shims) with a lead plug embedded in the center. The elastomer provides the isolation component and the lead core, with diameter ranging between 15% and 33% of the bonded diameter of the bearing, provides the energy dissipation or damping com- ponent, due to the plastic deformation of the lead [Fujita, 1998]. The hysteresis of LR bearings resembles that of elastoplastic materials. The lead core relieves the need for additional damping devices, with tuning

being done by varying its diameter. Caution should be taken with the lead's temperature variation since large values can reduce characteristic strength. Fatigue of the lead could be disregarded since lead recrystallizes at normal temperatures [Constantinou et al., 1998].

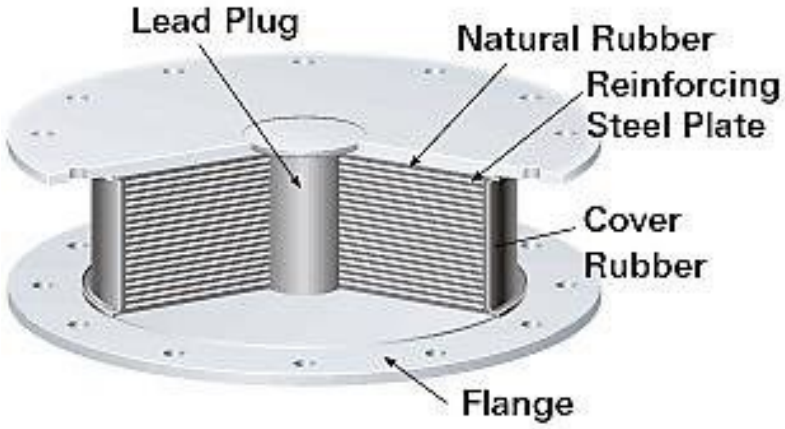

Figure 2.4: Cross section of a lead rubber bearing (adapted from Naeim & Kelly et al. [1999]).

Sliding bearings consist of a top steel concave plate, an articulated slider, and a base plate that is either plain or also concave, depending on the bearing type. These bearings provide stiffness in the vertical direction through direct contact of the bearing elements, whereas horizontal stiffness is provided by sliding. Each surface area between two elements is coated with a material that has an extremely low friction coefficient, ususally polytetrafluoroethylene (PTFE). This is a solid made entirely of carbon and fluorine and has one of the lowest friction coefficients of any solid, allowing smooth sliding with as little resistance as possible. The other bearing elements are made of high-strength stainless steel. Upon dislocating from the initial configuration during seismic motion, re-centering is achieved through the elements' geometry or using additional damping devices.

Friction pendulum bearings (FPB) have a plain base plate, articulated slider and a concave top dish, whose curvature is designed to provide a restoring force to the bearing and return it to its initial configuration. In addition to this, when seismic motion causes sliding along the concave surface the bearing provides a lifting vertical component to the system which reduces vertical displacements. The radius of the con- cave contact surface and the friction coefficient are the parameters designed to give the Friction Pendulum bearings desirable dynamic properties, such that very high axial loads could be supported at large lateral displacements [Warn and Ryan, 2012].

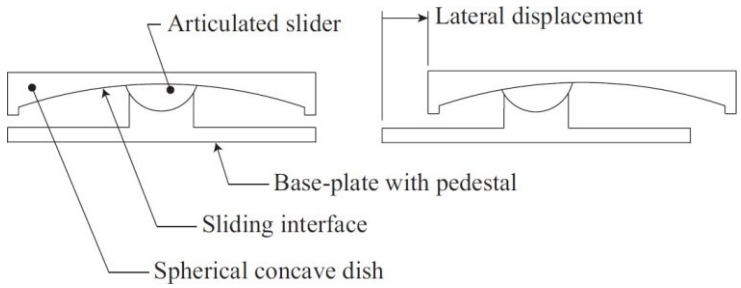

Figure 2.5: Friction Pendulum bearing undeformed and deformed configurations (adapted from Warn and Ryan [2012]).

Triple pendulum is a multi-spherical sliding bearings. This device consists of four spherical sliding surfaces and three independent pendulum mechanisms, as shown in Figure 2.8. In particular, the response during low intensity seismic event is controlled by the internal pendulum mechanism, with two concave plates and a rigid slider, whereas the outer stainless steel concave surfaces provide two independent pendulum mechanisms that con- trol the response during medium or high level of ground motions [Zayas et al., 2016], [Pecchillo, 2019].

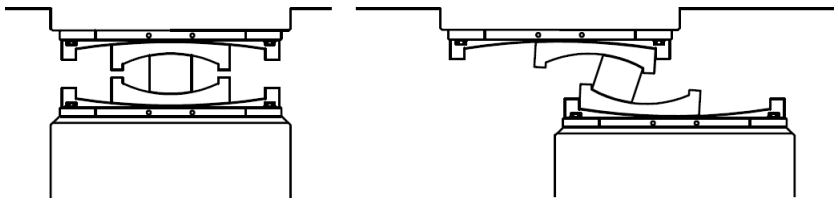

Figure 2.6: Triple Pendulum bearing undeformed and deformed configurations (adapted from Zayas et al. [2016]).

2.3 3D Seismic Isolation

Elastomeric bearings can be further divided according to their damping capacities:

1. Bearings that cannot provide sufficient damping to the system and have to be accompanied by additional damping devices;
2. Bearings that are able to produce the required amount of damping without additional damping devices.

The first group refers to low damping rubber bearings (LDR), whereas the second refers to high damping (HDR) and lead rubber (LR) bearings. One factor responsible for the difference in damping capacities between the bearings without a lead core is the composition of the elastomer. Different treatment during vulcanization and compounding as well as different

quantities of certain fillers (typically carbon black) have a large effect on hardness, stiffness, creep, stress relaxation and the elongation at break.
A geometrical property with significant influence on the bearings' stiffness is the shape factor (S):

$$S = \frac{D}{4t_r} \tag{2.1}$$

Where D is the diameter of the reinforcing steel shims and t_r is the rubber layer thickness. A small rubber layer thickness results in higher vertical stiffness, which in turn means that the isolation capacity in the vertical direction would be low. Analogous to this, a thicker rubber layer would result in a lower vertical stiffness and with that, a better isolation in the vertical direction. Having in mind the relationship between t_r and S, it can be concluded that bearings with a high shape factor can provide isolation only in the horizontal direction, whereas bearings with a lower value of S can provide sufficient isolation in both horizontal and vertical direction. It is important to remember that the shape factor is associated only with the thickness of a single layer of rubber and not the total rubber thickness in the bearing, so its value has no significant correlation with isolation in the horizontal direction. Furthermore, studies have shown that even though variation in the shape factor influences vertical stiffness, the normal stress in the steel reinforcement remains unaffected by this variation.
The loading scenario for rubber bearings gives rise to some phenomena, such as buckling, that represent a multiaxial issue and require several checks to be performed on the bearing design to ensure safety under both service and critical conditions.
The bearing properties that must be determined to design an elastomeric bearing-based seismic isolation system are:

- **Horizontal stiffness** of the bearing, linked to a specific horizontal natural frequency;
- **Vertical stiffness** of the bearing, linked to a predominant vertical frequency;
- **Stability** of the bearing under combined vertical load and lateral displacement.

To shed light on vertical response in general, and on the stability problem, the following sections are focused on the theoretical background of the mathematical existing model for elastomeric bearing: the Haringx's theory of bearing stability and the Two-spring model for elastomeric bearing. The formulations for the computation of horizontal and vertical stiffness of a bearing are deeply discussed in Chapter 3, with particular attention on the coupling between horizontal and vertical motions and their reciprocal influence. [Kelly et al., 1989; Kumar et al., 2015; Pecchilo, 2019].

2.4 Haringx's Theory of Rubber Bearing Stability

Over the course of a few years, Haringx published several articles on highly compressible helical springs and rubber rods and their potential use in vibration-free mountings. His theory was later proven to be able to predict the buckling load and analyze the effects of the vertical loads on damping and shear in bearings by Gent [1964].
The behavior of an elastomeric in terms of buckling resembles that of a slender column with a small stiffness in shear. With respect to this, the bearing can be considered as a beam for which the plane sections normal to the central axis remain plane after deformation, but not necessarily normal to the central axis [Timoshenko and Gere, 1961].

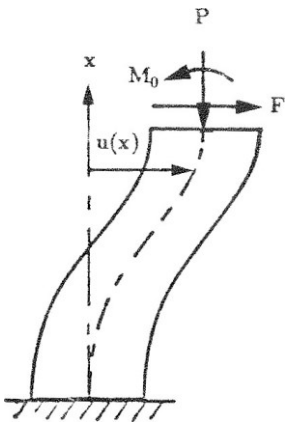

Figure 2.9: Haringx column in deformed configuration (adapted from Kelly et al. [1989]).

Figure 2.9 describes an elastic column of length l that is fixed at the bottom and has constrained rotation but free translation at the top. It is loaded by a compressive force P and a moment M_0 due to the constraint.
The problem is defined with:

- the displacement of the central axis, u (x);
- the rotation of a face originally normal to the undeformed axis, φ(x).

Leading to two contributions to the deformation:

- the shear deformation $u'(x) - \varphi(x)$;
- the curvature $\varphi'(x)$.

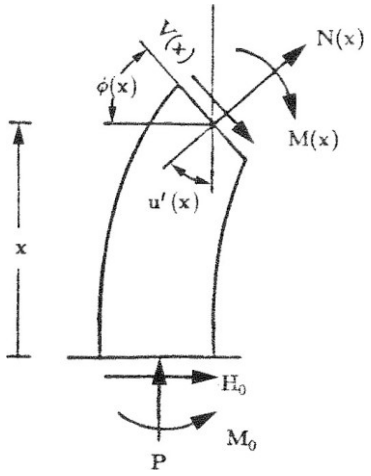

Figure 2.10: Internal forces in a generic cross section of the deformed column (adapted from Kelly et al. [1989]).

Figure 2.10 describes the post-deformation configuration of the column, where the equilibrium equations are:

$$M(x) = M_0 - Pu(x) + H_0(x) \tag{2.2}$$

$$V(x) = P\varphi(x) - H_0 \tag{2.3}$$

The constitutive equations expressing the problem are as follows:

$$M(x) = EI_{eff}\varphi'(x) \tag{2.4}$$

$$V(x) = GA_{eff}[(u'(x) - \varphi(x)] \tag{2.5}$$

To account for the steel shims in the bearings, the effective members from the constitutive equations become $EI_{eff} = E_r I_s$ and $GA_{eff} = GA_s$.
Another approach by [Kelly, 1993] offers a more accurate representation by taking into account the effect of the thickness of the steel shims on the slenderness and the elastic modulus, expressed as:

$$EI_{eff} = E_r I_s = \frac{E_c}{3} I \frac{h}{T_r} \tag{2.6}$$

$$GA_{eff} = GA_s = GA \frac{h}{T_r} \tag{2.7}$$

By combining the constitutive and equilibrium expressions, the governing differential equation of the problem can be reached in terms of both the displacement and the rotation as:

$$\frac{EI}{1+\frac{P}{GA_s}}u'' + Pu = H_0 x + M_0 \tag{2.8}$$

$$\frac{EI}{1+\frac{P}{GA_s}}\varphi'' + P\varphi = H_0 \tag{2.9}$$

where the first equation is expressed through u and the second through φ. From here, the general solutions are as follows:

$$u(x) = Acos\alpha x + Bsin\alpha x + \frac{H_0}{P}x + \frac{M_0}{P} \tag{2.10}$$

$$\varphi(x) = Ccos\alpha x + Dsin\alpha x \frac{H_0}{P} \tag{2.11}$$

The coefficient α holds the expression:

$$\alpha^2 = \frac{P}{EI_{eff}}\left(1+\frac{P}{GA_s}\right) \tag{2.12}$$

The boundary conditions of the general solutions are:

$$\begin{gathered} u(0) = 0 \\ \varphi(0) = 0 \\ H_0(0) = 0 \\ \varphi(l) = 0 \end{gathered} \tag{2.13}$$

From this a new expression containing α is obtained, which can then be combined with the previous explanation of α^2 in order to arrive at:

$$\alpha l = \pi \tag{2.14}$$

$$P\left(1+\frac{P}{GA_s}\right) = \frac{\pi^2 EI_{eff}}{l^2} \tag{2.15}$$

where the right hand side is defined as the Eulerian buckling load $P_E = \frac{\pi^2 EI_{eff}}{l^2}$ and $GA_s = P_s$. After exchanging these new terms into the equation above and making some adjustments, the critical buckling load can be expressed as:

$$P_{cr} = \sqrt{P_E p_s} \tag{2.16}$$

2.5 Two-Spring Model of an Elastomeric Bear- ing

The previous section described the behavior of a bearing in buckling without

accounting for the effect of the lateral displacements, which if non-zero would affect the height and stiffness of the bearing. This influence can be captured by using a model with two springs [Koh and Kelly, 1988] that will couple the lateral displacements with the vertical stiffness. [Constantinou, 2006] discusses such a model through a column whose configuration and boundary conditions represent a bearing's behavior.

Consider a rigid column of length h equal to the total height of the rubber layers and the steel shims. The column is put on a rigid plate on two

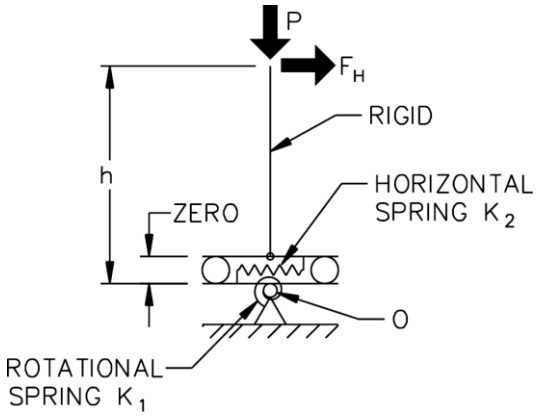

Figure 2.11: The two-spring model (adapted from Constantinou et al. [2006]).

frictionless rollers of negligible dimension, which in turn sit on another rigid plate. A horizontal spring, characterized by a stiffness K2 (force per unit length), constrains the relative displacement, s, between the two plates. The bottom plate is simply supported in the middle and the relative rotation, θ, is constrained by a rotational spring, characterized by a stiffness K1 (moment per unit radian). A vertical compression load P and a horizontal force FH are applied at the free end of the column [Kelly et al., 1989; Pecchillo, 2019].

Assuming small displacements only, the lateral displacement u and the reduction of the column height v are computed as:

$$u = s + h\theta \tag{2.17}$$

$$v = s\theta + h\frac{\theta^2}{2} \tag{2.18}$$

The equilibrium equations are expressed with respect to the rotation point O and the displacement directions s, in the following form:

$$P\theta + F_H + K_2 S = 0 \tag{2.19}$$

$$Pu + F_H h - K_1\theta = 0 \tag{2.20}$$

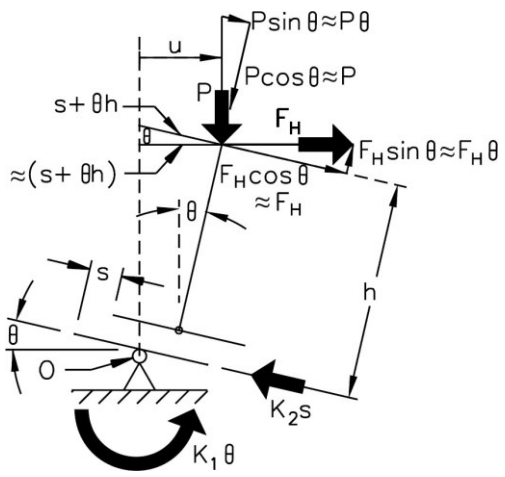

Figure 2.12: Forces and moments acting on the deformed configuration of the Two-spring model (adapted from Constantinou et al. [2006]).

To obtain the stiffness of the springs, each one is observed as if the other one tends to infinity. They are expressed as:

$$K_1 = P_E h \tag{2.21}$$

$$K_2 = \frac{GA_s}{h} = \frac{GA_s}{T_r} \tag{2.22}$$

Hence, the solutions to the equilibrium equations are:

$$\theta = \frac{F_H}{GA_s} \frac{GA_s + P}{P_E - P(1 + \frac{P}{GA_s})} \tag{2.23}$$

$$\frac{s}{h} = \frac{F_H}{GA_s} \frac{P_E}{P_E - P(1 + \frac{P}{GA_s})} \tag{2.24}$$

Taking into account that $K_H = \frac{F_H}{u}$, the horizontal stiffness can be computed including the influence from the vertical load as:

$$K_H = \frac{GA}{T_r}\left(1 - \frac{P^2}{P_{cr}^2}\right) \tag{2.25}$$

where $P_E \gg P$ and $P_E \gg GA_s$ and the higher order terms are neglected.
The total displacement in the vertical direction is computed as:

$$u_{tot} = u + P\frac{T_r}{E_c A} \tag{2.26}$$

where the first term is the lateral contribution and the second is the contribution due to the vertical load.

As for the vertical stiffness, the equation is obtained by assuming that the bearing height is very close to the total height of the rubber layers and that $P \gg GA$.

$$K_u = \frac{E_c A}{T_r} \frac{1}{1 + \frac{3}{\pi}(2\frac{u}{r})^2} \tag{2.27}$$

where r is the radius of gyration, computed as:

$$r = \sqrt{\frac{I}{A}} \tag{2.28}$$

Experimental data points out that the value for the vertical stiffness obtained with the two-spring model is sufficiently accurate [Warn and Whittaker, 2006].

Chapter 3

Mathematical and Numerical Model of Elastomeric Bearings for 3D Seismic Isolation

This chapter will encompass the mechanical behavior of an elastomeric bearing in all principal directions, as well as its numerical implementation in a software designed for seismic engineering and earthquake simulations. The first two sections will focus on the bearing behavior in the vertical and horizontal directions, accordingly. The third section will discuss the parameters relevant for rotation and torsion in elastomeric bearings. After that, the following sections will cover how this mechanical behavior is interpreted in OpenSees (Open System for Earthquake Engineering Simulation), a software framework that, unlike most popular civil engineering tools, relies completely on a programming language to build an entire model and perform certain analyses only through lines of code. It is capable of performing both serial and parallel finite element analyses is perfectly suited for investigating hazard in the field of geotechnics and structural engineering. The programming language in question is “tcl”, which has many similarities to C++,C and Fortran.

3.1 Mechanical Behaviour in Vertical Direction

The stiffness in vertical direction of elastomeric bearings mainly controls the vertical frequency of a seismically isolated structure. Therefore, to design a three-dimensional isolation system that protects the structure also from vibrations in vertical direction (in addition to horizontal directions), the need to predict the behaviour under compressive loads becomes fundamental [Kelly, 1993]. In case of major earthquakes, large variations in axial loads are expected due to extreme shaking of the ground and the coupling of horizontal and vertical responses needs to be considered [Pecchillo, 2019].
This means that actions in a certain direction should be expected to have an effect on the bearing's properties in an orthogonal direction, such as:

- as the lateral displacement u_h increases, the axial stiffness K_v decreases;
- as the axial load P increases, the shear stiffness K_H decreases;
- a reduction in the axial stiffness K_v causes a reduction in the critical buckling load P_{cr}, thus reducing as well the shear stiffness K_H.

It is obvious that severe seismic motions have a complex impact on the bearings. The correlation between the lateral displacement and the vertical stiffness is captured in a simplified model by Koh and Kelly [1988] based on Haringx's theory on rubber bearing stability [1949b]. It is a two-spring model with some assumptions where Kv is given as:

$$K_v = \frac{E_c A}{T_r} \frac{1}{1 + \frac{3u_h}{\pi^2 r}} = K_{v0} \frac{1}{1 + \frac{3u_h}{\pi^2 r}} \tag{3.1}$$

where

- E_c is the compression modulus of the rubber bearing;
- A is the area of the bonded rubber layers;
- T_r is the total height of the rubber;
- r is the radius of gyration, as defined in Equation (2.24);
- K_{v0} is the vertical stiffness at zero lateral displacement, i.e. $u_h = 0$.

One way to compute Ec is in accordance with a hypothesis proposed by Gent and Lindley [1959] that suggests total incompressibility (ν=0.5). With respect to this hypothesis, the compression modulus for a circular elastomeric bearing is as follows:

$$E_c = E(1 + 2S^2) \tag{3.2}$$

Where E is the Young modulus of the elastomer and S is the shape factor. This hypothesis is governed by the assumptions:

- horizontal plane sections parallel to the rigid plate remain plane and parallel to it after deformation;
- the lateral surface deforms in parabolic fashion;
- normal stresses are equal to the mean pressure in the three orthogonal directions.

Another hypothesis also by Gent and Lindley [1959] takes into consideration the compressibility of the volume. In this case, the equation for the compression modulus would be:

$$\frac{1}{E_c^J} = \frac{1}{E_c} + \frac{1}{K} \tag{3.3}$$

where E_c is the modulus as calculated in Equation (3.2) and K is the bulk modulus. Although the second expression is closer to the bearing realistic behavior, the first one has been deemed acceptable in the case of bearings with a low shape factor.

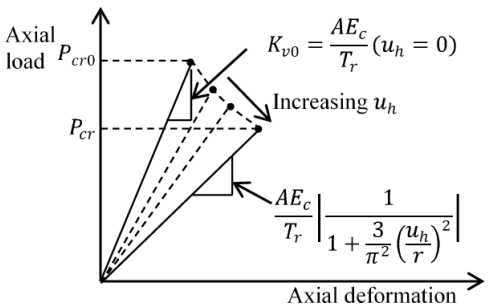

Figure 3.1: Axial load-deformation curve in compression (adapted from Kumar et al. [2015]).

Figure 3.1 shows the aforementioned relationship between lateral displacements and the vertical stiffness of the bearing. As long as u_h=0 the

vertical stiffness is equal to K_{v0}, which provides the critical buckling load Pcr0. After initial lateral displacements occur, the value of the vertical stiffness is reduced, thus reducing the critical buckling load and forming a lower inclination on the load-deformation curve in compression.
The critical buckling load for a certain value of lateral displacement can be computed as a function of the overlapping area.

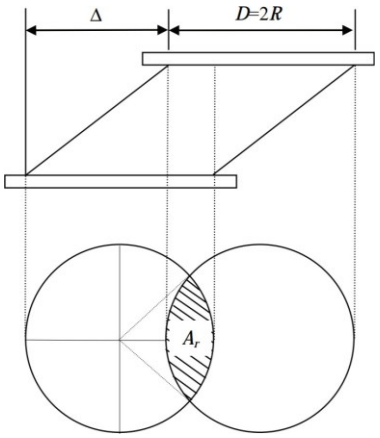

Figure 3.2: Reduced area of elastomeric bearing (adapted from Warn and Whittaker [2006]).

$$P_{cr} = P_{cr0}\frac{A_r}{A} \tag{3.4}$$

Where A_r is the overlapping area between the top and bottom sections of the bearing after displacements have occurred, and is equal to:

$$A_r = \frac{D^2}{4}(\delta - sin\delta) \tag{3.5}$$

where

$$\delta = 2cos^{-1}\left(\frac{u_h}{D}\right) \tag{3.6}$$

Mathematically, this suggests that once u_h=D the bearing would have zero buckling capacity, experimental studies have shown that even in this case P_{cr} would still be larger than zero. A linear approximation proposed by Warn and Whittaker [2006] suggests that after the ratio between the overlapping and the bonded area falls under 0.2, the critical buckling load remains constant.

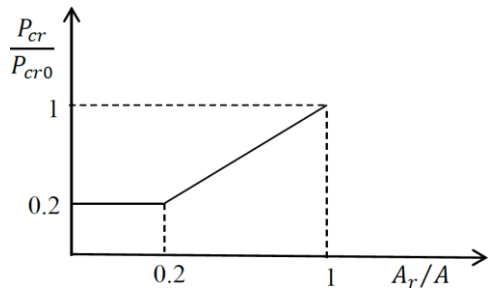

Figure 3.3: Bi-linear variation of buckling load (adapted from Kumar et al. [2015]).

$$\begin{aligned} for \quad & \frac{A_r}{A} \geq 0.2 \qquad P_{cr} = P_{cr0}\,\frac{A_r}{A} \\ for \quad & \frac{A_r}{A} < 0.2 \qquad P_{cr} = 0.2P_{cr0} \end{aligned} \tag{3.7}$$

It is crucial to note that Figures 3.1 and 3.3 describe the bearing behavior solely in compression. Tension in elastomeric bearings is associated with cavitation, an occurrence that is accompanied by the irreversible damage due to formation of micro cracks in the volume of rubber. When the bearing is loaded beyond the point of cavitation and unloaded, it returns along a new path and cavitation strength is reduced. The area enclosed between loading and unloading amounts to the hysteretic energy due to damage in the bearing. Subsequent loading follows the latest unloading path elastically until strain exceeds the past maximum value max u , below which loading has the effect of only opening and closing of existing cavities within the rubber. Once loading exceeds the past maximum value of tensile strain, the formation of new cavities leads to increased damage [Kumar, 2013].

3.2 Mechanical Behaviour in Horizontal Direction

With respect to the approximation of the two-spring model of an elastomeric bearing be Kelly [1993], the horizontal stiffness is:

$$K_H = \frac{ttA}{T_r}\left|\frac{1}{1-\frac{P}{P_{cr}}}\right| = K_{H0}\left|\frac{1}{1-\frac{P}{P_{cr}}}\right| \tag{3.8}$$

where K_{H0} is the horizontal stiffness while the axial load is zero, and P_{cr} is the critical buckling load, calculated as in Equation (3.7). It is obvious from the formulation that the axial load has an a crucial effect on the stiffness in horizontal direction.

The coupling between vertical and horizontal is included in the model that describes the coupling between horizontal directions. In particular, the model

for elastomeric bearing in horizontal shear is a bidirectional smooth bi-linear hysteretic one, showed in Figure 3.4, and is based on the formulation by Park et al. [1986] [Pecchillo, 2019].

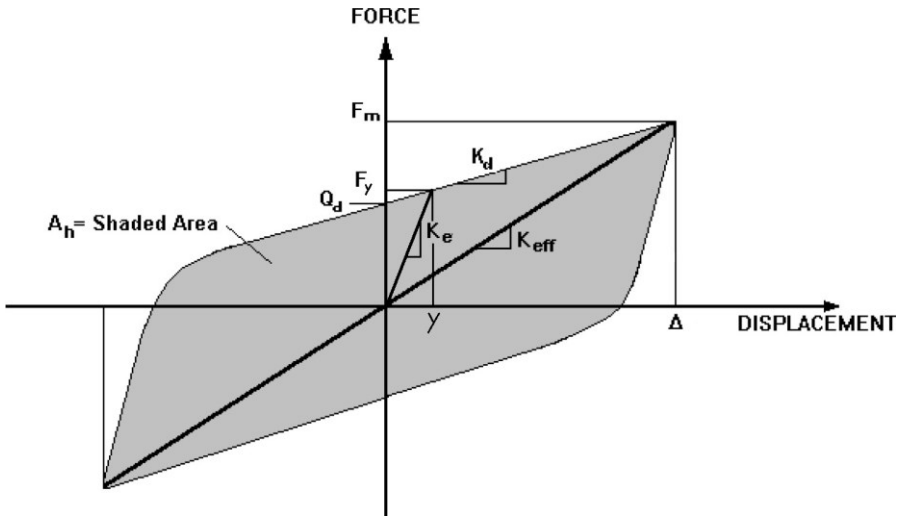

Figure 3.4: Idealized smooth behaviour of elastomeric bearing in shear (adapted from Kelly [2001]).

The hysteresis loop is characterized by parameters typical of seismic isolation design:

– The initial elastic stiffness, K_e;

– The post-elastic stiffness, K_d;

– The effective stiffness, K_{eff} ;

– The yield strength, F_y;

– The yield displacement, Y ;

– The characteristic strength, Q_d;

– The maximum displacement, Δ;

– The maximum force, F_m.

The effective shear modulus can be computed as follows:

$$tt_{eff} = \frac{K_{eff} T_r}{A} \tag{3.9}$$

where the effective stiffness K_{eff} is obtained through the ratio of the sums of the absolute values of the restoring force and the maximum displacements as:

$$K_{eff} = \frac{|F^+| + |F^-|}{|\Delta^+| + |\Delta^-|} \tag{3.10}$$

The shear modulus is variable as it depends on the shear strains. For an increase in the strains up to 100% the shear modulus continuously decreases, but after that it is almost constant up to 200%. For practical purposes, the value of the shear modulus is assumed as constant, but these variations caused by the varying strains have to be taken into consideration.
To acquire the restoring forces, the isotropic expression for the model is used:

$$\frac{F_x}{F_y} = c_d\left(\frac{\dot{U}_x}{\dot{U}_y}\right) + K_d\left(\frac{U_x}{U_y}\right) + Q_d\left(\frac{Z_x}{Z_y}\right) \tag{3.11}$$

where:

- F_x and F_y are the restoring forces in orthogonal directions;
- U_x and U_y are the displacements in those directions;
- $\dot{U}_x$ and $\dot{U}_y$ are the derivatives of the displacements, i.e. the velocities;
- Z_x and Z_y are hysteretic components of the restoring forces.

Z_x and Z_y both have units of displacement and are functions of time histories of U_x and U_y. The biaxial interaction is given as:

$$Y\begin{Bmatrix}\dot{Z}_x \\ \dot{Z}_y\end{Bmatrix} = \left(A[I] - [\begin{matrix} Z_x^2(\gamma Sign(\dot{U}_x Z_x) + \beta) & Z_x Z_y(\gamma Sign(\dot{U}_y Z_y) + \beta) \\ Z_x Z_y(\gamma Sign(\dot{U}_x Z_x) + \beta) & Z_x^2(\gamma Sign(\dot{U}_y Z_y) + \beta)\end{matrix}]\right) \tag{3.11}$$

Parameters γ and β control the shape of the hysteresis loop and A is the amplitude of the restoring force [Kumar, Whittaker and Constantinou, 2013], and it must hold that:

$$\frac{A}{\gamma + \beta} = 1 \tag{3.12}$$

When yielding occurs, the solution of the system is:

$$\begin{gathered} -Z_x = cos\theta \\ Z_y = sin\theta \\ \theta = tan^{-1}(\frac{\dot{U}_y}{\dot{U}_x}) \end{gathered} \tag{3.13}$$

where θ is the angle between the direction of the motion and the resultant force.

The characteristic strength Q_d that contributes to the hysteretic part of the restoring force is dependent on the effective damping of the system β_{eff}, computed as:

$$\beta_{eff} = \frac{1}{2\pi}\left[\frac{EDC}{K_{eff}\Delta^2}\right] \tag{3.14}$$

where Δ is the displacement of the system due to earthquake shaking obtained from smoothed response spectra and EDC is the energy dissipated per cycle at displacement Δ [Kumar, Whittaker and Constantinou, 2013] . For the idealized behavior in Figure 3.4, EDC can be computed as:

$$EDC = 4Q_d(\Delta - \mathrm{Y}) \tag{3.15}$$

where Y is the displacement of the system at the yielding point. For lead rubber bearings, the characteristic strength is determined using the effective yield stress of the lead core. It is important to note that in the case of low damping rubber bearings, the characteristic strength cannot be obtained directly. An effective damping of the system is assumed, and Q_d is computed as:

$$\beta_{eff} = \frac{1}{2\pi}\left[\frac{4Q_d(\Delta - \mathrm{Y})}{K_{eff}\Delta^2}\right] \leq \frac{2Q_d}{\pi K_d \Delta} \tag{3.16}$$

$$Q_d \geq \frac{\pi}{2}\beta_{eff} K_d \Delta \tag{3.17}$$

The characteristic strength of LDR bearings can be estimated if the value of displacement Δ due to earthquake shaking is known from the simplified analysis. The above procedure can also be used for high damping rubber bearings, since their force-displacement response is similar to that shown in Figure 3.4 but with larger energy dissipated per cycle, so the same path of reasoning can be followed (e.g., Constantinou et al., 2011).

3.3 Mechanical Behaviour in Rotation and Torsion

The torsion and rotation of an individual elastomeric bearing have a fairly small effect on the overall response of the seismically isolated building. Due to this fact, the bearing behavior under torsion and rotation can be represented by linear elastic springs with the following stiffnesses:

$$K_r = \frac{E_r I_s}{T_r}$$
$$K_t = \frac{G I_t}{T_r} \tag{3.18}$$

respectively, where E_r is the rotation modulus of the bearing, I_s is the moment of inertia about the axis of rotation in the horizontal plane and I_t is the moment of inertia about the vertical axis [Kumar, Whittaker and Constantinou, 2013].

3.4 Numerical Model in OpenSees

There are a few structural softwares that offer a numerical model of an elastomeric bearing. The scope of this thesis is focused on the modelling and analyzing of a seismically isolated structure using OpenSees, an object-oriented, open source software framework sponsored by the Pacific Earthquake Engineering Research Center (PEER). This section will cover some of the basic principles of OpenSees, as well as its capabilities to capture the behavior of elastomeric bearings.

3.4.1 OpenSees Framework

Although still under development, OpenSees offers the user vast control over the manner of defining analysis procedures and results. Moreover, it makes it possible and fairly easy for multiple users to share and edit work and the scope of the output. It is designed to be flexible, extensible and object-oriented, i.e. Opensees makes extensive use of object composition allowing users to combine components in manners that are not available in commercial or other research codes [McKenna, 2011]. Admittedly the lack of a graphical interface is not quite typical for a structural engineering software, some of the perks of using an interpreter as OpenSees include quick modification of the design and analysis properties, notable reduction in time consumption of designing structures with a high level of modular repetition and a smaller chance for errors since OpenSees requires all aspects of the design and analysis process to be manually defined. However, the current database of OpenSees may prove to be somewhat limited for the cause of modelling more complex structures, which would lead to certain simplifications and reduced accuracy of the model. Every operation in OpenSees is written in the programming language Tcl, to which the interpreter adds commands that are bound to a C++ procedure. For the purpose of this thesis, this section will focus more on the commands added to Tcl in particular for the needs of structural design.
The commands essential for this can be grouped in the following modules:

1. **ModelBuilder**: used to construct the objects of the structure in the model.
2. **Recorder**: used to select the quantities to be monitored during analysis procedures and the outputs of results.
3. **Analysis**: used to define the solution procedure to advance the model from state at time t_i to state at time $t_i + dt$ [Pecchillo, 2019].

The modelBuilder command is used at the beginning of any modelling procedure to specify the number of dimensions in which the problem will be observerd and in accordance with this the number of degrees of freedom. Afterward, in order to introduce the elements that make up the structure, it is necessary to define the type and properties of all the materials they consist of. Here OpenSees offers a plethora of commands that represent different stress-strain relationships, mainly grouped under the "uniaxialMaterial" command for uniaxial, or under "ndMaterial" for stress-strain relationships at the gauss-point of a continuum element. The following step is to define all the nodes that will represent a beginning or end of each object through their coordinates (2 coordinates for 2D or 3 coordinates for a 3D problem). The same line of code can specify the lumped mass (if any) in a certain node, or the "mass" command can be used after the nodes have been defined. The procedure also requires that the constraints be defined as free with a "0" or fixed with a "1" in the "fix" command. The commands for the elements of the structure can be written only after all previous prerequisites are met. The elements hold the force vectors and stiffness matrices needed for the analysis.
Once the model is complete, the next step is to apply the loads, which begins with defining the time series that represent the relationship between the time in the domain and the load factor that will be applied to the loads. The second step is writing the command for the load patterns that hold the intensity, location and direction of the loads. Each load pattern is associated with a "timeSeries" object and can contain nodal loads, elemental nodes or single point constraint objects.
After having defined the model and the loads, the type of analysis needs to be selected. The "analysis" command offers the choice between a static analysis and transient analyses with either a constant or a variable time step dt. However, before an analysis is initiated, several of its components that will determine how the analysis runs need to be manually defined by the user.

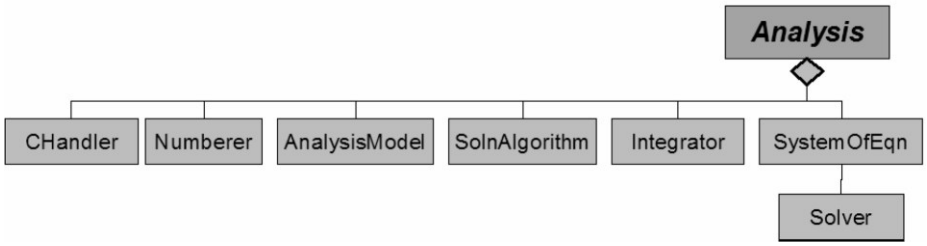

Figure 3.5: Analysis objects on OpenSees (adapted from Mazzoni et al. [2006]).

Finally, the needed information from the analysis is acquired through recorder objects that monitor what is happening during the analysis and generate the output afterward. Recorder objects can be focused on monitoring both nodes and elements, providing various information (node displacements, reactions, internal forces, stiffnessess etc.).

3.4.2 Reference Coordinate Systems

OpenSees recognizes three different reference coordinate systems:

- basic coordinate system;
- local coordinate system;
- global coordinate system.

Each reference coordinate system is associated with a different aspect of the model and the analysis. The basic coordinate system is related to the information on the elements (displacements, stiffness matrices, forces). The local coordinate system holds the nodal response, whereas the global coordinate system is used for the system of equations for the whole model.
During the analysis process, the contents of the basic coordinate system (stiffness matrices and force vectors) are transformed first into the local reference system, and then into the global one. Once the system of equations there reaches a solution, the transformation process is ran backward.
OpenSees has a geometric transformation command which creates a coordinate transformation object used to transform the element's stiffness and resisting force from the basic to the global coordinate system.

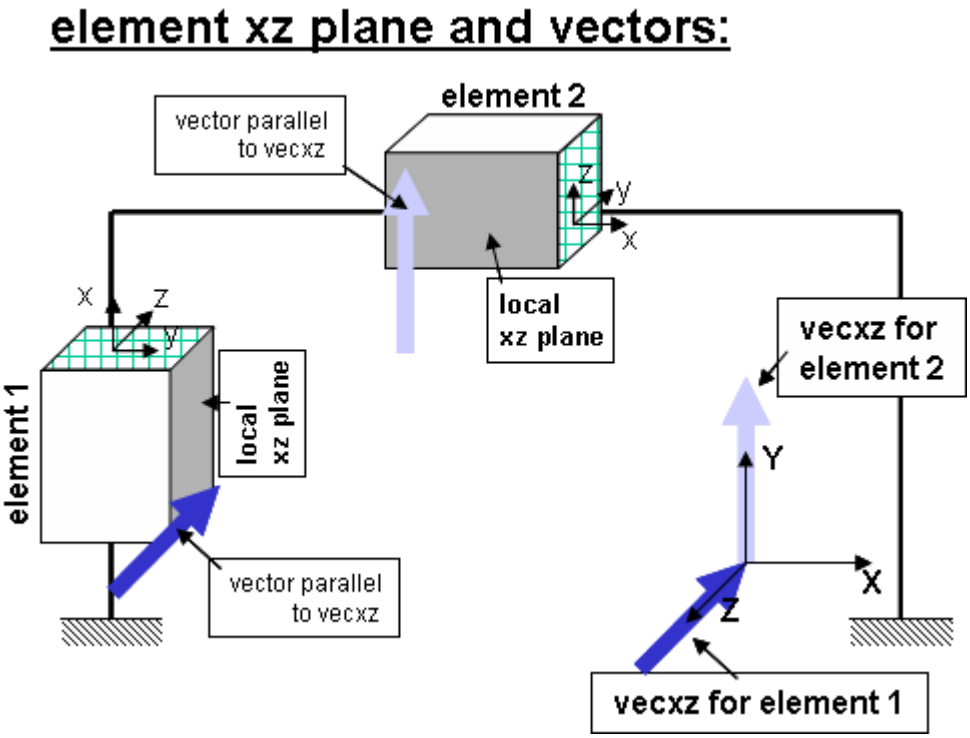

Figure 3.6: Linear coordinate transformation (adapted from Mazzoni et al. [2006]).

3.4.3 Element ElastomericX

The OpenSees element that will be used to interpret the elastomeric bearings in this thesis is the "ElastomericX" object, used for 3D problems. With it the bearing is modelled as a 2-node, 12 degree of freedom (DOF) discrete element. It is an extension of the Bouc-Wen OpenSees bearing element, only instead of requiring material models as input arguments, the ElastomericX only needs the geometric and material properties of the elastomeric bearing as arguments.

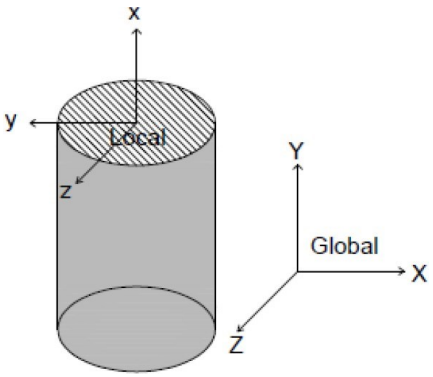

Figure 3.7: Coordinate systems of a vertical element in OpenSees (adapted from Kumar et al. [2015]).

The top and bottom nodes are connected by six springs that interpret the mechanical behavior of the bearing in the six basic directions (Figure 3.9).

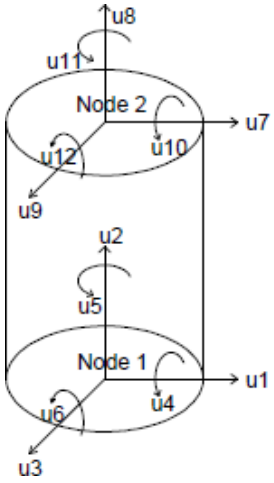

Figure 3.8: Model of the 3D continuum geometry of an elastomeric bearing (adapted from Kumar [2016]).

The general form of the element force vector is expressed as:

$$f_b = \begin{bmatrix} Axial \\ Shear\ 1 \\ Shear\ 2 \\ Torsion \\ Rotation\ 1 \\ Rotation\ 2 \end{bmatrix} \tag{3.19}$$

All springs are uncoupled, apart for the two shear spings for which a bidirectional coupled model is used. The coupling between the vertical and horizontal directions is taken into account indirectly by expressing the mechanical properties in one direction in dependence of the response parameters in the other direction [Kumar, 2016]. As covered in Section 3.3, torsion and rotation do not significantly affect the response, so the torsional and two rotational springs are linear uncoupled.
The stiffness matrix of the bearing is given as:

$$K_b = \begin{bmatrix} Axial & 0 & 0 & 0 & 0 & 0 \\ 0 & Shear1 & 0 & 0 & 0 & 0 \\ 0 & 0 & Shear2 & 0 & 0 & 0 \\ 0 & 0 & 0 & Torsion & 0 & 0 \\ 0 & 0 & 0 & 0 & Rotation1 & 0 \\ 0 & 0 & 0 & 0 & 0 & Rotation2 \end{bmatrix} \tag{3.20}$$

It should be noted that the two-spring model [Koh and Kelly, 1987] does not consider the off-diagonal terms regarding the coupling of axial behavior with shear and torsion, which would be non-zero in an exact model [Kumar, 2016]. The values of axial and shear stiffness as a function of the axial load and lateral displacement can be obtained through Equations (3.1) and (3.8).

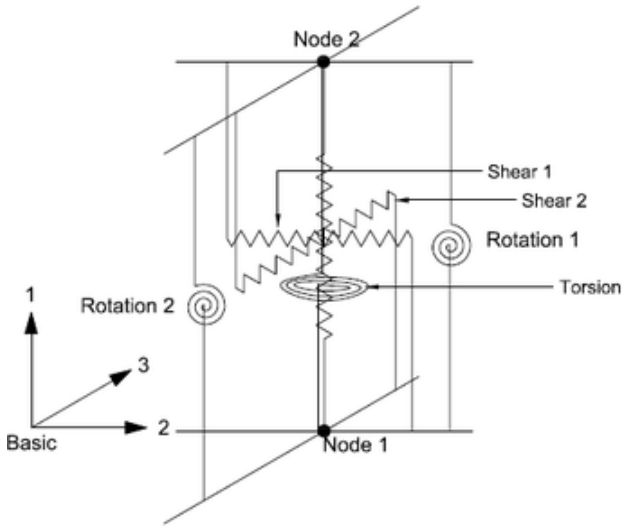

Figure 3.9: Degrees of freedom and discrete spring representation of an elastomeric bearing (adapted from Kumar [2016]).

During the analysis, the state of the model and all of its parameters is calculated at the end of each time step Δt.
In the axial direction, the progression of the parameters begins with the variation of the lateral displacements, expressed as:

$$u_h = \sqrt{u_{b,y}^2 + u_{b,z}^2} \tag{3.21}$$

where $u_{b,y}$ and $u_{b,z}$ are the displacements along the y and z axis of the basic coordinate system, respectively. Each new value for the lateral displacement leads to new values for the axial stiffness K_v (Equation (3.1)) and the angle δ (Equation (3.6)), which in turn leads to a new value for the overlapping area A_r (Equation (3.5)). This is followed by a change in the critical buckling load (Equation (3.4)), which governs the buckling problem. If in any time step the axial load becomes larger than the critical buckling load, i.e. if the bearing buckles it will lose the load carrying capacity, however for numerical reasons in the analysis a residual stiffness a thousand times smaller than K_v will be assumed.
In the horizontal direction, in accordance with the Bouc-Wen formulation the elastomeric bearing is observed as having two components to its response – one is viscoelastic with an elastic stiffness k_e and the other is hysteretic with an initial elastic stiffness k_0. The initial bearing stiffness is equal to the sum of the two components, whereas the post-yield stiffness is equal to the former component, expressed through the post-yield stiffness ratio α as:

$$\alpha = \frac{k_e}{k_e + k_0} \tag{3.22}$$

The viscoelastic component's stiffness is in fact what was previously defined

as K_{H0} in Equation (3.8), the horizontal bearing stiffness for a zero axial load.

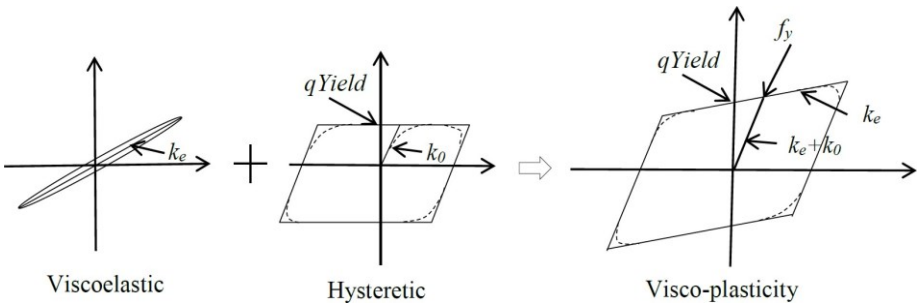

Figure 3.10: Numerical model of the response in shear (adapted from Kumar et al.

The post-yield stiffness ratio along with the characteristic strength of the bearing computed in Equation (3.17) give the yield strength as:

$$f_y = \frac{Q_d}{1-\alpha} \tag{3.23}$$

For a known constant value of the shear modulus, the viscoelastic stiffness is expressed as:

$$k_e = \frac{GA}{T_r} \tag{3.24}$$

where the value for G is experimentally obtained for a lateral displacement $\Delta = T_r$ (100% shear strain).
An additional parameter governing the behavior in the horizontal direction is the damping. Upon computing k_e as in Equation (3.24) and the effective damping β_{eff} as in Equation (3.16), the damping c_d can be obtained from the expression for the critical damping:

$$\begin{aligned} \beta_{eff} &= \frac{c_d}{c_{cr}} \\ c_{cr} &= 2\sqrt{k_e m} \\ c_d &= 2\beta_{eff}\sqrt{k_e m} \end{aligned} \tag{3.25}$$

The torsion and rotation remain represented with uncoupled linear elastic springs with the stiffness defined previously in Section 3.3. As mentioned before, their effect has a lesser influence on the model response.

Finally, the format of the command to create an elastomeric bearing object in OpenSees with the aforementioned parameters is the following:

element ElastomericX $eleTag $Nd1 $Nd2 $Fy $alpha $Gr $Kbulk $D1 $D2 $ts $tr $n <<$x1 $x2 $x3> $y1 $y2 $y3> <$kc> <$PhiM> <$ac> <$sDratio>

<$m> <$cd> <$tc> <$tag1> <$tag2> <$tag3> <$tag4>

where "$" symbolizes that what follows is the value of the parameter and "< >" implies that the parameter within is optional and may be given a default value if not otherwise specified.

Input	Deftnition
$eleTag	tag associated to the bearing (unique)
$Nd1	bottom end node
$Nd2	top end node
$Fy	yield strength
$alpha	post-yield stiffness ratio
$Gr	shear modulus
$Kbulk	bulk modulus
$D1	internal diameter
$D2	external diameter
$ts	thickness of a single steel shim
$tr	thickness of a single layer of rubber
$n	number of rubber layers
$x1 $x2 $x3	vector components in global coordinates defining local x-axis
$y1 $y2 $y3	vector components in global coordinates defining local y-axis
$kc	cavitation parameter (default=10.0)
$PhiM	damage parameter (default=0.5)
$ac	strength reduction parameter (default=1.0)
$sDratio	distance of the shear centre from the bottom node, as a fraction of the element length (default=0.5)
$m	mass of the isolator (default=0.0)
$cd	viscous damping parameter (default=0.0)
$tc	thickness of the rubber cover (default=0.0);
$tag1	tag to include the cavitation and post-cavitation behaviour in tension
$tag2	tag to include the variation in the buckling load capacity due to lateral displacement
$tag3	tag to include the variation in horizontal shear stiffness with axial load

$tag4	tag to include the variation in vertical stiffness with lateral displacement

Table 3.1: Input arguments of `ElastomericX`.

The last four tags require an input of either “1” or “0” to define if those factors will be included in the analysis or neglected, respectively.

Chapter 4

Design of a 3D Elastomeric Bearing-based Isolation System

This chapter covers the design procedure of a 3D base isolation system with elastomeric bearings in accordance with the European Standards. In addition to this, an alternative approach is introduced, whose concept is based on a hypothesis that should benefit an analysis of this scope by relieving certain strict requirements, without taking a hazardous toll on safety.

The introduction of a three-dimensional isolation system to a structure primarily represents a division of the structure, both physically and in terms of stiffness. The isolation devices form a gap and divide the structure into a substructure (the foundations) and a superstructure (the rest of the structure above the isolation gap). This design has a tremendous effect on the overall stiffness, causing a reduction and increasing the flexibility of the structure. In the vertical direction, this causes a relief in the damage otherwise taken by vibrations, whereas in the horizontal direction a shift in the natural period of the structure occurs, moving it into the long range and reducing the negative effect of certain modes.

The high deformation capacity of the elastomeric bearings allows a much more stable and uniform behavior of the superstructure, further ensured by the reduction of the top accelerations, which in turn reduce the maximum drifts. However, to exploit the bearing's deformation capacity and to guarantee safety, sufficient space must be secured between the bearings themselves and also any other objects in the isolation gap.

A useful note is that as much as they contribute to the flexibility in case of severe earthquakes, they also provide a certain degree of rigidity to aid the behavior under wind and service loads.

For the purpose of achieving these benefits from a seismic isolation system in this thesis, a solution using high damping rubber bearings will be utilized.

4.1 Design Procedure according to European Standards

The following design procedure draws from the Eurocode for the design of structures for earthquake resistance EN1998-1:2004 (EC8 for short), the European standards for anti-seismic devices EN15129:2017 (EN15129 for short) and the European standards for elastomeric bearings EN1337-3:2005 (EN1337 for short).

The beginning of the procedure is marked by the assumption of the structure's period T_0, which should belong to the long period range of 2-4 seconds. The higher end of this interval is associated with a low stiffness that would lead to larger displacements, due to which the aim will be toward the interval between 2-3 seconds.
Once the assumption on the period has been made, the natural frequency of the system can be expressed as:

$$\omega = \frac{2\pi}{T_0} \tag{4.1}$$

Assuming that the mass is known, the effective stiffness can be obtained through the definition of the natural circular frequency, which is:

$$\omega = \sqrt{\frac{K_{eff}}{m_t}} \tag{4.2}$$

$$K_{eff} = \omega^2 m_t \tag{4.3}$$

For an isolation system where all the bearings have the same material and geometrical properites, the horizontal stiffness of a single bearing is computed by simply dividing the effective stiffness by the total number of bearings in the system n_i:

$$K_H = \frac{K_{eff}}{n_i} \tag{4.4}$$

The horizontal stiffness is a function of the surface area A, the height of the elastomer T_r and the shear modulus G. Since an assumption on the material properties is needed, EN15129 §8.2.2.1 offers a range for the value of the shear modulus between $0.3MPa$ and $1.5MPa$. Kelly [2001] suggests a slightly narrower range based on the hardness of the rubber compound.

Hardness IRHD± 2	Shear Modulus G
37	0.40 MPa
40	0.45 MPa
45	0.54 MPa
50	0.64 MPa
55	0.81 MPa
60	1.06 MPa

Table 4.1: Values of the shear modulus suggested by Kelly

Another assumption should be made on the bearing's geometry, i.e. the diameter and the rubber height. These parameters define the shape factor, whose value can be an indicator of the bearings capacity to provide sufficient isolation in both the vertical and horizontal direction. A shape factor with a lower value (smaller difference in the values of the diameter and the rubber height) is more appropriate for isolation in the vertical in addition to the horizontal direction. To this aim, the threshold for the shape factor value below which the bearing is considered to provide vertical isolation is set at $S = 5$. After a value for the shear modulus has been chosen and the shape factor is known, the elastic compression modulus can be computed according to EN15129 §8.2.3.3.2 as:

$$E_c = 3G(1 + 2S^2) \tag{4.5}$$

For all purposes this value can be considered equal to that computed in Equation (3.2), as the difference is negligible, if any.
In terms of the height of the rubber, apart from the total height, additional notable parameters are the height of a single rubber layer and the number of rubber layers in a bearing. The latter can be easily expressed once the former is approximately assumed, as:

$$n = \frac{T_r}{t_r} \tag{4.6}$$

where it is important to note that the value computed in this manner might be a decimal number, which is physically impossible for a uniform thickness of all rubber layers. Due to this, the closest integer value for n is approximated and subsequently a new, exact value for T_r is obtained. Using the new T_r, a new horizontal stiffness is computed with Equation (4.4) and then by running Equations (4.3), (4.2) and (4.1) backward a new value for the period is reached, which is no longer an assumption but the actual effective period T_{eff}.
The same path of reasoning is applied to the computation of the vertical period of the structure, aiming also to acquire a value in the long range which would otherwise not be the case for a non-isolated structure. The ideal interval for the vertical period however, is notably smaller than the one for the horizontal

period, about 0.3-0.5 seconds, since larger values are correlated with the rocking phenomena.

After the aforementioned parameters have been defined, it is necessary to perform an evaluation of the stability of the bearing in accordance with EN15129.

The design shear strain caused by vertical loads is given in EN 15129 §8.2.3.3 as:

$$\varepsilon_{c.E} = \frac{6SN_{Ed,Max}}{A_r E_c} \tag{4.7}$$

where:

- S is the shape factor;
- $N_{Ed,Max}$ is the maximum vertical load;
- A_r is the reduced surface area caused by non-seismic loads;
- E_c is the compression modulus.

Following is the design strain due to angular rotation, which is covered by EN1337 §5.3.3.4. For the case of a circular bearing where a minimum rotational angle of $\alpha_d = 0.003\, rad$ has been assumed for each orthogonal direction, the strain $\varepsilon_{\alpha,d}$ is computed as:

$$\varepsilon_{\alpha,d} = \frac{D^2 \alpha_d}{n t_r^2} \tag{4.8}$$

where:

- α_d is the rotation angle;
- D is the bearing outer diameter;
- n is the number of rubber layers;
- t is the thickness of each rubber layer.

The design shear strain due to earthquake-imposed horizontal displacement d_{bd} is computed as:

$$\varepsilon_{q,E} = \frac{d_{bd}}{T_q} \tag{4.9}$$

where T_q is the thickness of the elastomer active during shear. The shear strain due to maximum horizontal displacement is set to be:

$$\varepsilon_{q,max} = \frac{d_{Ed}}{T_q} \tag{4.10}$$

where:

$$d_{Ed} = \gamma_x d_{bd} \tag{4.11}$$

The horizontal displacement d_{bd} can be obtained from the horizontal elastic response spectrum and γ_x represents a magnification factor and is equal to 1.2. The maximum total design shear strain, comprised of all the aforementioned parameters, is expressed as:

$$\varepsilon_{t,d} = K_L\left(\varepsilon_{c.E} + \varepsilon_{q,max} + \varepsilon_{\alpha,d}\right) \leq \frac{7.0}{\gamma_m} \tag{4.12}$$

where K_L is a loading factor which is equal to unity for all cases except designing bridges, and γ_m is a partial factor for elastomers. It is a recommendation that its values is taken as 1.
The horizontal elastic response spectrum is a function of the damping correction factor η, which is governed by the damping ratio ξ (previously discussed as β_{eff} in Equation (3.16)). In accordance with EC8 §3.2.2, the damping correction factor is expressed as:

$$\eta = \sqrt{\frac{10}{(5+\xi)}} \tag{4.13}$$

where ξ is considered as a percentage, so $\eta = 1$ for a damping ratio of 5%.
After obtaining the correction factor and finding the elastic response spectrum the coincides with T_{eff}, it holds that:

$$S_{e,\xi} = \eta S_e\left(T_{eff}\right) \tag{4.14}$$

Which is sufficient to compute the earthquake-imposed displacement as:

$$d_{bd} = \frac{S_{e,\xi}\left(T_{eff}\right)}{\omega^2} \tag{4.15}$$

Following is the stability verification, governed by the critical buckling load which is expressed as:

$$P_{cr} = \frac{\lambda G A_r DS}{T_r} \tag{4.16}$$

where the coefficient λ equals 1.3 for rectangular bearings, or as 1.1 for circular bearings. The main condition of the stability verification is the following:

$$N_{Ed,Max} \leq \frac{P_{cr}}{2} \tag{4.17}$$

The verification proceeds in two possible cases, depending on the difference in the values of $N_{Ed,Max}$ and P_{cr}:

$$\begin{aligned} for \quad & \frac{P_{cr}}{2} > N_{Ed,Max} \geq \frac{P_{cr}}{4} \quad \rightarrow \quad 1 - \frac{2N_{Ed,Max}}{P_{cr}} \geq 0.7\delta \\ for \quad & N_{Ed,Max} < \frac{P_{cr}}{4} \quad \rightarrow \quad \delta \leq 0.7 \end{aligned} \tag{4.18}$$

where:

$$\delta = \frac{d_{Ed}}{D} \tag{4.19}$$

It should be noted that these criteria ensure fail-safe service conditions of a bearing and include an ample level of safety, which is to state that the limit conditions demanded here are not placed at the limit capacity of the node. Furthermore, should the case be that the lateral displacements are equal to the diameter (for circular bearings), the bearing still exhibits some residual carrying capacity.

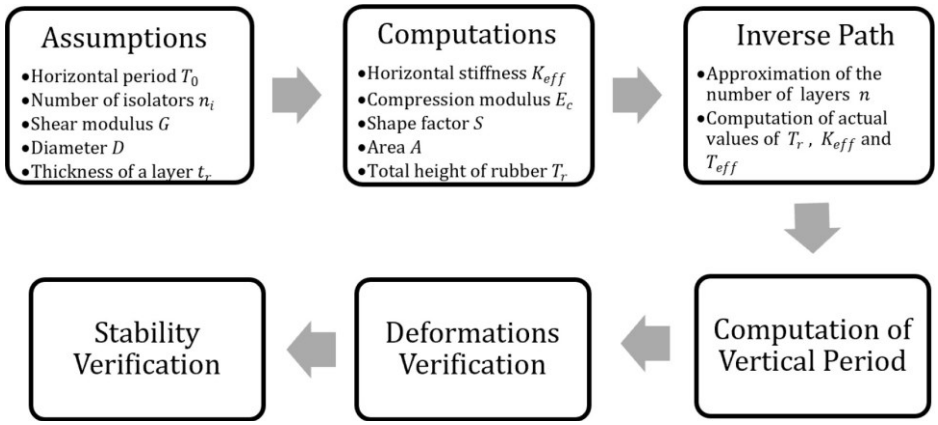

Figure 4.1: Design and Verification Process.

4.2 Alternative Design Approach

The design procedure offered by the European Standards described above offers a safe and well established approach to the seismic isolation of structures, although it is obviously complicated, with several dependencies which require almost certain repeating of the steps included. The goal of providing isolation in the vertical direction in addition to the horizontal requires a low value of the shape factor, which comes at the cost of lowered stiffness of system in both directions. This is coupled with the obvious need for a high critical buckling load which can be accomplished by selecting a large value for the shear modulus, which in turn would increase the stiffness and omit the effect of a low shae factor. These connections between the

numerous parameters involved makes the process of calibrating the ideal values quite cumbersome. Due to this, an alternative approach is introduced which focuses on the high probability that the precautions taken with the European Standards take an unnecessary toll on the practicality of designing.

The procedure described in EN15129 considers the maximum design axial force NEd,Max as the sum of the structure's self-weight, the axial force caused by the vertical component of the earthquake as well as the rocking effect caused by the horizontal motion. However, as previously mentioned, there is an undeniable difference in the long ranges belonging to the horizontal and the vertical periods. The former should be between 2 and 3 seconds, whereas the latter in the interval between 0.3 and 0.5 seconds. This large difference points out that the probability of the maximum effects from the horizontal and the vertical earthquake components acting in the same instance is considerably low. In light of this fact, the alternative approach proposes considering two separate conditions:

1. *Static load combined with horizontal seismic action* – assuming that the horizontal earthquake component is at its peak and the lateral displacement has reached the highest value, the maximum axial load is computed as the sum of the structure's self weight and the overturning moment caused by the horizontal ground motion (rocking). The effect of the earthquake's vertical component is neglected.

2. *Static load combined with vertical seismic motion* – the largest earthquake-imposed load in the vertical direction is considered and the rocking effect from the horizontal earthquake component is neglected. The maximum axial load is computed as the sum of the self-weight and the vertical earthquake component. For this case a notably smaller lateral displacement should be assumed.

Once both values for the vertical load are obtained, one value is used to perform the design procedure discussed in the previous Section, while the verification is performed using the other value. To "safeproof" this approach, a check should be performed to ensure that when the lateral displacement reaches its peak the axial load will not be at the maximum value and vice versa. It is worth noting that the stability requirement reported in Equation (4.17) is defined to guarantee a safety factor equal to 2. This condition is strongly conservative and can be slightly relaxed, maintaining a great level of safety [Pecchillo, 2019].

Chapter 5

Design of a 3D Seismic Base Isolation System for a Case Study

This chapter utilizes the design procedure described in Chapter 4 in order to define a 3D base isolation system for a structure with large sensitivity to high frequency vibrations in the horizontal and vertical directions. The system is composed of high damping rubber bearings with a low value for the shape factor, in hopes to shift both the horizontal and vertical periods in the long range. Predicting the behavior of such a system is quite a difficult task and implementing it is very expensive, so it is done only in cases where the vertical vibrations are of extreme importance for the structure. In this particular case, the structure is the E-ELT and it is considered that the proposed solution is suitable for the problem at hand. The first section of this chapter introduces the purpose and importance of the E-ELT, with a scheme of the structure following in the second section. Section 5.3 describes the acting loads, and finally Section 5.4 reports the design procedure and the obtained properties for the elastomeric bearings.

5.1 E-ELT Structure

The European Extremely Large Telescope (E-ELT for short) or "the world's biggest eye on the sky" as some have called it, is a 1083 million euro, 11-year programme funded by the European Southern Observatory (ESO) and is meant to provide research capabilities to the European astronomical community in the following decades. It is located on Cerro Armazones as part of the La Silla Paranal Observatory, which has been proven to be one of the best astronomical sites on the planet. The main jewel of the structure will be a state-of-the-art mirror with a record size of 39.3 meters in diameter and will view an area of the sky close to one ninth the size of the full Moon. In addition to this, a large

quantity of other expensive and highly sensitive instruments will inhibit the ELT's structure, which will be positioned at an altitude of 3064 meters above the sea level. The proportions of this project in combination with the chosen location make a seismic isolation protective system the perfect option for the ELT. The sensitivity of the equipment in the structure will require considerable reduction of the effects of an earthquake that is unfortunately not an uncommon occurrence for this part of the continent. Moreover, the high altitude leads to local temperatures that agree with the thermal requirements of elastomeric bearings.

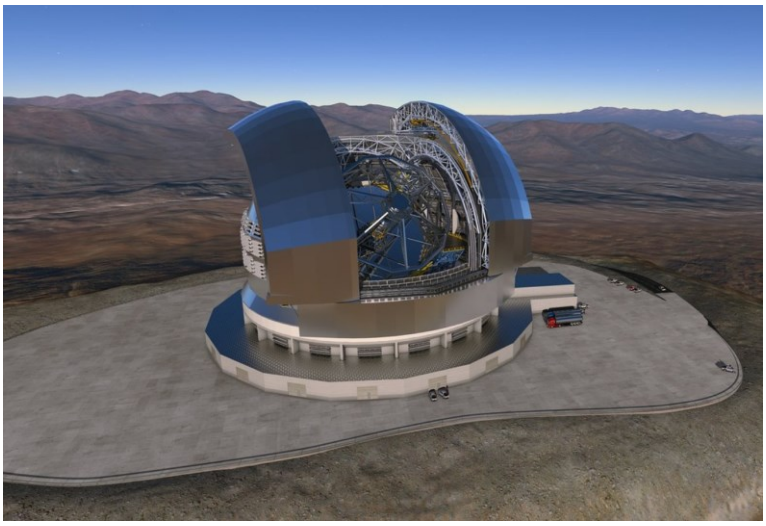

Figure 5.1: Rendering of the E-ELT (adapted from ESO [2019]).

As seen in Figure 5.1, the telescope is covered and protected by a dome with the ability to open from the middle, uncovering an enormous surface for the mirror. The opening doors of the dome move along tracks, supported by four girders. The dome is supported by its own foundation, a reinforced concrete annulus with an 11.8 meter height and a thickness of 1 meter. A windscreen is also added in order to provide protection from high-speed winds.

Figure 5.2: Rendering of the telescope (adapted from ESO [2019]).

The entirety of the structure inside the dome constitutes the main structure, which stands on a concrete pier of considerable proportions, approximately 86.4 meters in diameter with a height of 9.3 meters. The piers lifts the azimuth the ground level and ensures a that the primary mirror is 10 meters above the ground at all times. The top of the pier holds a crown structures that supports upward facing bogies for the dome rotation. The dome foundatons have a spacious opening that is 8 meter wide and 7 meters high made for the moving of large objects during construction and operation.

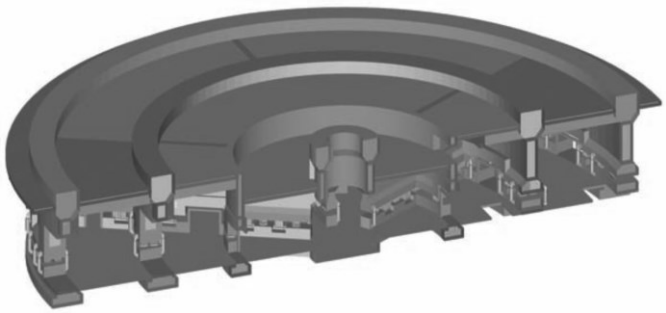

Figure 5.3: Telescope concrete pier (adapted from ESO [2011]).

The telescope pier has two annular rings that support the azimuth tracks of the telescope, one of which has a diameter of 51.5 meters and the other 34 meters. The other components of the pier are the 40cm-thick slabs at the top and bottom, as well as radial walls on every 15 degrees to increase the stiffness. The floor is located at the 8.125-metre level and extends outside the pier outer diameter to allow access to the lower part of the outer track for maintenance. The inner floor is similar to the dome floor with the same load-carrying

capacity ($20\ \frac{kN}{m^2}$) [ESO, 2011].

According to the construction proposal for the ELT, the design includes an isolation system within the telescope pier underneath the main structure's foundation, with the isolation plane being above the bottom concrete slab of the pier. The same is comprised of springs, viscous damping devices and pre-loaded units working in unison and providing an equivalent damping of 27%. This shifts the period in the long range with a fundamental frequency of $0.51Hz$.

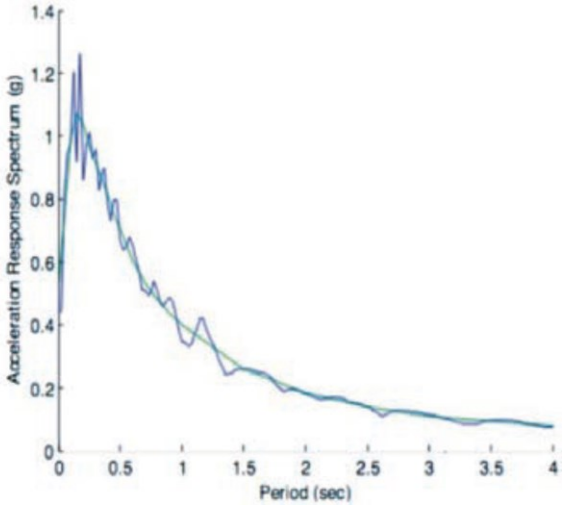

Figure 5.4: Horizontal elastic response spectrum (adapted from ESO [2011]).

The damping greatly reduces the earthquake's effect on the superstructure, lowering the horizontal accelerations above the isolation plane to $0.14g$, in correspondence with the No Collapse Requirement (NCR).

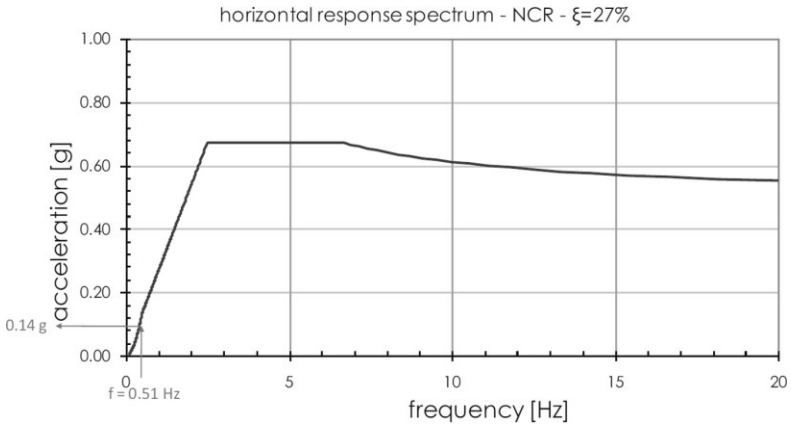

Figure 5.5: Horizontal response spectrum due to equivalent damping of 27% (adapted from ESO [2011]).

5.2 Scheme of the Structure

The earthquake protective system of the ELT is designed for thorough seismic

isolation of the structure as a whole, including devices underneath the tracks of the dome. This thesis is focused on the isolation of the main structure, hence the topic of the discussion will be the elastomeric bearings installed in the two annular rings of the telescope pier described above. The behavior of the pier is assumed to be perfectly rigid and its total mass will be expressed as a point mass located at the center of the annular rings, at a height equal to half of the pier height. To simplify, the main structure will be considered as an elastic beam with a height of 18.84 meters, equal to the estimated height of the rotation point which coincides with the height of the Nasmyth platforms. The mass of the main structure will be expressed as a lumped mass, placed at the top of the elastic beam.

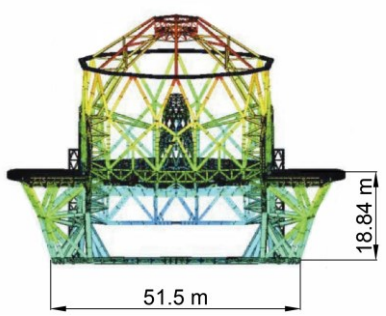

Figure 5.6: Dimensions of the main structure (adapted from ESO [2011]).

Mode	Frequency	Mode shape
1	2.91 Hz	Horizontal in Y
2	3.19 Hz	Horizontal in X
8	5.17 Hz	Vertical

Table 5.1: Eigenfrequencies of the main structure (adapted from ESO [2011]).

Table 5.1 shows the modes that represent the overall behavior of the main structure in two orthogonal horizontal directions and the vertical direction.

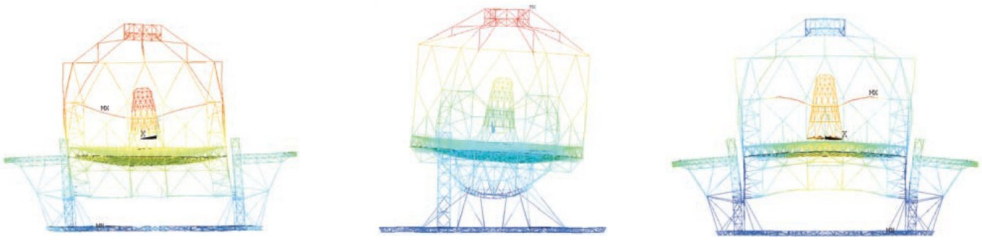

Figure 5.7: Deformed shape of the mode 1, mode 2 and mode 8 of the main structure (adapted from ESO [2011]).

The eigenfrequency values from Table 5.1 can be used to obtain the natural frequencies of the system, from which the stiffness in the vertical and horizontal direction can be derived. The absence of torsional modes, at least in the first ten modes of vibration of the main structure, allows to consider as zero the torsional mass and the torsional moment of inertia. Assuming that the main structure has an average Young's modulus of EYoung = 200 GPa, close to the modulus of elasticity of the steel, the geometrical properties of the equivalent elastic beam result [Pecchillo, 2019]:

$$\begin{aligned} A &= 0.338m^2 \\ I_x &= 12.299m^4 \\ I_y &= 14.78m^4 \end{aligned} \tag{5.1}$$

The beam representing the main structure is modelled in OpenSees using an "elasticBeamColumn" element.

5.3 Acting Loads

Considering the size of the ELT, it should be no surprise that its mass is of serious proportions, which further explains the need for implementation of an isolation system. Table 5.2 shows the mass contribution of the components supported by the bearings:

Component	Description	Mass
Telescope Pier	Concrete walls and slabs	17815 ton
	Concrete floors	794 ton
Main Structure	Telescope and sub-units	3400 ton

Table 5.2: Mass budget (adapted from ESO [2011]).

For the purpose of analyzing an individual elastomeric bearing, the sum of these mass contributions will be divided by the total number of bearings, since the geometry of the problem and the disposition of the bearings allow the consideration that each bearing carries an equal part of the total load.
The design of the isolation system is performed considering the seismic event as the predominant variable action on the structure. The actual values of the seismic actions in horizontal and vertical directions should be obtained through a numerical dynamic analysis. However, to apply the design pro- cedure, it is possible to initially consider the seismic actions as equivalent static loads and, successively, perform the numerical dynamic analysis.
The initial assumptions of the design procedure are based on the required horizontal response of the bearing, i.e. the dimensioning of the bearing isthat the 3D isolation system is made of high damping rubber bearing characterized by low shape factor, an effective damping ξ equal to 10% is selected

[Pecchillo, 2019].
Recalling that the desired effect of the isolation system is to shift the isolation period in the long range which is between 2 and 3 seconds, the assumption made at the beginning on the value of the period is $T = 2.5s$.
In accordance with the horizontal elastic response spectrum provided by the European Southern Observatory (Figure 5.2), an isolation period of 2.5s corresponds to $S_e(T_H) = 0.18g$. Using Equation (4.13) the correction factor is computed to be $\eta = 0.816$, which is applied to the obtained acceleration value of $S_e(T_H)$ to arrive at the actual value:

$$S_{e,\xi}(T_{eff}) = S_e(T_{eff})\eta = 0.147g \tag{5.2}$$

The largest recorded horizontal displacement computed through Equation (4.15) is $d_{bd} = 0.231m$ and this is then multiplied with the coefficient $\gamma_x = 1.2$ to arrive at:

$$d_{Ed} = \gamma_x d_{bd} = 0.277m \tag{5.3}$$

Which is the maximum horizontal displacement induced by the seismic motion.
An assessment on the shear on the basis of the elastic response spectrum (Figure 5.4) is performed as:

$$V_b = m_t S_{e,\xi}(T_{eff}) \tag{5.4}$$

The base shear is proportionally distributed between the masses of the structure. For the specific model of the ELT, this is the point mass representing the mass of the telescope pier and the one representing the mass of the main structure atop the elastic beam. The two shear components are computed as:

$$V_{tp} = \frac{m_{tp}}{m_{tp} + m_{ms}} V_b \tag{5.5}$$

$$V_{ms} = \frac{m_{ms}}{m_{tp} + m_{ms}} V_b \tag{5.6}$$

where V_{tp}, V_{ms}, m_{tp} and m_{ms} are the shear and mass components of the telescope pier and the main structure, respectively. These shear components multiplied by their distance from the base give the overturning moment caused by the horizontal seismic motion:

$$M_{rock} = V_{tp} h_{tp} + V_{ms} h_{ms} \tag{5.7}$$

The values required to compute the shear components and the overturning moment are as follows:

$$m_{tp} = 18609t$$
$$m_{ms} = 3400t$$
$$h_{tp} = 4.65m$$
$$h_{ms} = 28.14m$$

Making reference to Equation (5.4), the base shear is $V_b = 31739kN$, leading to an overturning moment of $M_{rock} = 262560kNm$.

To compute the rocking effect using the overturning moment, the structure will be observed as a beam supported by elastic springs, represented by the elastomeric bearings. The moment is causing a rotation around the center and the axial force acting on a single spring will depend on the distance between that spring and the center of rotation. Once the overturning moment is obtained, the axial force N_{rock} is computed as:

$$N_{rock} = \frac{x_i - x_g}{\sum_i (x_i - x_g)^2} M_{rock} \tag{5.7}$$

where x_i is the coordinate of the i-th bearing and x_g the coordinate of the center of rotation which is located in the center of the azimuth rings. The most affected bearings are the ones that are the furthest of the center. For this configuration, half of the bearings will experience a compressive loading, whereas the ones opposite of them will experience a tensile loading. The total number of bearings supporting the structure is 144, with half of this number under each of the azimuth rings. The bearings are placed symmetrically, with one for each 5 degrees of the rings, also making sure that every third bearing along the arc is supporting a radial wall, since the radial walls in the telescope pier are placed at a distance of 15 degrees each.

The value for the axial force is $N_{rock} = 197kN$

The other component of the axial force is caused by the vertical earthquake-induced motion. The one provided response spectrum of the ELT coincides with the one defined by Eurocode 8 referring to the case for soil type A, so this is the scenario that will be discussed.

The beginning and the end of the stationary segment occur at frequencies of $2.5Hz$ and $7Hz$, corresponding to a period of $0.4s$ and about $0.15s$, respectively. The same values define parameters T_B and T_C in EC8 §3.2.2, so in accordance with Table 3.4 in EC8 §3.2.2.3, the vertical response spectrum will be defined by:

$$T_B = 0.05s$$
$$T_c = 0.15s$$
$$T_D = 1s$$
$$a_{vg} = 0.9a_g = 0.36g$$

where a_g is the peak ground acceleration in horizontal direction and a_{vg} is the peak ground acceleration in vertical direction, and is 90% of the former.

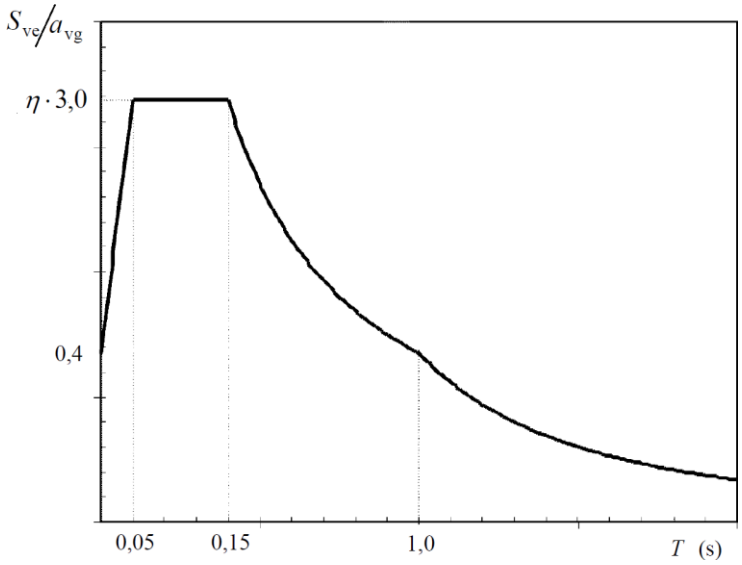

Figure 5.8: Vertical elastic response spectrum (adapted from EC8).

Assuming a response in the long range with a period of $0.3s$ and following the vertical response spectrum properties given in EC8 §3.2.2.3, the acceleration of the damped system is computed as:

$$S_{ve,\xi}(T_v) = 3.0 a_{vg} \eta_v \frac{T_C}{T} = 0.39g = 3.9 \frac{m}{s^2} \tag{5.8}$$

Hence, the axial force contribution due to vertical earthquake-induced motion is:

$$N_{ve} = \frac{m_{tot} S_{ve,\xi}(T_v)}{n} = 596kN \tag{5.9}$$

Finally, the total axial design force $N_{Ed,Max}$ which is used for the verification procedure given by EN15129 is computed as the sum of the self-weight, the rocking effect and the contribution from the vertical earthquake component:

$$N_{Ed,Max} = N_{ve} + N_{rock} + \frac{m_{tot} g}{n} = 2292kN \tag{5.10}$$

Given that the absolute value of N_{ve} alone is smaller the sum of the other two contributions to $N_{Ed,Max}$, it can be concluded that even in the case of an upward vertical ground motion, the elastomeric bearings will not experience

tensile loading.

5.4 Design of the 3D Isolation System

The isolation design proposal of this thesis aims to achieve sufficient isolation in both horizontal and vertical direction, provided by 144 high damping rubber bearings, each with an effective damping of 18%. An equal number of bearings is installed under both azimuth rings and their layout ensures a symmetry in the system. The centers of damping and stiffness are located at the center of the two azimuth rings and have zero coordinates along the global x and z axis. The same is true for the center of the mass, hence the torsion effects will not impose an issue for the structure.
The design of the bearings will be performed following the alternative approach described in Section 4.2 which allows uncoupling of the maximum axial forces induced by the vertical and the horizontal components of the earthquake. This approach is based on the idea that the vertical and horizontal isolation periods will not coincide, which must be verified through a dynamic analysis in OpenSees.
As mentioned before, the approach examines two possible cases for a maximum axial force:

- Coupling of the static load and the horizontal earthquake component:

$$N_1 = \frac{m_{tot} g}{n} + N_{rock} = 1696kN \tag{5.11}$$

- Coupling of the static load and the vertical earthquake component:

$$N_2 = \frac{m_{tot} g}{n} + N_{ve} = 2095kN \tag{5.12}$$

To proceed with the design, an isolation period in the horizontal direction is assumed with a value of $2.5s$. The natural frequency is then:

$$\omega_0 = \frac{2\pi}{T_{eff,0}} = 2.51 \frac{rad}{s} \tag{5.13}$$

The assumed value of the shear modulus should provide sufficient stiffness, as well as buckling capacity. However, sacrificing a portion of the stiffness would lead to increased displacements, which would imply improved flexibility as well. For this particular case the shear modulus is assumed to be $G = 0.64MPa$.
The rubber in the bearings is composed of layers with a uniform thickness that is now assumed to be $0.09m$. The diameter of the bearings is $1.2m$, which leads to a shape factor of $S = 3.33$. Since this value is lower than 5, it can be expected that the bearings will be able to isolate the structure in the vertical

direction.

The effective stiffness of the structure is computed as:

$$K_{eff,0,tot} = \omega_0^2 m_{tot} = 138659 \frac{kN}{m^2} \tag{5.14}$$

The effective stiffness of a single bearing is obtained by simply dividing the total stiffness by the number of bearings in the system, and is equal to:

$$K_{eff,0} = \frac{K_{eff,0,tot}}{n} = 962.9 \frac{kN}{m^2} \tag{5.15}$$

The compression modulus depends on the shape factor and the shear modulus and it results:

$$E_c = 3G(1 + 2S^2) = 44.5MPa \tag{5.16}$$

The surface area of the bearing is $A = 1.13m^2$, so the total height of the bearing can be computed as:

$$T_{r.0} = \frac{GA}{K_{eff}} = 0.626m \tag{5.17}$$

The number of required layers of rubber with the assumed thickness is:

$$n = \frac{T_{r.0}}{t_r} = 6.95 \tag{5.18}$$

As mentioned before, the number of rubber layers has to be an integer, so the closest value that is also higher than the required one is $n = 7$. After making the necessary adjustment to the number of layers, the parameters calculated thus far on the basis of assumptions are now computed again, this time as final and effective values:

$$\begin{aligned} T_r &= 0.63m \\ K_{eff} &= 1148 \frac{kN}{m^2} \\ \omega &= 2.5 \frac{rad}{s} \\ T_{eff} &= 2.51s \end{aligned} \tag{5.19}$$

Following is the computation of the vertical isolation period, which depends on the vertical stiffness of the elastomeric bearings. The stiffness for a single bearing is computed as follows:

$$K_v = \frac{E_c A}{T_r} = 79820 \frac{kN}{m} \tag{5.20}$$

The total vertical stiffness is obtained by multiplying the stiffness of a single bearing with the total number of bearings in the system, which is used to compute the vertical period as:

$$T_v = 2\pi \sqrt{\frac{m_{tot}}{nK_v}} = 0.27s \tag{5.21}$$

After having obtained such values for the horizontal and vertical period, it can be stated that both belong in their respective long range, which correlates to a design solution with an implemented seismic isolation system.
A verification of the bearing's state is necessary for both of the loading conditions proposed by the approach.
For the case of the self-weight combined with the horizontal earthquake component, the deformations computed using the equations discussed in Chapter 4 are as follows:

$$\begin{gathered} \varepsilon_{c,E} = 0.673 \\ \varepsilon_{\alpha,d} = 0.038 \\ \varepsilon_{a,max} = 0.361 \leq 2.5 \\ \varepsilon_{t.d} = 1.072 \leq \frac{7.0}{1} \end{gathered} \tag{5.22}$$

The values are within the permitted limits and satisfy the requirements.
As for the stability criteria, the verification is performed as in Equation (4.18) with respect to the ratio of the critical buckling load and the design axial force:

$$\begin{gathered} P_{cr} = 5047kN \\ \frac{P_{cr}}{2} > N_{Ed,Max} \geq \frac{P_{cr}}{4} \\ 1 - \frac{2N_{Ed,Max}}{P_{cr}} = 1 - 0.672 = 0.328 > 0.212 \end{gathered} \tag{5.23}$$

For the case of self-weight combined with the vertical earthquake component, the deformation values are the following:

$$\begin{gathered} \varepsilon_{c,E} = 0.832 \\ \varepsilon_{\alpha,d} = 0.038 \\ \varepsilon_{a,max} = 0.361 \leq 2.5 \\ \varepsilon_{t.d} = 1.231 \leq \frac{7.0}{1} \end{gathered} \tag{5.24}$$

The stability verification shows:

$$\begin{gathered} P_{cr} = 5047kN \\ \frac{P_{cr}}{2} > N_{Ed,Max} \geq \frac{P_{cr}}{4} \\ 1 - \frac{2N_{Ed,Max}}{P_{cr}} = 0.169 < 0.212 \end{gathered} \tag{5.25}$$

Upon completing the verifications for both cases of maximum axial load, it is shown that for the case of self-weight combined with the horizontal earthquake contribution the final stability check exceeds the required value, to be precise $0.328 > 0.212$. However, keeping in mind that indeed $\frac{P_{cr}}{2} > N_{Ed,Max}$ and that the safety factor in question is 2, this deviation is considered acceptable.

Chapter 6

Analyses in OpenSees of the Case Study

This chapter is focused on the modelling and analysis process of the ELT using the open framework OpenSees. The first section elaborates the code used to build a simplified model of the structure, supported by the elastomeric bearings, as designed in the previous chapter. Following is a presentation of the results from the OpenSees analyses, obtained by recording the relevant parameters at each time step of the duration of an earthquake simulation. The final section is a commentary on the results in terms of behavior of the elastomeric bearings as part of a 3D base isolation system.

6.1 Model of the E-ELT

The OpenSees model of the designed bearing is created referring to the formulation of Kumar et al. [2015] and the element implemented by Kumar [2016]. However, the parameters required as input arguments of the element need to be selected such that represent the actual behaviour of the isolation device.

In particular, it is worth nothing that the expression for the computation of the restoring forces, based on the formulation by Park et al. [1986] and reported in Equation (3.11), describes in a correct manner the behaviour of lead rubber bearings, in which the hysteretic component is exploited by the internal lead core, but makes a mistake for what concerns elastomeric bearings. In fact, using that expression, the energy dissipation exploited by the rubber is taken into account twice: firstly by means of the parameter cd of the viscous energy dissipation, that represents the defined percentage of the critical damping of the bearing, and then by means of the characteristic strength Qd, i.e. the intercept of the hysteresis cycle curve with the y-axis. Both quantities depend on the effective damping β_{eff} , that is the ratio between the energy

dissipated per cycle and the elastic strain energy, so it is evident that the contribution of the damping is doubled. The major energy dissipation mechanism of the elastomer used for high damping rubber bearing is hysteretic rather than viscous. Due to this, the parameter cd is assumed to be zero.
The predominant contribution of hysteretic energy dissipation leads to non-linear hysteresis in the force-displacement graph. The behaviour is modelled as a bi-linear curve, with initial elastic stiffness and then a strain-hardening branch. The post-elastic stiffness ratio α, i.e. the ratio between the the post-elastic stiffness and the elastic stiffness, is suggested by Kelly [2001] to be in the range of 1/3 − 1/4 for high damping rubber bearing, so the elastic stiffness is from three to four times the post-elastic one.
Elastomeric bearings are usually subjected to large strains, so the design of their properties is usually carried out at shear strain of 100%. In the case of the E-ELT, the aim to reach a vertical isolation, in addition to the horizontal isolation, has implied thick layers of rubber that means a high value of the total height of the bearing. Due to this, the design horizontal deformation corresponds no longer to shear strain of 100% but to less than 50%. In fact, the design horizontal displacement reported in Equation (5.3) is far from $T_r = 0.63$ m, so the bearing subjected to high-intensity earthquakes will not reach the level of deformation assumed by Kumar et al. [2015]. Therefore, attention must be paid to the definition of the hysteresis cycle. In fact, the expression to compute the characteristic strength (Equation (3.17)) depends on quantities determined for $\Delta = T_r$, i.e. shear strain of 100%, but in this case $\Delta = T_r$ can not be reached, so the value of Q_d computed by means of Equation (3.17) can not be used. To shed light on the reasons for this, the idealized bi-linear behaviour in shear, shown in Figure 6.1, is considered, with u_{max} corresponding to the maximum lateral displacement, here referred as Δ.

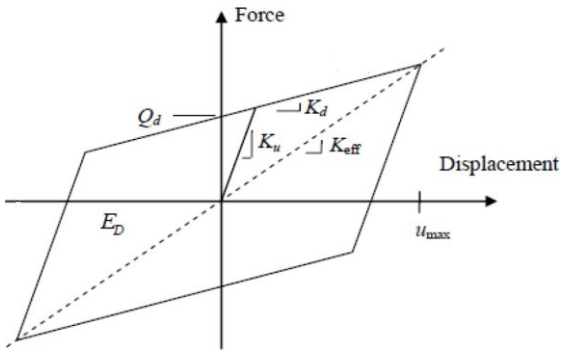

Figure 6.1: Idealized behaviour of elastomeric bearings in shear (adapted from Warn and Whittaker [2006]).

The area enclosed in the curve represents the energy dissipated per cycle and it can be computed in an approximate manner through Equation (3.15), that is a linear function of the maximum displacement Δ. The elastic strain energy is defined as $K_{eff}\ \Delta^2$ that is a square function of the maximum dis- placement.

Thus, if the maximum displacement Δ decreases, both energies decrease but the elastic strain energy decreases faster than the energy dis- sipated per cycle, so the value of the effective damping β_{eff} results higher than the initial one, as evident from Equation (3.14). Moreover, since the effective stiffness is computed through Equation (3.10), if the maximum dis- placement Δ decreases, the effective stiffness K_{eff} increases. Kumar et al. [2015] assumes the effective stiffness K_{eff} to be very similar to the post- elastic stiffness Kd such that it has no influence if it is considered the latter rather than the former and this is acceptable for a shear strain of 100%. Conversely, for lower shear strain, the effective stiffness must be computed as:

$$K_{eff} = K_d + \frac{Q_d}{\Delta} \tag{6.1}$$

Hence, for value of the shear strain lower than 100%, the system turns out to be stiffer ($K_{eff} > K_d$) and more damped ($> \beta_{eff}$), so the procedure proposed by Kumar et al. [2015] leads to a hysteresis cycle that does not represent the actual behaviour of the designed bearing. In particular, due to the fact that the post-elastic stiffness K_d is defined as a function of the geometrical and material properties of the bearing, that are fixed, and the elastic stiffness is computed as the product between the post-elastic stiffness K_d and the post-elastic stiffness ratio α, that are fixed, the characteristic strength Q_d remains the only quantity that can be modified to define a correct force-deformation curve. Therefore, the definition of the characteristic strength is performed through an iterative procedure that aims at finding a value of Q_d for which the ef- fective damping at a shear strain corresponding to the design horizontal displacement results as the designed value, i.e. β_{eff} = 10%. The geome rical and material properties of the bearing are known and the post-elastic stiffness ratio is fixed. Considering Δ = d_{bd}, the procedure starts assuming a value of the characteristic strength Q_d, from which it is possible to compute the yield strength F_Y through Equation (3.26) and the corresponding yield displacement Y as the ratio between the yield strength and the lateral displacement Δ. Then, the area enclosed in the hysteresis cycle can be obtained by means of Equation (3.16) and, once the post-elastic stiffness has been calculated as $K_d = GA/T_r$, the effective stiffness K_{eff} is found through Equation (6.1). Finally, the effective damping can be computed using Equation (3.16) and the result must be in accordance with the initial hypothesis of β_{eff} = 10%. If the check is fulfilled, the initially assumed value of the characteristic strength Q_d describes correctly the energy dissipation of the bearing. Conversely, if the effective damping β_{eff} does not match with the initial hypothesis, another value of the characteristic strength must be assumed and the procedure must be repeated. In particular, if the effective damping β_{eff} results lower than the required one, a higher value of the characteristic strength Q_d has to be selected. [Pecchillo, 2019].

Following the procedure previously discussed by Pecchillo [2019], the obtained value for the characteristic strength is $Q_d = 46kN$, leading to a yield

strength of $F_y = 69kN$. After completing this adjustment with respect to the realistic behavior of the structure, the next step is the implementation of model in OpenSees.

The modelling of the structure begins with the definition of the spatial dimension of the object and the degrees of freedom of the nodes using the *BasicBuilder* command as:

```
#Create Model Builder
model BasicBuilder -ndm 3 -ndf 6
```

Next is the definition of the node coordinates using the *node* command:

```
#Define nodes
node $nodeTag $x $y $z
```

The node representing the center of mass of the telescope pier has the coordinates (0,4.65,0) along the x, y and z axes, respectively, and an additional node (0,9.3,0) represents the top of the pier and the beginning of the main structure. The mass of the main structure is represented by a point mass in the node with coordinates (0,28.125,0). The rest of the nodes in the model are associated with the top and bottom point of the elastomeric bearings.
The masses of the telescope pier and main structure are appointed for each individual degree of freedom using the *mass* command as:

```
#Define mass
mass 1 18609.0 18609.0 18609.0 18609.0 18609.0 18609.0
mass 3 3400.0  3400.0 3400.0 0.0 0.0 0.0
```

The *fix* command is used to define the constraints for each degree of freedom of the nodes:

```
#Define constraints
fix $nodeTag (ndf $constrValues)
```

where the value of *$constrValues* can be 1 for a fixed DOF or 0 for a free DOF. The bottom of the bearings is intact to the foundations, so all the degrees of freedom for the bottom nodes of the bearings are constrained, whereas all other nodes are completely free.
The following step is to create the physical link between the node representing the telescope pier mass and the nodes representing the top of the elastomeric bearings. This is done using *elasticBeamColumn* elements with extremely high mechanical properties that should simulate a near-perfectly rigid bond. However, using these elements would allow a transfer of a moment from the pier to the bearings when in fact, this cannot occur in the real structure. Due to this, additional “clone” nodes are created with the exact same coordinates as the nodes representing the top of the bearings, and are then connected to their

"original" nodes using an *equalDOF* constraint object that will impose the same translational displacements of the original nodes to their clones. The rotational DOFs of the clone nodes are left unbound and the link between the pier and the bearings is actually created between the node with the pier mass and the clone nodes, instead of the original nodes. In this manner, the transfer of the moment to the bearings is avoided, thus the model behavior stays true to that of the real structure. The *equalDOF* constraint objects are defined as:

```
#Define equalDOF
equalDOF $rNodeTag $cNodeTag $dof1 $dof2 $dof3
```

where *$rNodeTag* is the retained "master" node and *$cNodeTag* is the constrained "slave" node, on which are imposed the displacements of the former for the defined degrees of freedom.
Before defining element objects, a coordinate transformation object is introduced for the purpose of transferring the element stiffness and restoring force from the basic to the global coordinate system:

```
#Define geometric transformation
geomTransf Linear 1 0 0 -1
```

The connections between the bearings and the telescope pier mass are created with *elasticBeamColumn* elements that have the following properties:

Table 6.1: Designed input arguments of elasticBeamColumn elements for telescope pier

Input	Value	Input	Value
$eleTag	1001	$Iz	12.299
$Nd1	$telescope pier mass	$Iy	14.78
$Nd2	$top of bearing	$transfTag	1
$A	0.338	$massDens	default
$E	210000000000.0	-cMass	default
$G	70000000000.0		
$J	10.0		

The input for forces in OpenSees is in kilonewtons and the area is in square meters. Consequently, the stresses are in [$\frac{kN}{m^2}$].
The properties for the *elasticBeamColumn* portraying the main structure are listed below:

Table 6.2: Designed input arguments of elasticBeamColumn elements for main

structure

Input	Value	Input	Value
$eleTag	1000	$Iz	12.299
$Nd1	$telescope pier top	$Iy	14.78
$Nd2	$main structure lumped mass	$transfTag	1
$A	0.338	$massDens	default
$E	210000000.0	-cMass	default
$G	70000000.0		
$J	10.0		

The elastic and shear modulus of the *elasticBeamColumn* elements used for the telescope pier are 1000 times greater than that of the main structure, since their role is to provide a completely rigid link between the pier and the elastomeric bearings. This value is considered to be sufficient, whereas using an even higher value might cause convergence issues in OpenSees.
The last part of the model are the elastomeric bearings, implemented using *ElastomericX* elements with the following parameters:

Table 6.3: Designed input arguments of `ElastomericX`.

Input	Value	Input	Value
$eleTag	1	$y1 $y2 $y3	1 0 0
$Nd1	$bottom node	$kc	default
$Nd2	$top node	$PhiM	default
$Fy	69.4 kN	$ac	default
$alpha	0.33	$sDratio	default
$Gr	640.0	$m	default
$Kbulk	2000000	$cd	0.179
$D1	0	$tc	default
$D2	1.2 m	$tag1	0
$ts	0.0062	$tag2	0
$tr	0.09	$tag3	0
$n	7.0	$tag4	0
$x1 $x2 $x3	0 1 0		

Once the structure itself is complete, the gravity load is applied by defining a *timeSeries* object and the load pattern. The value of the gravity load is governed by the sum of the masses of the telescope pier and the main structure.

```
#Define timeSeries
timeSeries Linear 1
#Create a plain load pattern for static analysis
pattern Plain 1 1  {
load 1 0.0 [expr -$P] 0.0 0.0 0.0 0.0};
```

To execute a dynamic analysis, additional *timeSeries* objects are defined using records of the ground motion in all directions of a severe earthquake. To be specific, the earthquake in question is the one from El Centro (1940), since its elastic response spectra in the horizontal directions is quite similar to the spectrum of El Cerro Armazones for the value of the horizontal period defined for the ELT in this thesis.

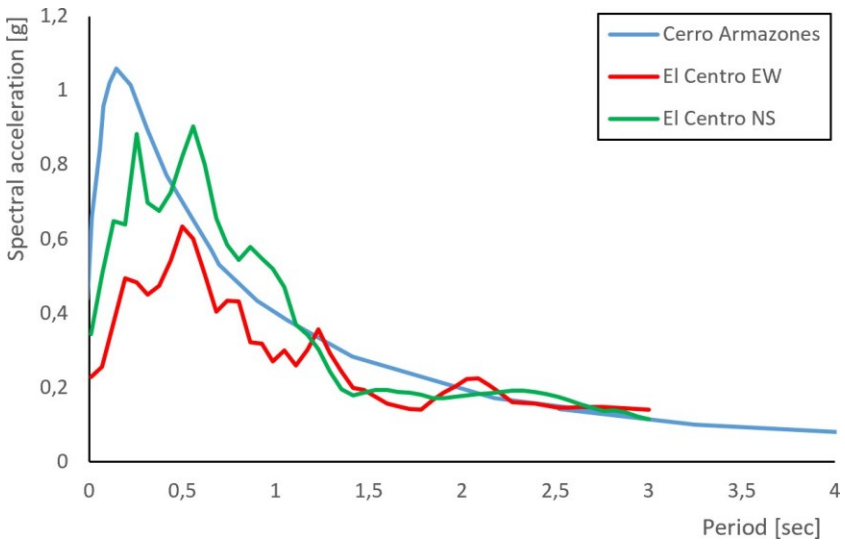

Figure 6.2: Superimposition of horizontal pseudoacceleration elastic response spectra.

Figure 6.2 shows the ground accelerations during the El Centro earthquake in East-West, North-South and vertical direction.

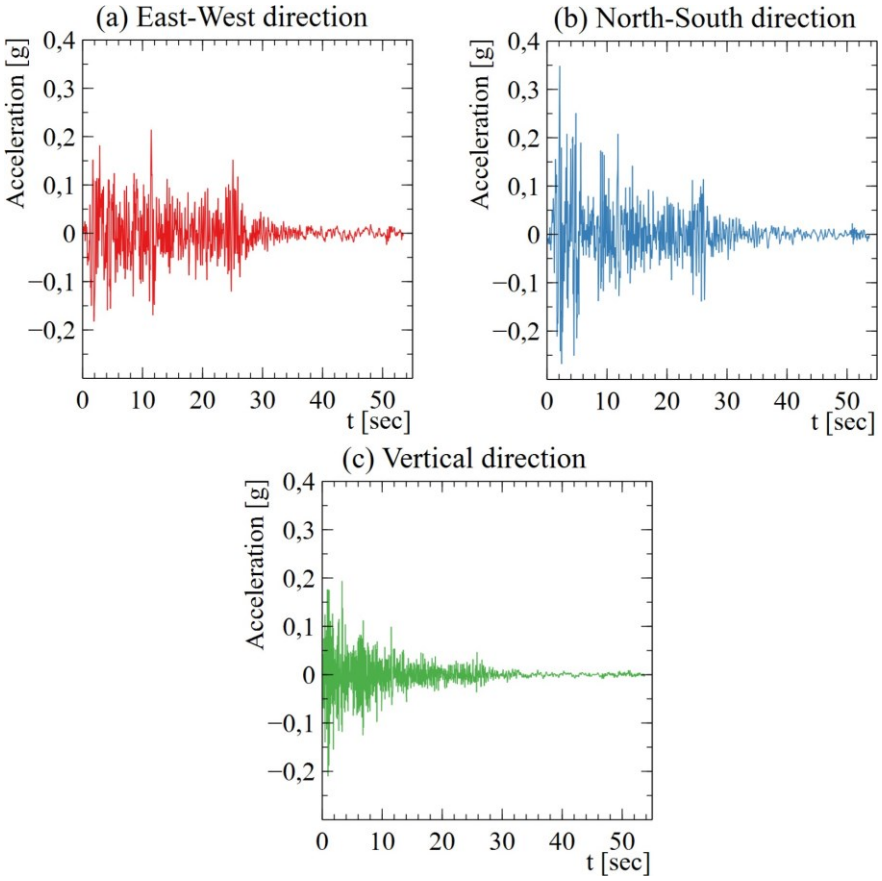

Figure 6.3: El Centro accelerograms in the three directions.

These accelerograms are implemented in the OpenSees analysis as follows:

```
#Set constant gravity loads and reset time in the domain
loadConst -time 0.0
#Define the time interval
set dt 0.02
#Define the time series path
timeSeries Path 10 -dt $dt -filePath elcentroNS.txt
-factor $0.4g;
timeSeries Path 20 -dt $dt -filePath elcentroUP.txt
-factor $0.4g;
timeSeries Path 30 -dt $dt -filePath elcentroEW.txt
-factor $0.4g;
```

```
#Create load patterns for dynamic  analysis
pattern  UniformExcitation   2  1  -accel 10
pattern  UniformExcitation   3  2  -accel 20
pattern  UniformExcitation   4  3  -accel 30
```

The relevant results from the analysis are monitored and extracted through *recorder* objects that can record various parameters for a certain node or element. The nodes of interest are the ones to which are assigned the point masses of the telescope pier and the main structure, for which the displacements and accelerations are recorded in all three directions. The elastomeric bearings whose behavior is monitored are the ones farthest apart on the global x and z axes for both azimuth rings, leading to a total of 8 bearings.

```
#Create recorder to monitor outputs
recorder Node -file telescope_pier_displacement.out -time -
node 1
-dof 1 2 3 4 5 6 disp;
recorder Node -file telescope_pier_acceleration.out -time -
node 1
-dof 1 2 3 4 5 6 accel;
recorder Node -file main_structure_displacement.out -time -
node 3
-dof 1 2 3 4 5 6 disp;
recorder Node -file main_structure _acceleration.out -time -
node 3
-dof 1 2 3 4 5 6 accel;
recorder Element -file ELTForce.out -time
-ele 73 basicForce;
recorder Element -file ELTDisplacement.out -time
-ele 73 basicDisplacement;
recorder Element -file ELTParam.out -time
-ele 73 Parameters.
```

The output of the recorders is provided in text documents, where the specified parameters are given as a function of time at each time step dt. Afterwards these parameters are represented in Excel graphs, again as a function of time. Following is a representation of the obtained results.

6.2 Analyses and Results

The ELT model as described in the previous section is studied through a transient analysis and the results are obtained via recorders that were previously introduced. The first performed analysis disregards the variation of the buckling load, horizontal and vertical stiffness. The analyses after that examine the behavior of the structure including a single parameter variation at a time. To clarify the following output, the eight bearings whose behavior is presented are named according to the azimuth ring they belong to and the degree of the angle they are located on, if the angle starts from the positive x axis of the global coordinate system. Their names and locations are as follows:

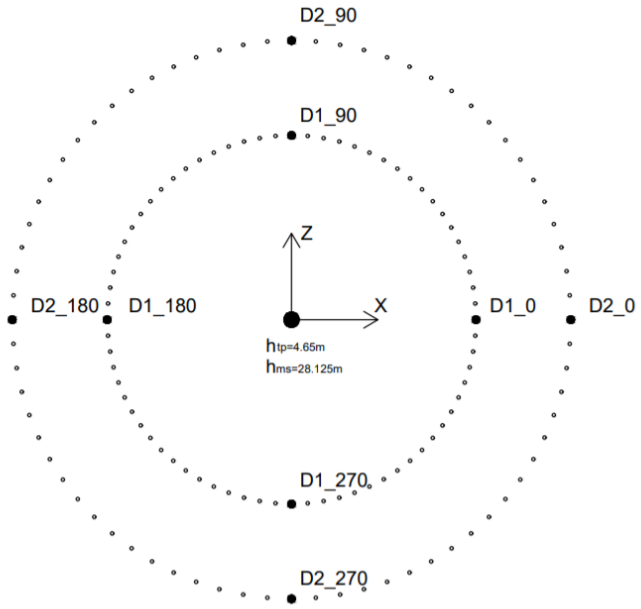

Figure 6.4: E-ELT model layout

- **D1_0** belongs to the inner azimuth ring and is located on the positive x axis
- **D1_90** belongs to the inner azimuth ring and is located on the positive z axis
- **D1_180** belongs to the inner azimuth ring and is located on the negative x axis
- **D1_270** belongs to the inner azimuth ring and is located on the negative z axis
- **D2_0** belongs to the outer azimuth ring and is located on the positive x axis
- **D2_90** belongs to the outer azimuth ring and is located on the positive z axis

- **D2_180** belongs to the outer azimuth ring and is located on the negative x axis
- **D2_270** belongs to the outer azimuth ring and is located on the negative z axis

It is important to note that the accelerations from the El Centro records in the North-South direction coincide with the x axis of the global coordinate system in OpenSees, whereas the accelerations in the East-West direction coincide with the global z axis.
The absolute displacements and accelerations are recorded for the nodes containing the masses of the telescope pier and the main structure, and those nodes will be called simply "telescope pier" and "main structure" in the following output contents.

6.2.1 Analysis with no Variation

This analysis considers the buckling capacity to be constant and equal to the one obtained in Equation (5.23). The same stands for the vertical and horizontal stiffness, which are considered as $K_v = K_{v0} = \frac{E_c A}{T_r}$ and $K_H = K_{H0} = \frac{GA}{T_r}$.
Following are graphs containing the force-displacement curves for the aforementioned bearings obtained through a 50 second simulation of the El Centro (1940) earthquake:

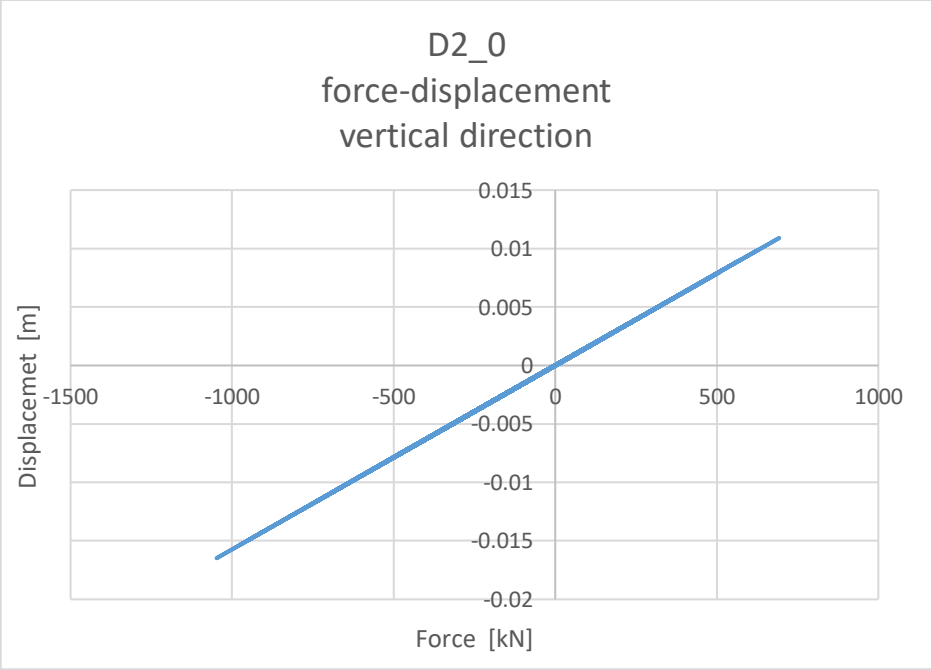

Figure 6.5: D2_0 force-displacement curve in vertical direction for no variation.

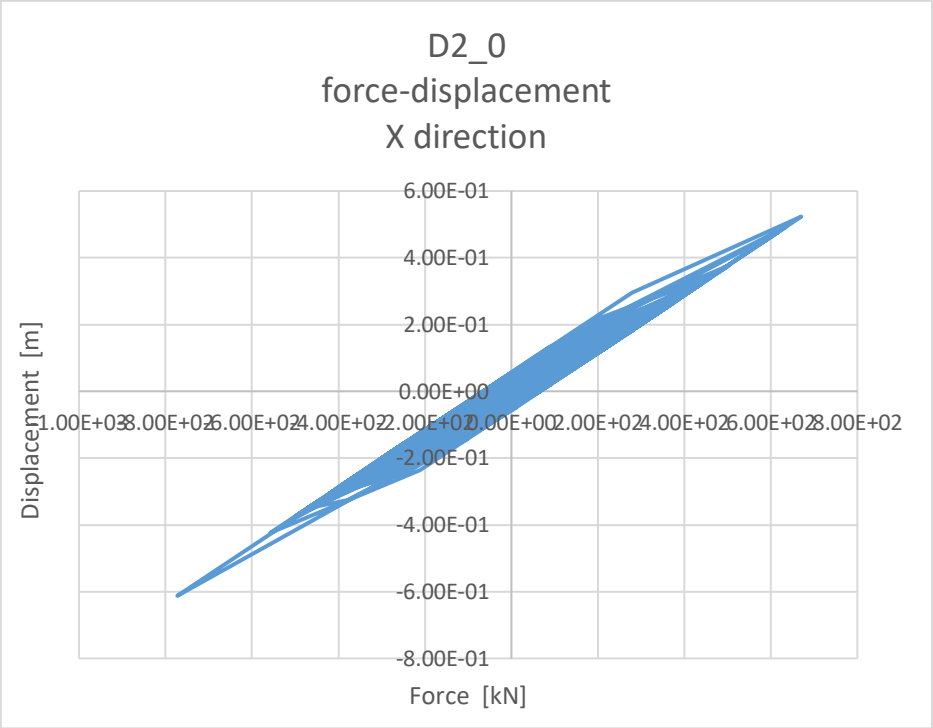

Figure 6.6: D2_0 force-displacement curve in North-South direction for no variation.

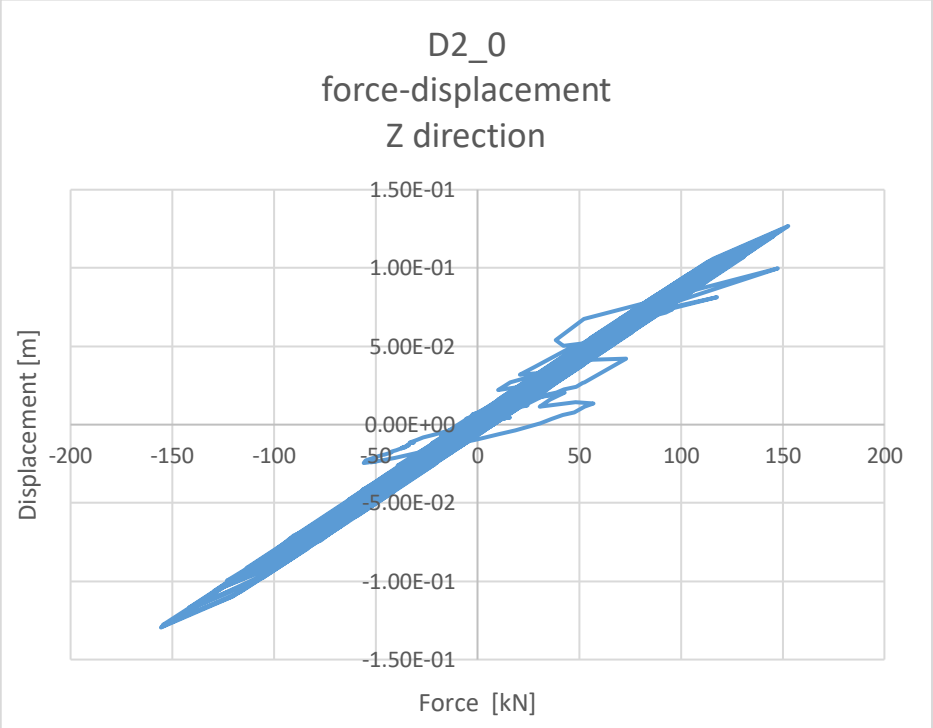

Figure 6.7: D2_0 force-displacement curve in East-West direction for no variation.

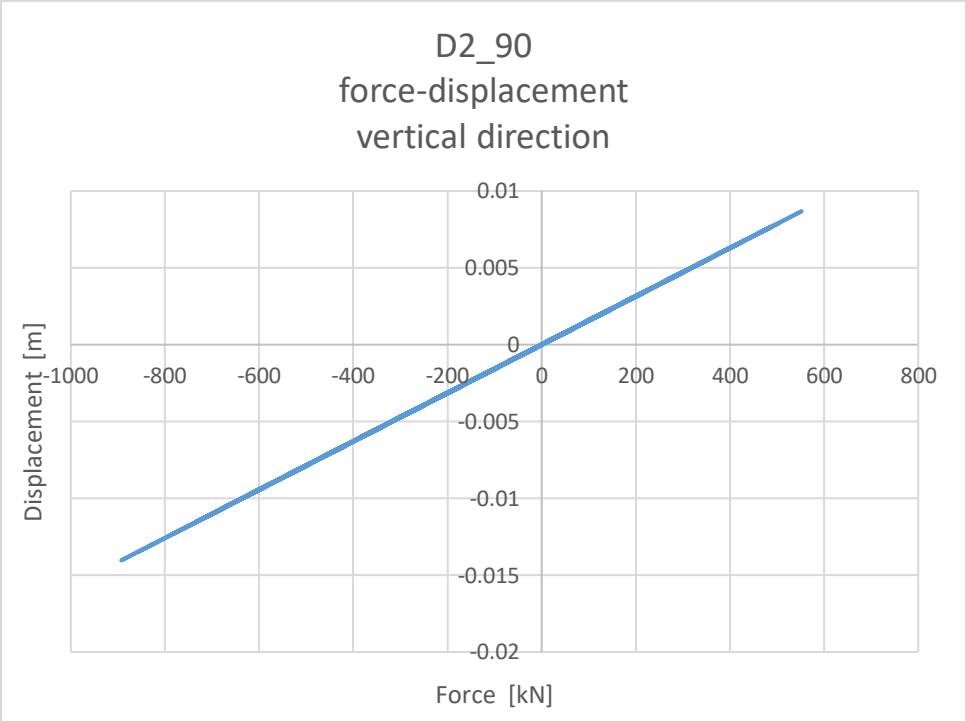

Figure 6.8: D2_90 force-displacement curve in vertical direction for no variation.

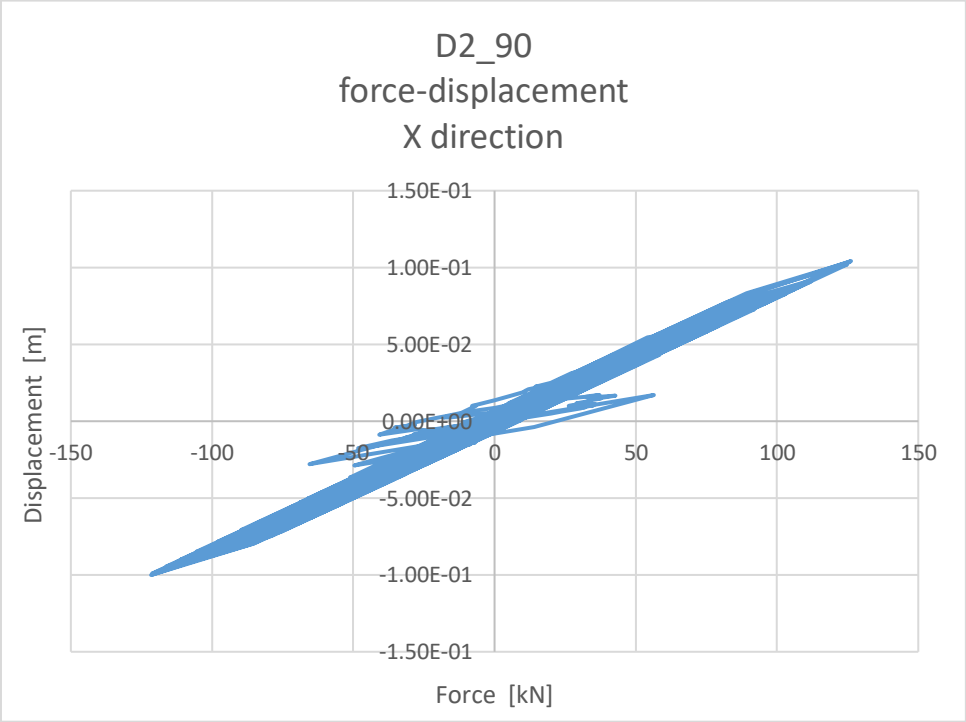

Figure 6.9: D2_90 force-displacement curve in North-South direction for no variation.

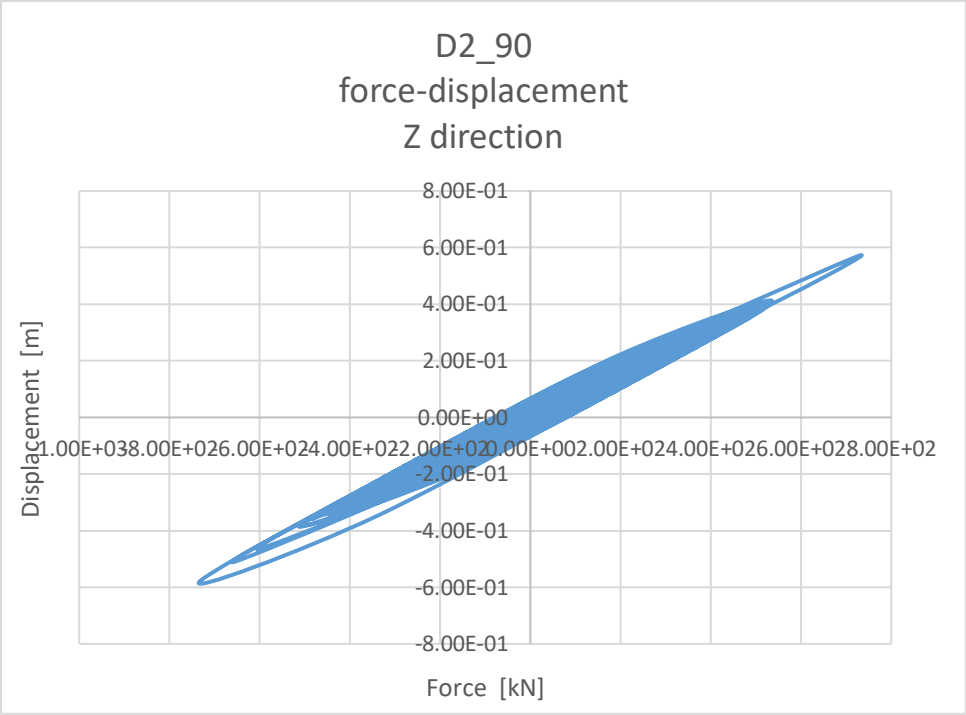

Figure 6.10: D2_90 force-displacement curve in East-West direction for no variation.

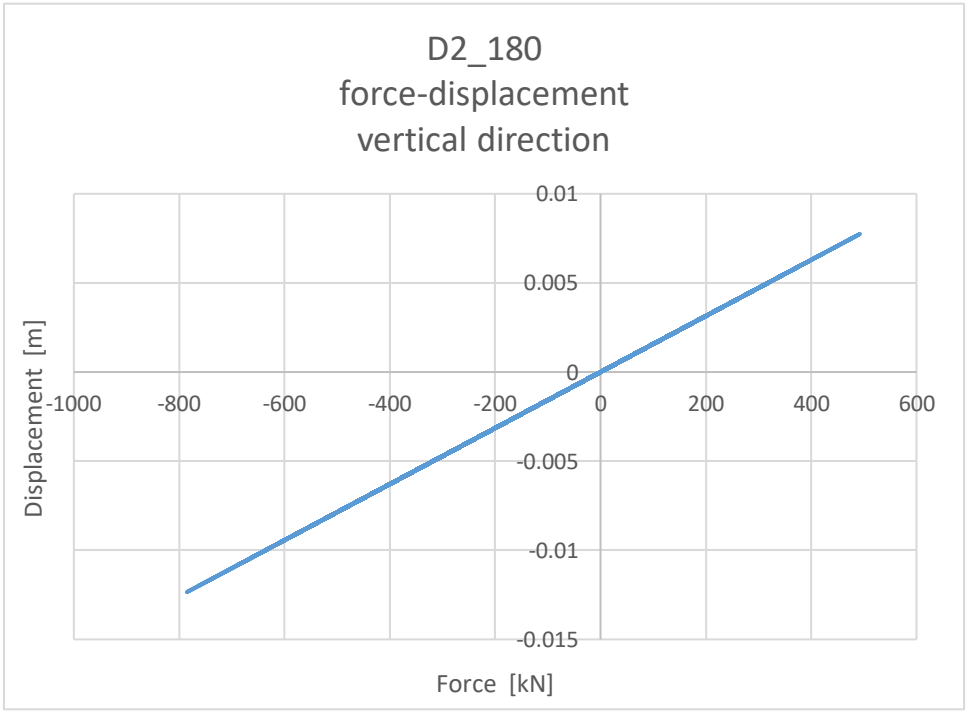

Figure 6.11: D2_180 force-displacement curve in vertical direction for no variation.

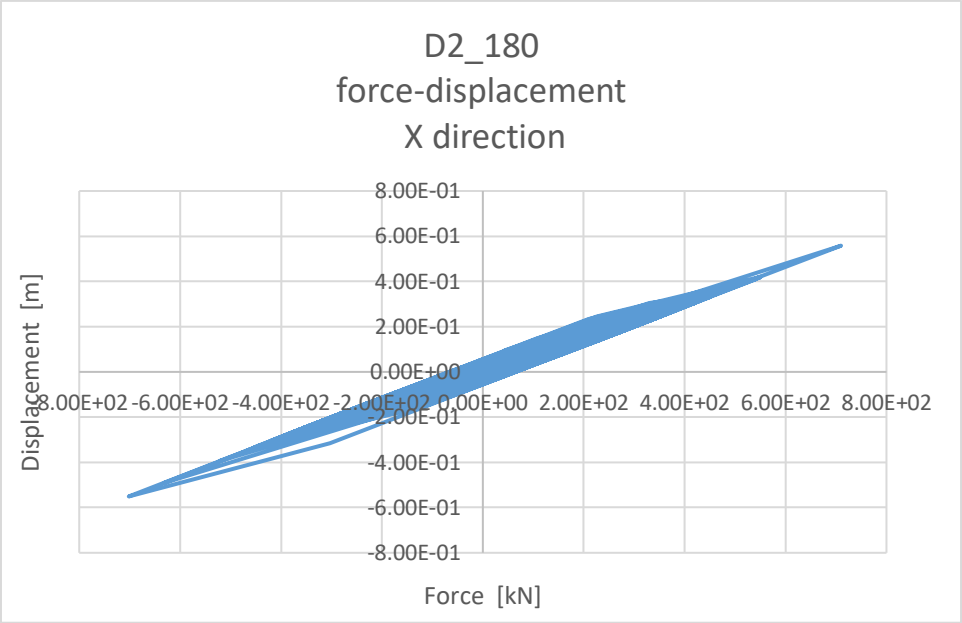

Figure 6.12: D2_180 force-displacement curve in North-South direction for no variation.

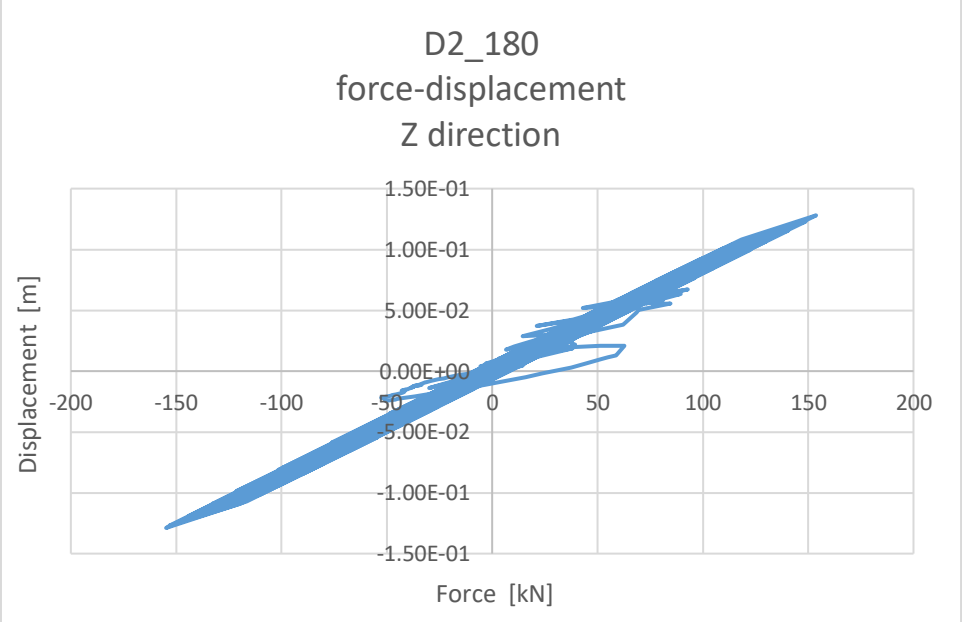

Figure 6.13: D2_180 force-displacement curve in East-West direction for no variation.

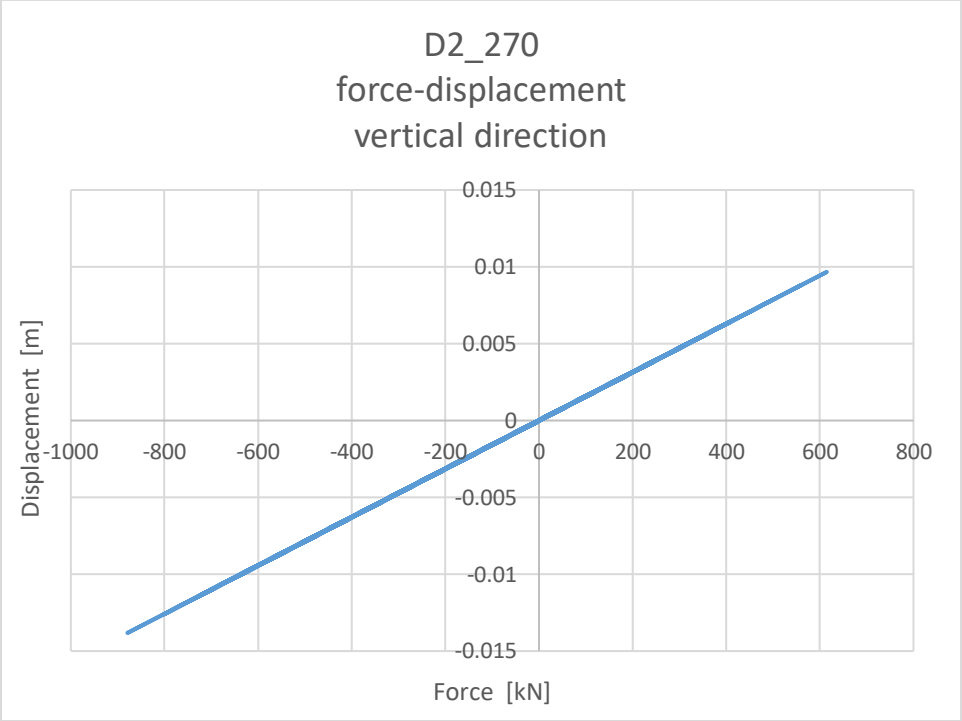

Figure 6.14: D2_270 force-displacement curve in vertical direction for no variation.

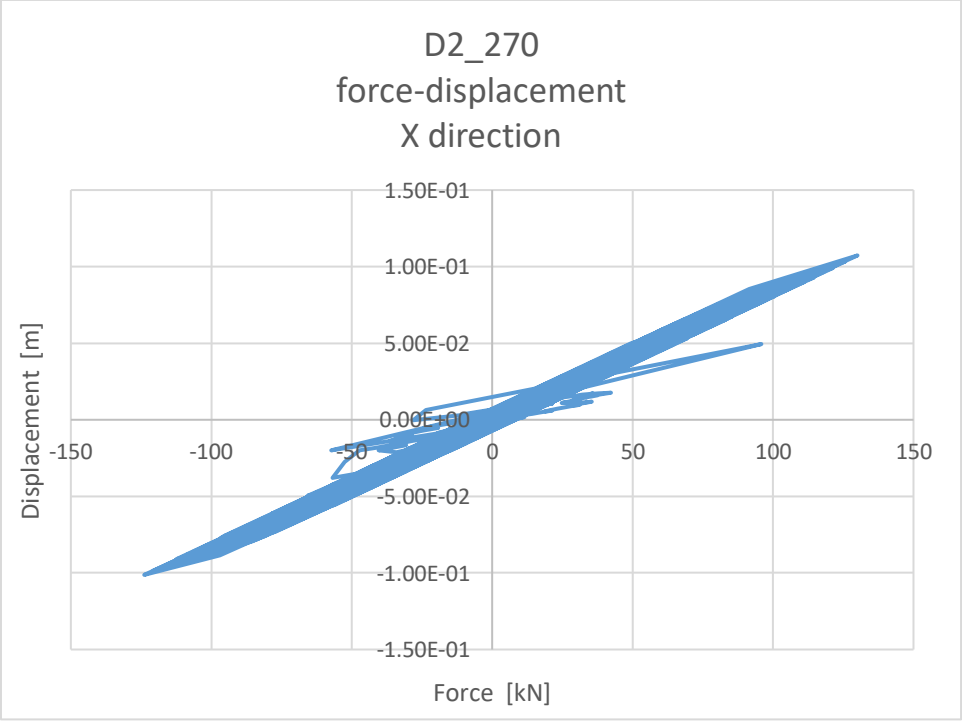

Figure 6.15: D2_270 force-displacement curve in North-South direction for no variation.

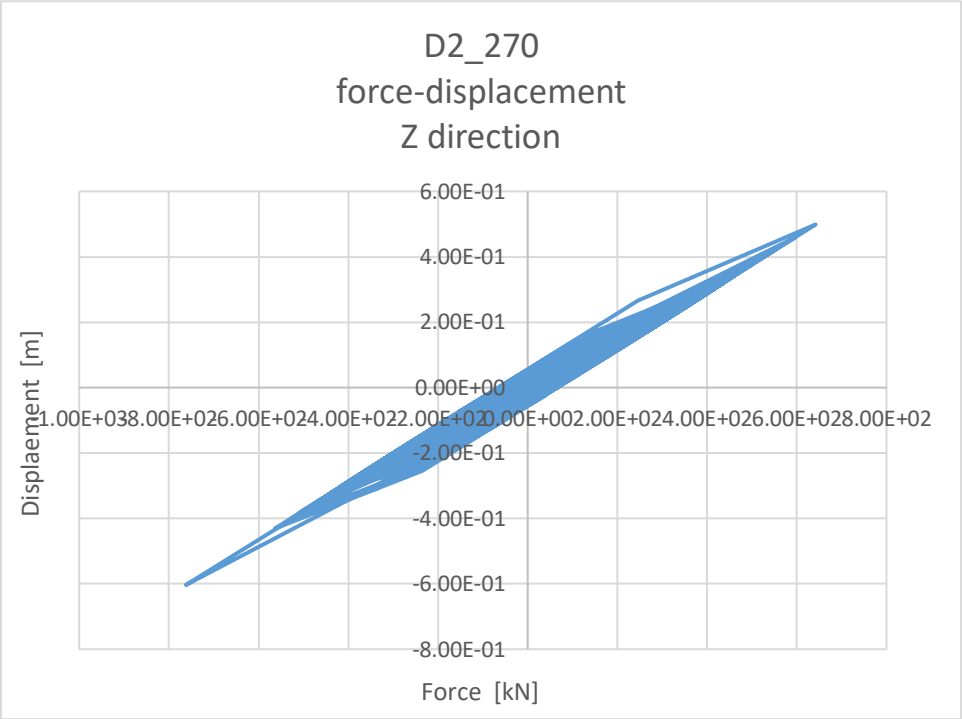

Figure 6.16: D2_270 force-displacement curve in East-West direction for no variation.

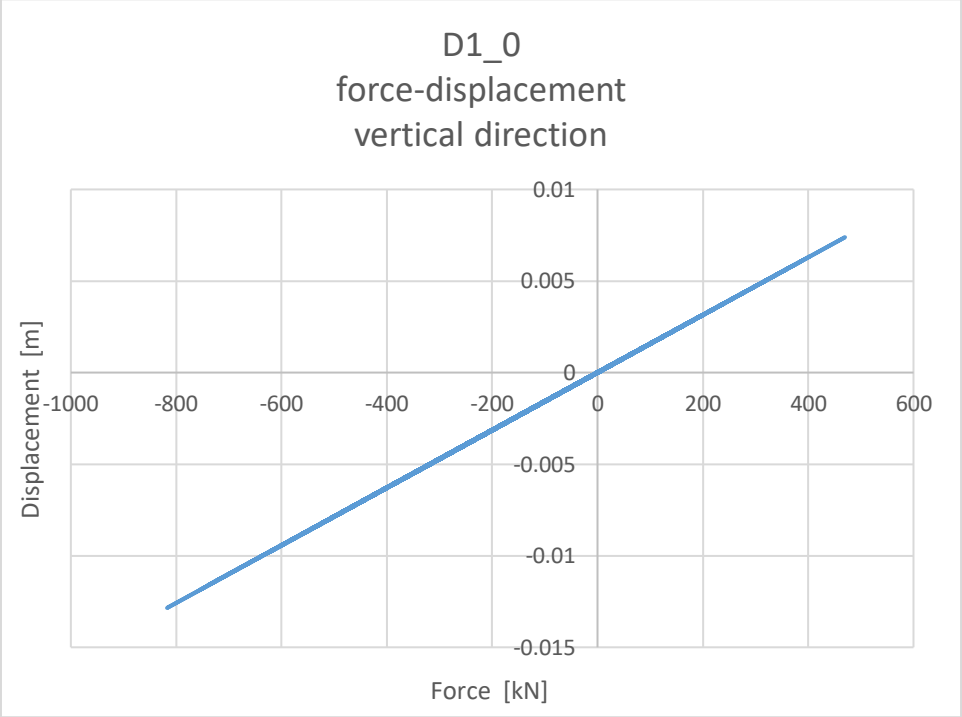

Figure 6.17: D1_0 force-displacement curve in vertical direction for no variation.

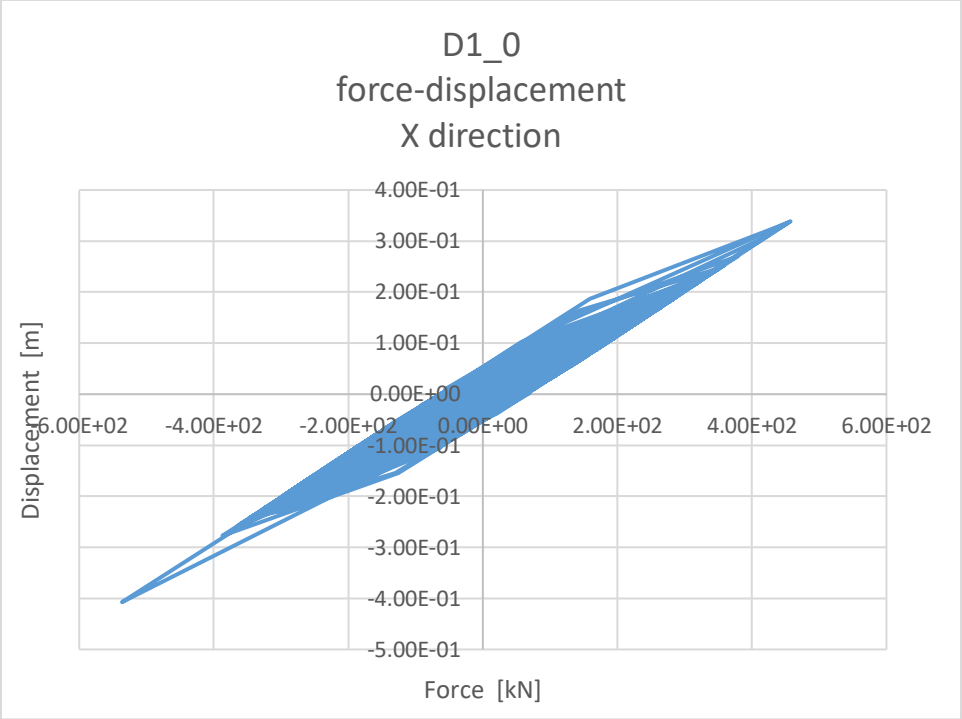

Figure 6.18: D1_0 force-displacement curve in North-South direction for no variation.

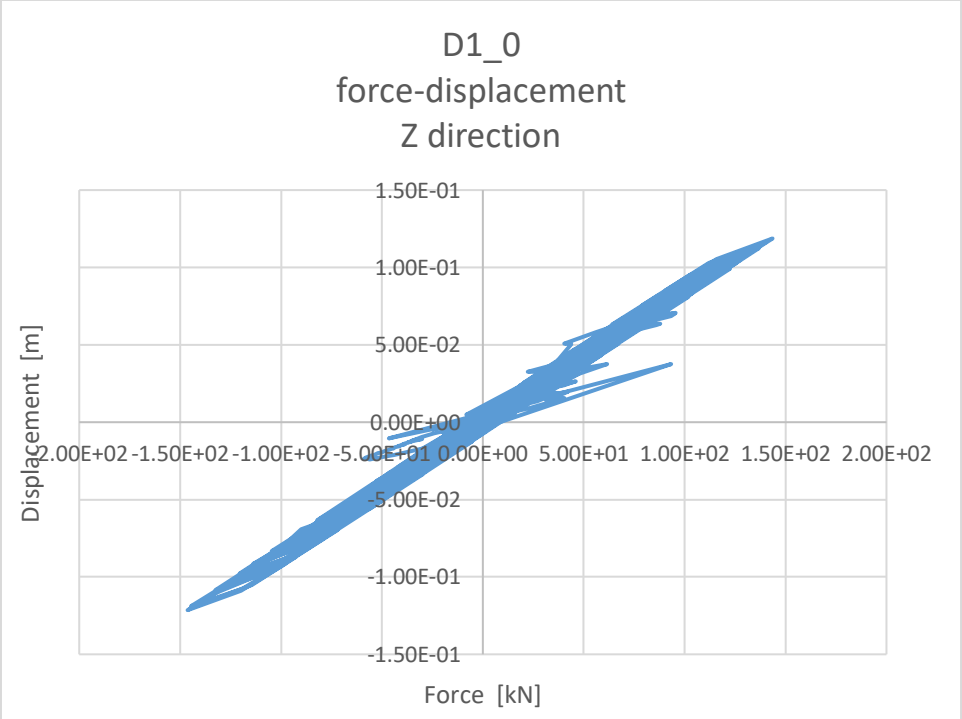

Figure 6.19: D1_0 force-displacement curve in East-West direction for no variation.

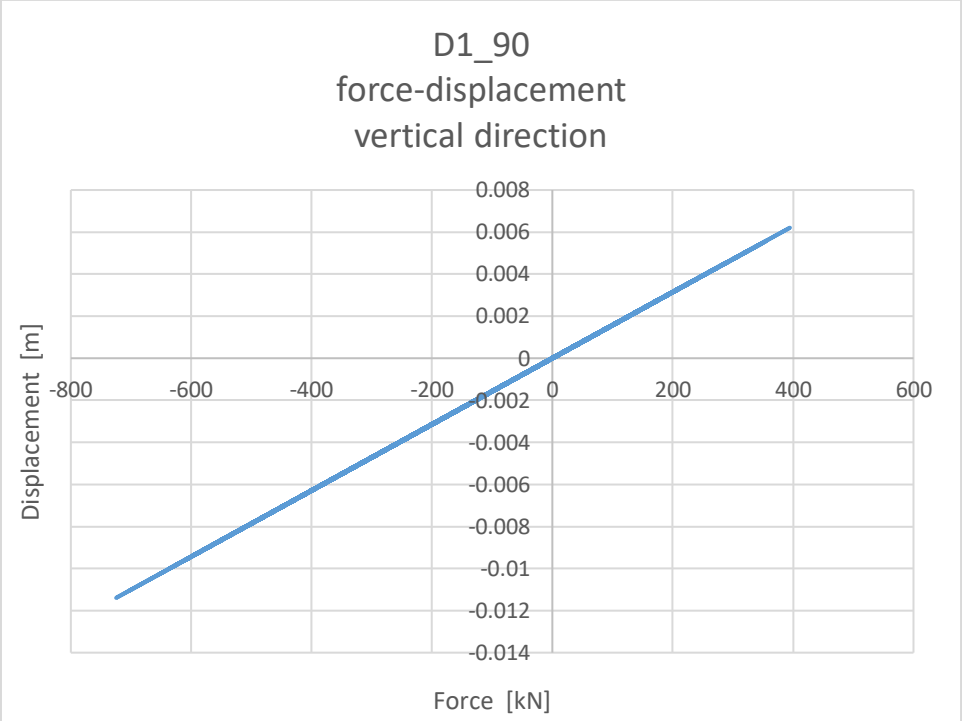

Figure 6.20: D1_90 force-displacement curve in vertical direction for no variation.

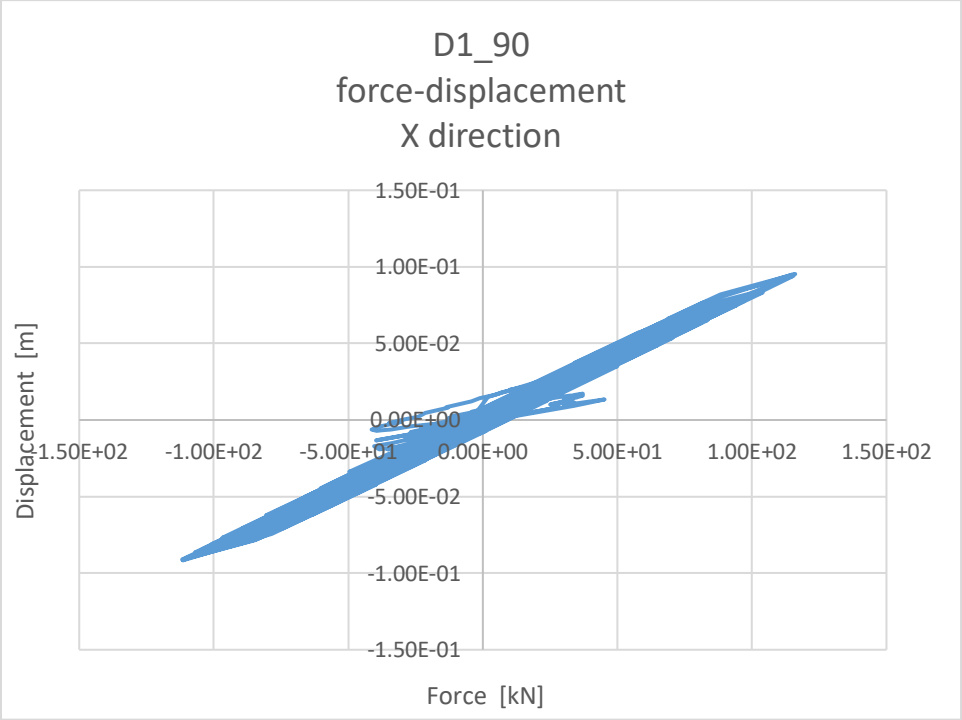

Figure 6.21: D1_90 force-displacement curve in North-South direction for no variation.

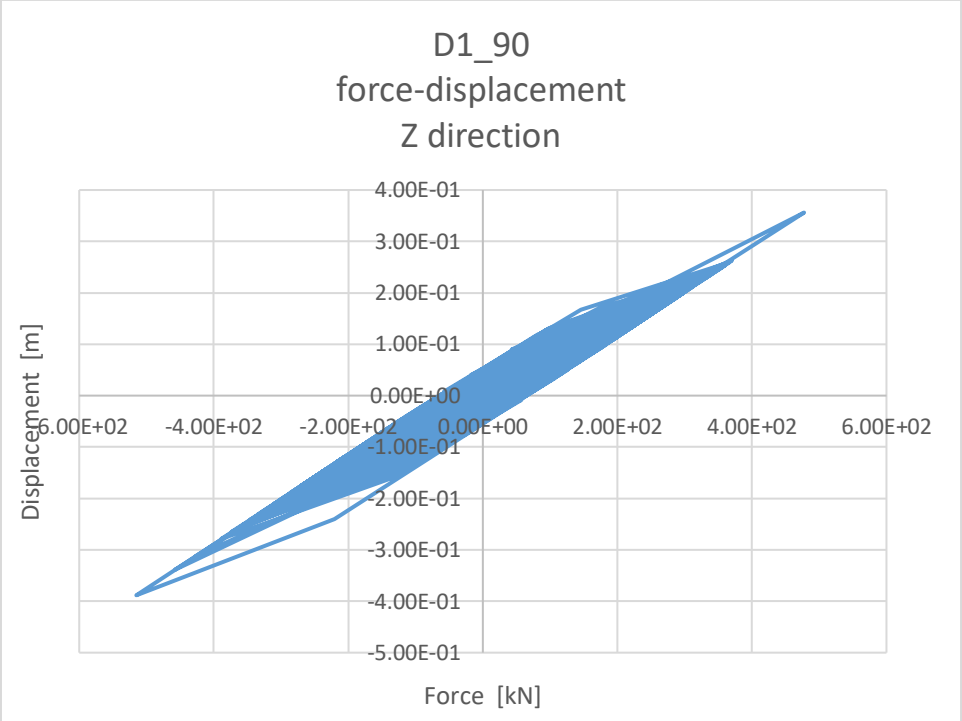

Figure 6.22: D1_90 force-displacement curve in East-West direction for no variation.

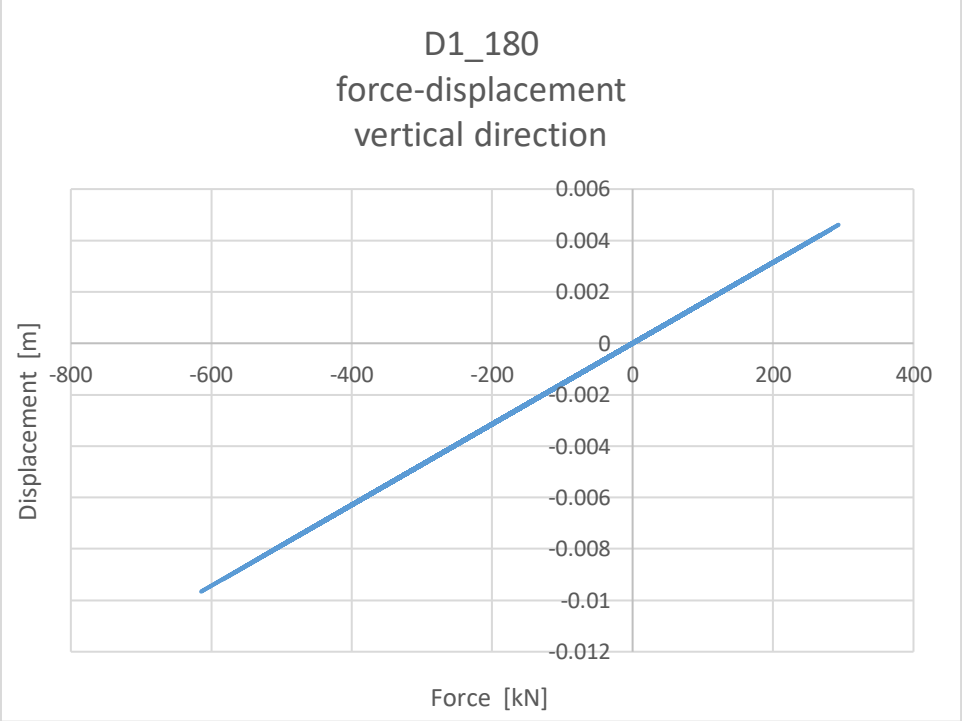

Figure 6.23: D1_180 force-displacement curve in vertical direction for no variation.

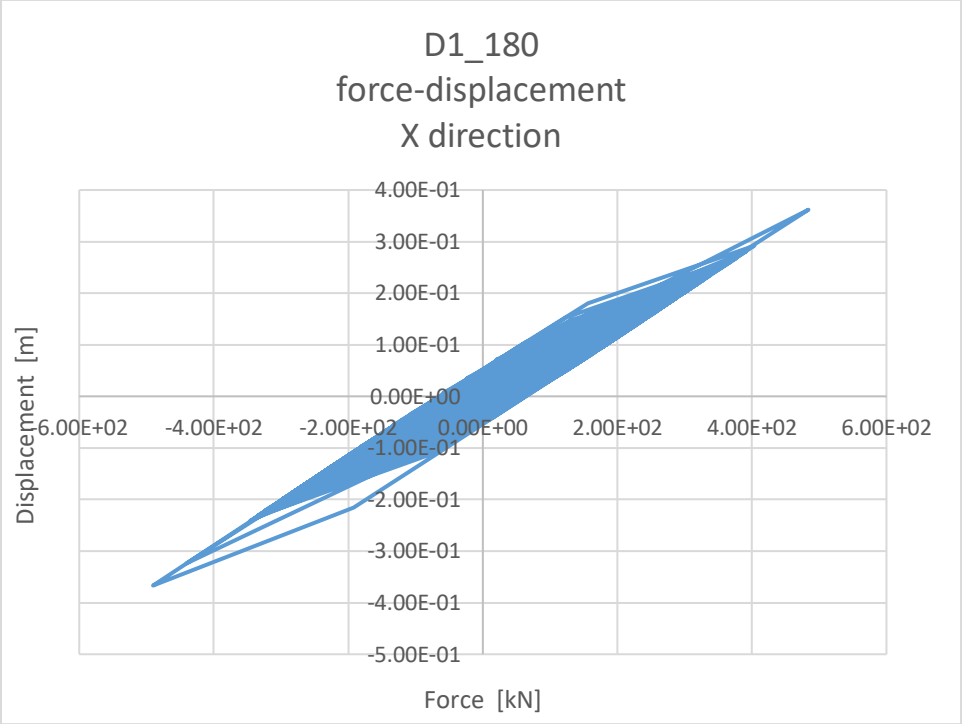

Figure 6.24: D1_180 force-displacement curve in North-South direction for no variation.

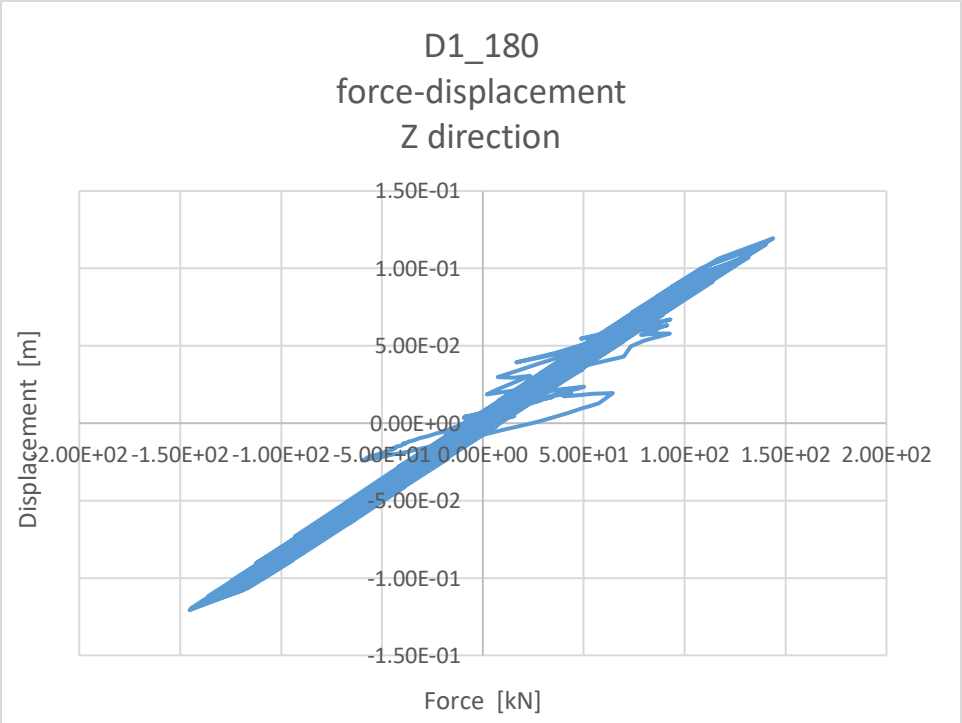

Figure 6.25: D1_180 force-displacement curve in East-West direction for no variation.

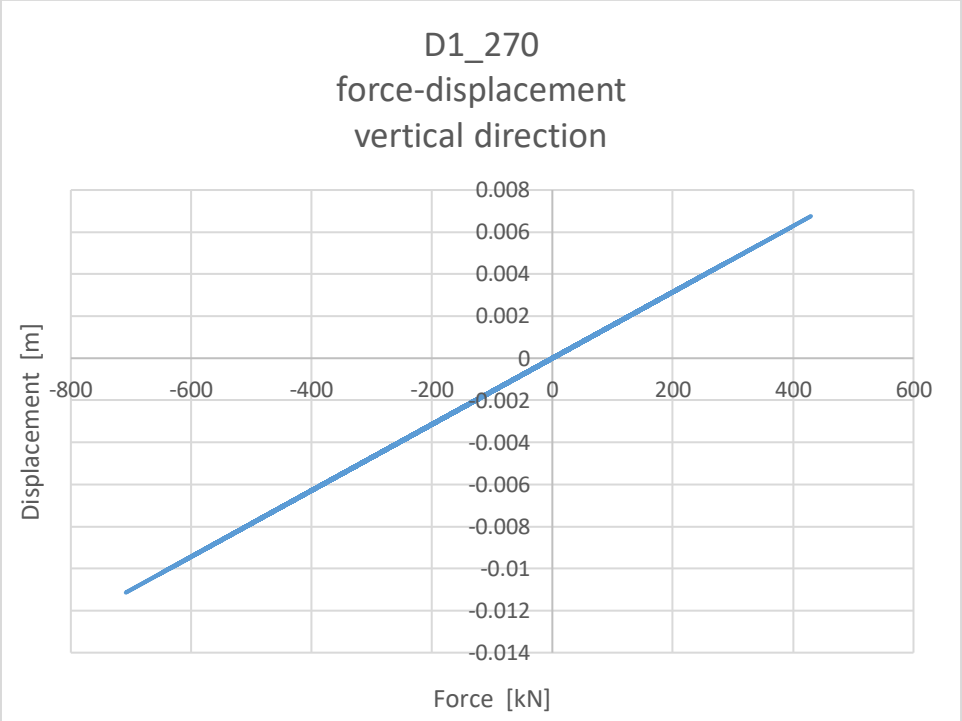

Figure 6.26: D1_270 force-displacement curve in vertical direction for no variation.

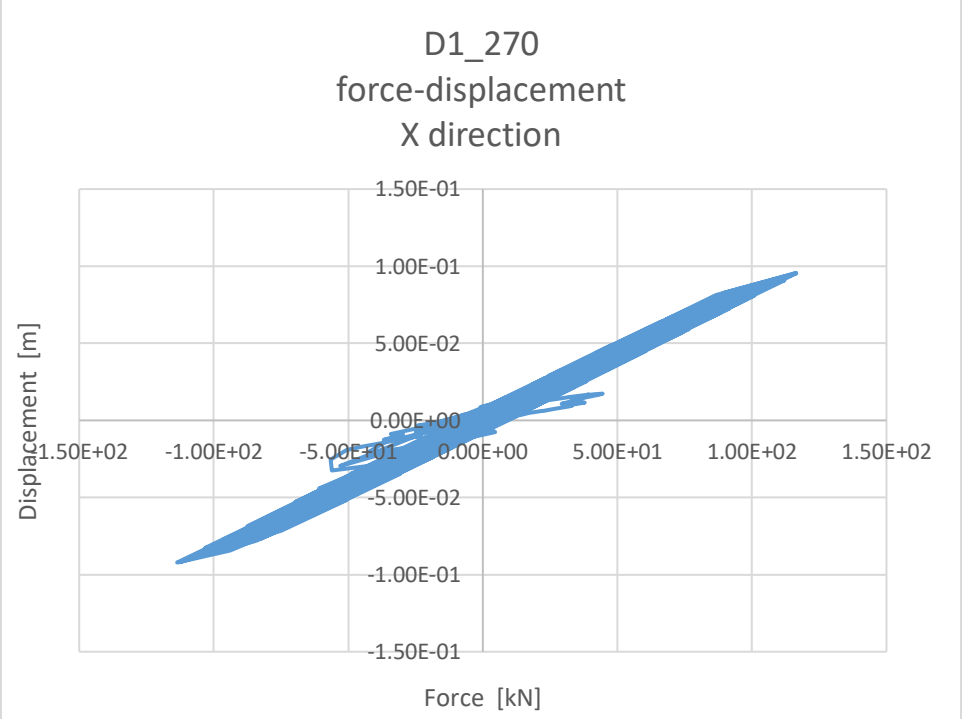

Figure 6.27: D1_270 force-displacement curve in North-South direction for no variation.

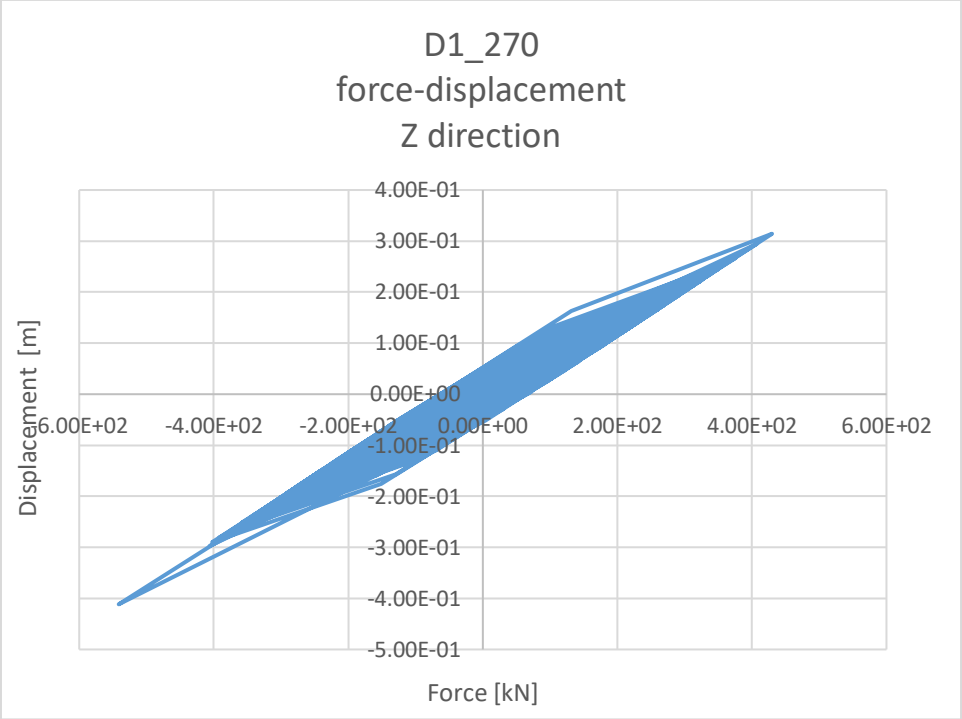

Figure 6.28: D1_270 force-displacement curve in East-West direction for no variation.

The shape of the curves obtained for the 8 bearings are in accordance with the symmetry of the system. In vertical direction, all bearings exhibit a perfectly elastic behavior with a curve stretching further in the negative domain due to the effect of the self-weight of the structure. The highest axial displacement is a compression of $0.016m$ corresponding to an axial compression force of $1048kN$, recorded for bearing **D2_0**.

In the horizontal plane, by observing the curves it is easy to recognize strong similarities to the idealized bi-linear behavior. The largest displacement in the *North-South* direction is $0.612m$, corresponding to a force of $773kN$, recorded for **D2_0**. The *East-West* direction is characterized by slightly smaller accelerations that cause a maximum displacement of $0.576m$ and maximum force of $731kN$ in the bearing **D2_90**.

Following are the recorded nodal displacements and accelerations for the telescope pier and main structure:

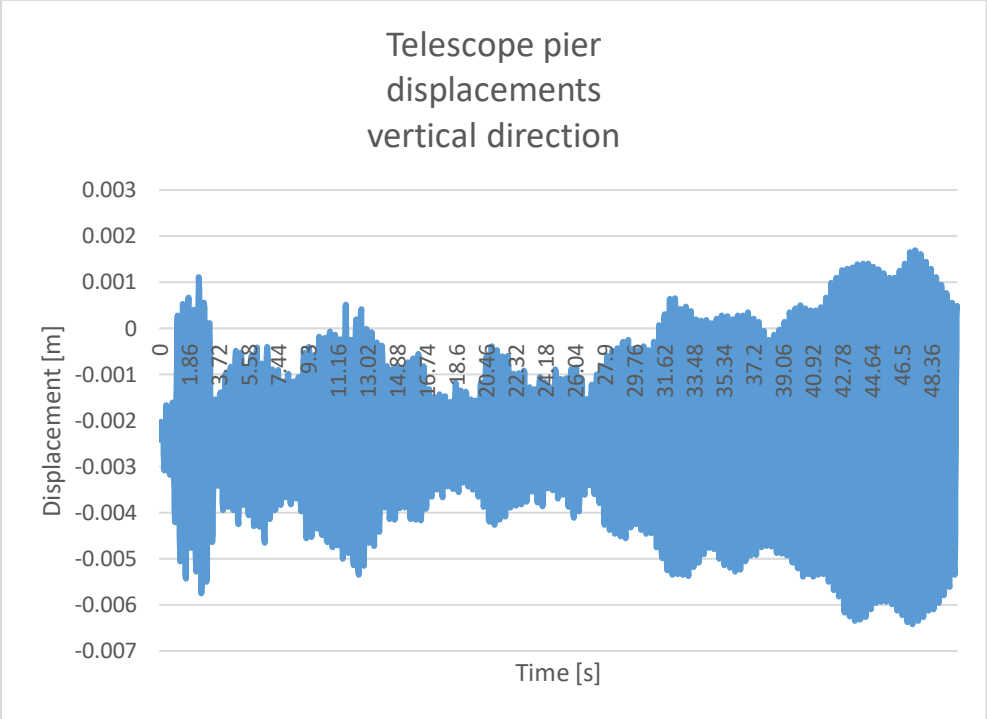

Figure 6.29: Telescope pier displacements in vertical direction for no variation.

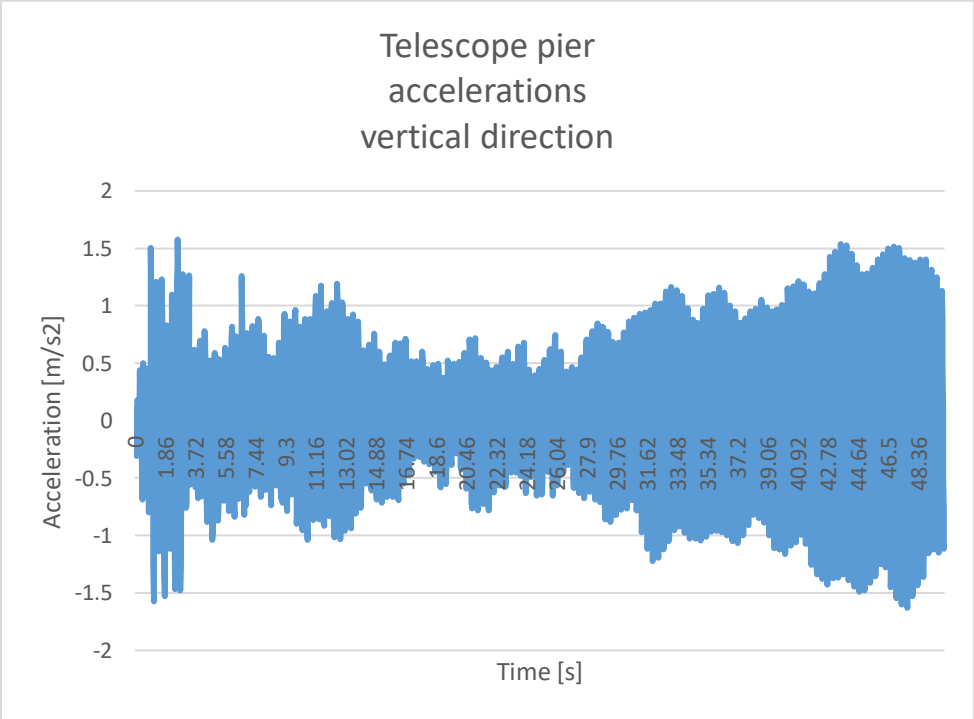

Figure 6.30: Telescope pier accelerations in vertical direction for no variation.

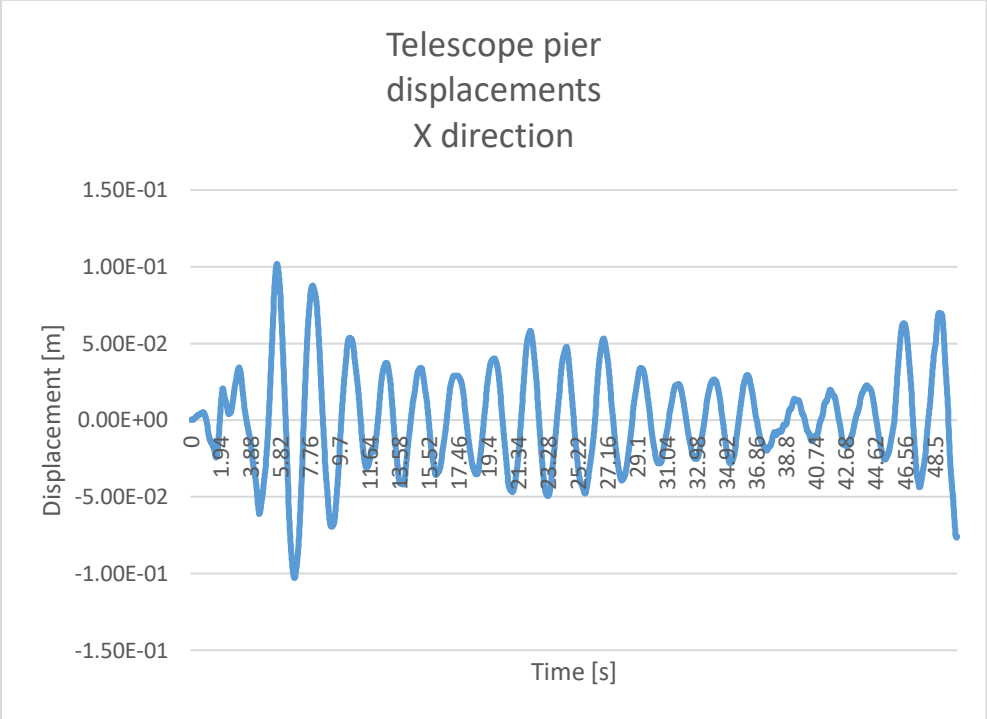

Figure 6.31: Telescope pier displacements in North-South direction for no variation.

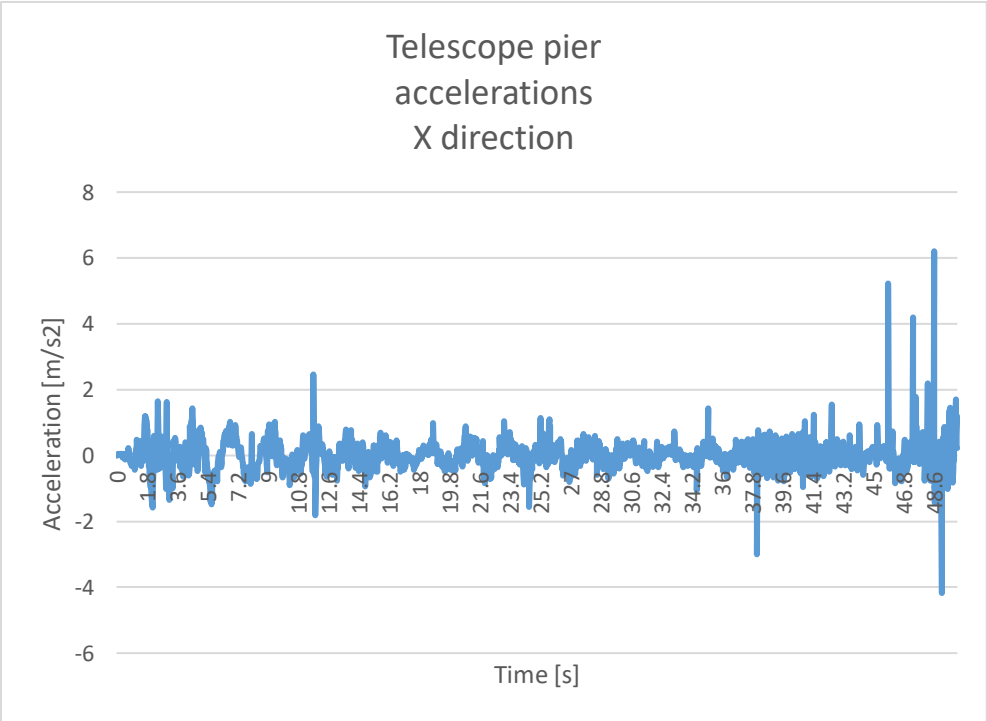

Figure 6.32: Telescope pier accelerations in North-South direction for no variation.

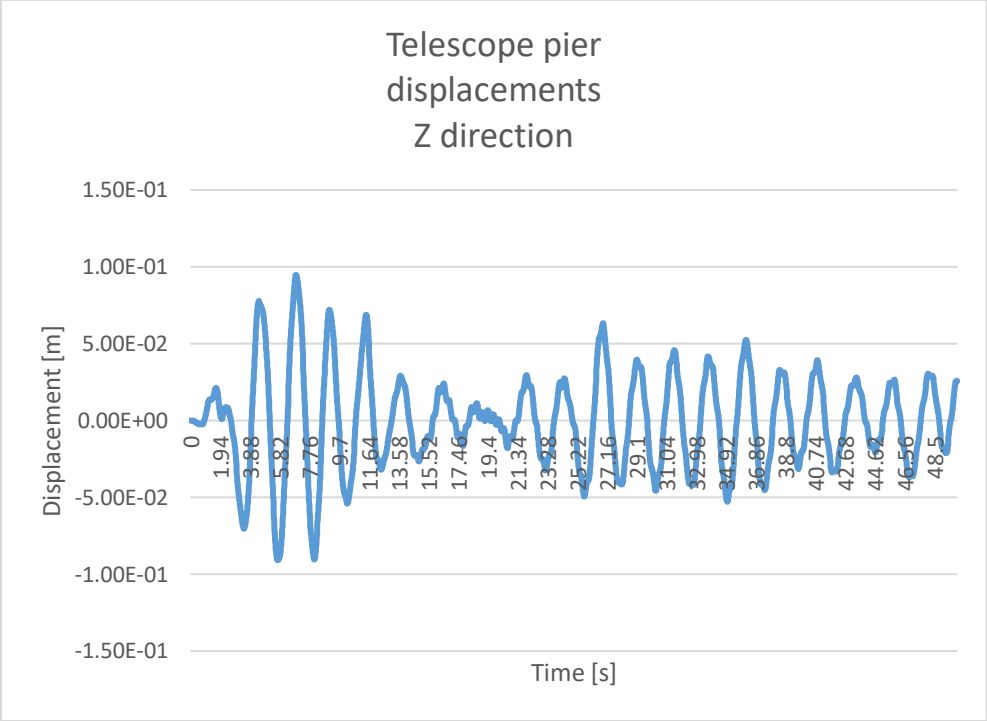

Figure 6.33: Telescope pier displacements in East-West direction for no variation.

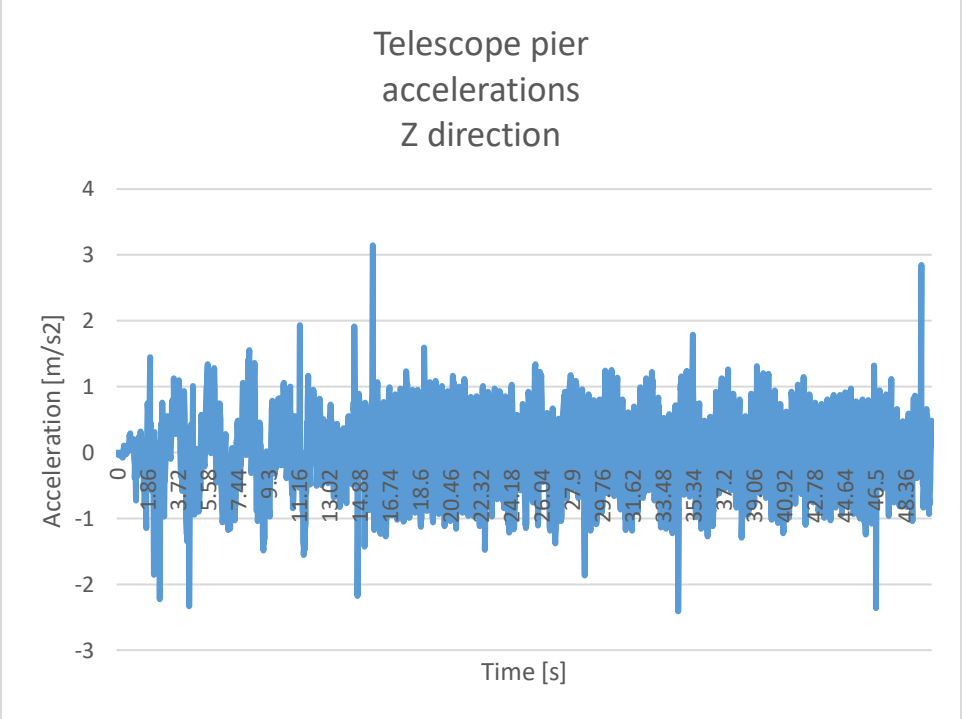

Figure 6.34: Telescope pier accelerations in East-West direction for no variation.

The time-dependent curves for the telescope pier behave in the expected sinusoidal fashion, with a notably denser plot for the vertical direction. The

largest displacement for the vertical direction is $0.006m$ downward. As for the horizontal plane, the *North-South* ground motion causes a larger displacement of $0.103m$, compared to $0.093m$ in the *East-West* direction.

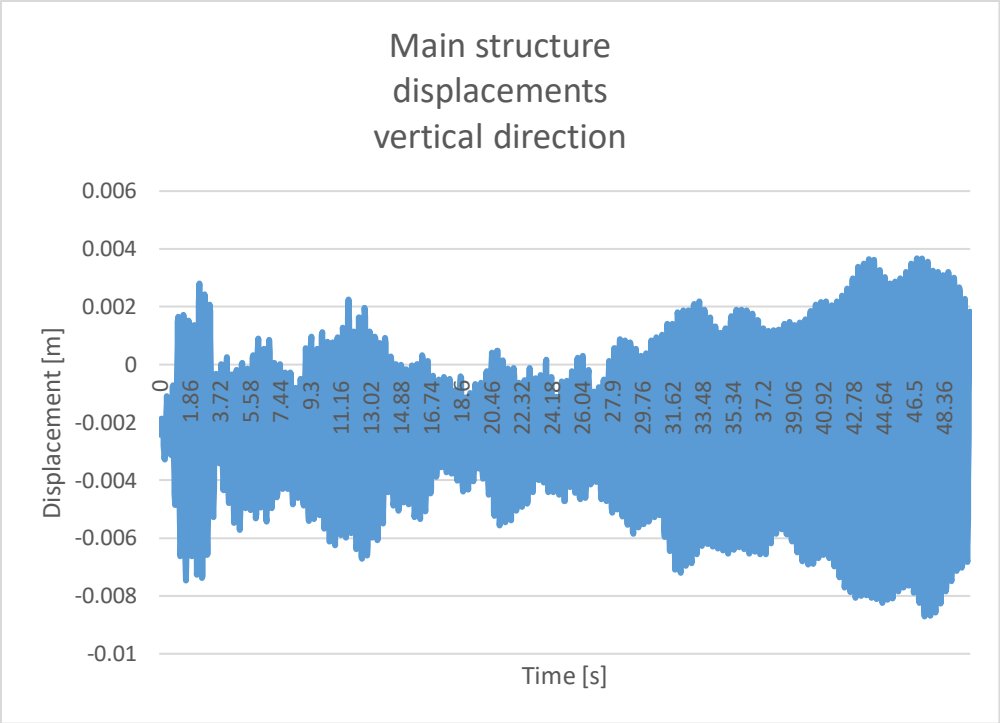

Figure 6.35: Main structure displacements in vertical direction for no variation.

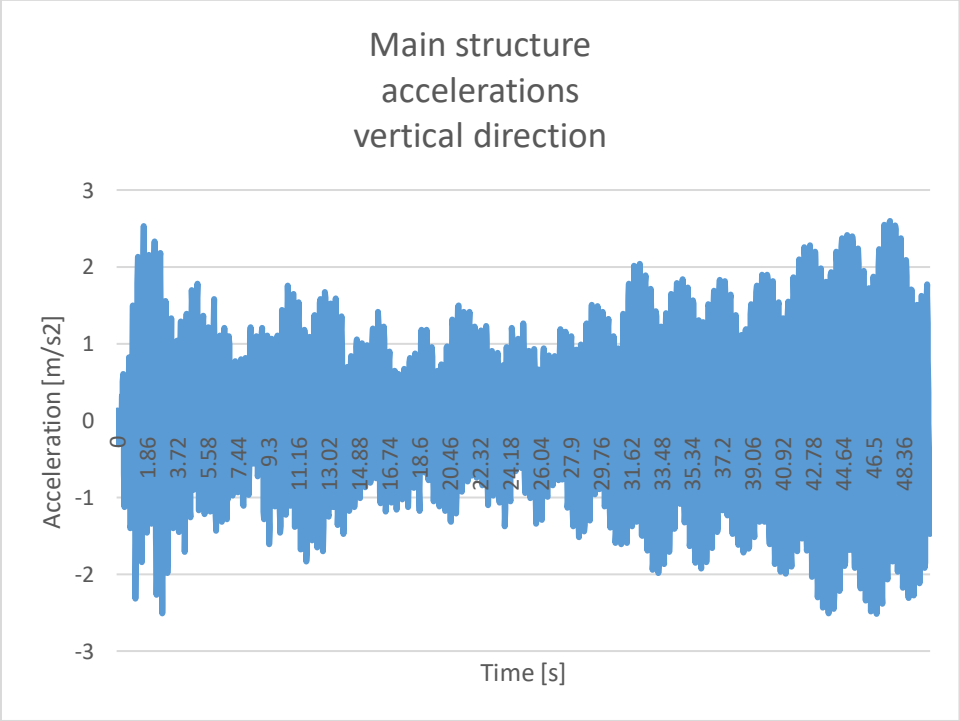

Figure 6.36: Main structure accelerations in vertical direction for no variation.

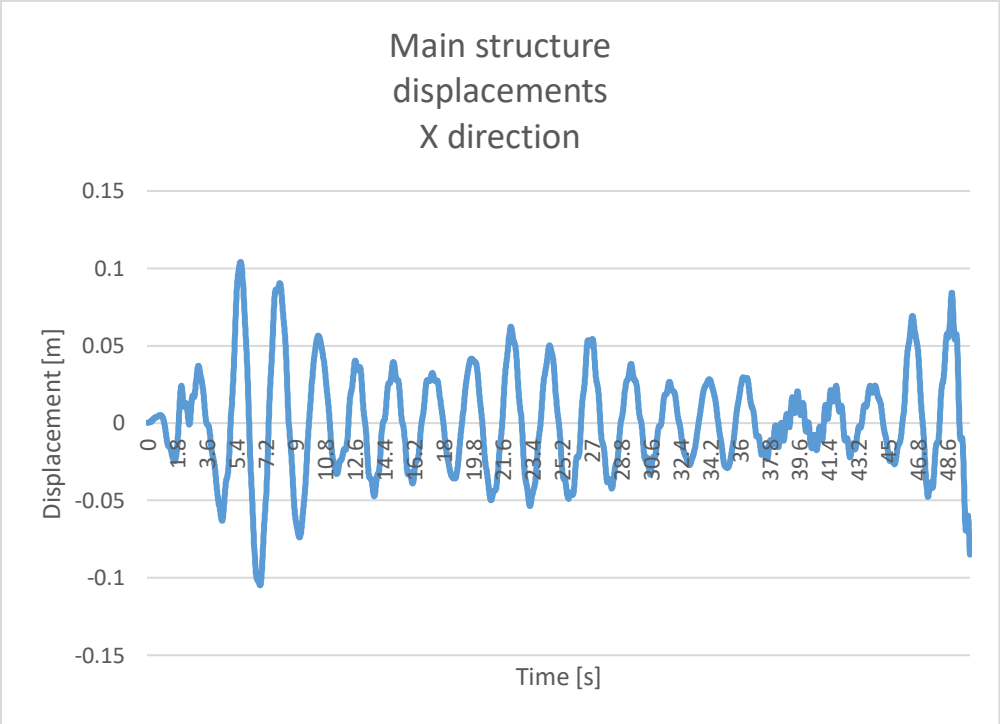

Figure 6.37: Main structure displacements in North-South direction for no variation.

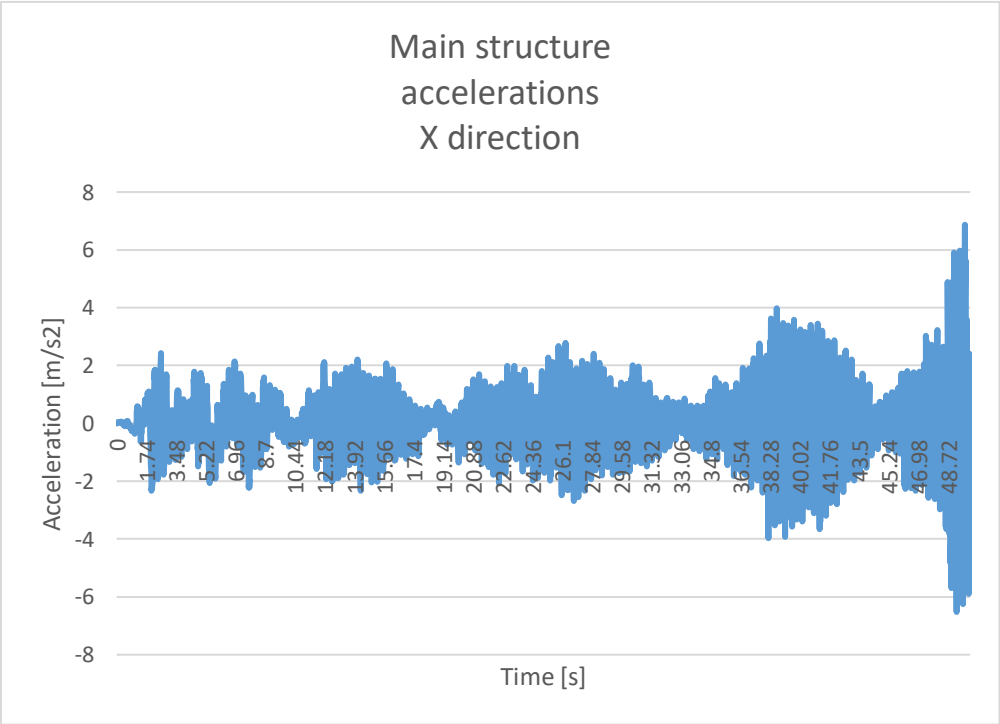

Figure 6.38: Main structure accelerations in North-South direction for no variation.

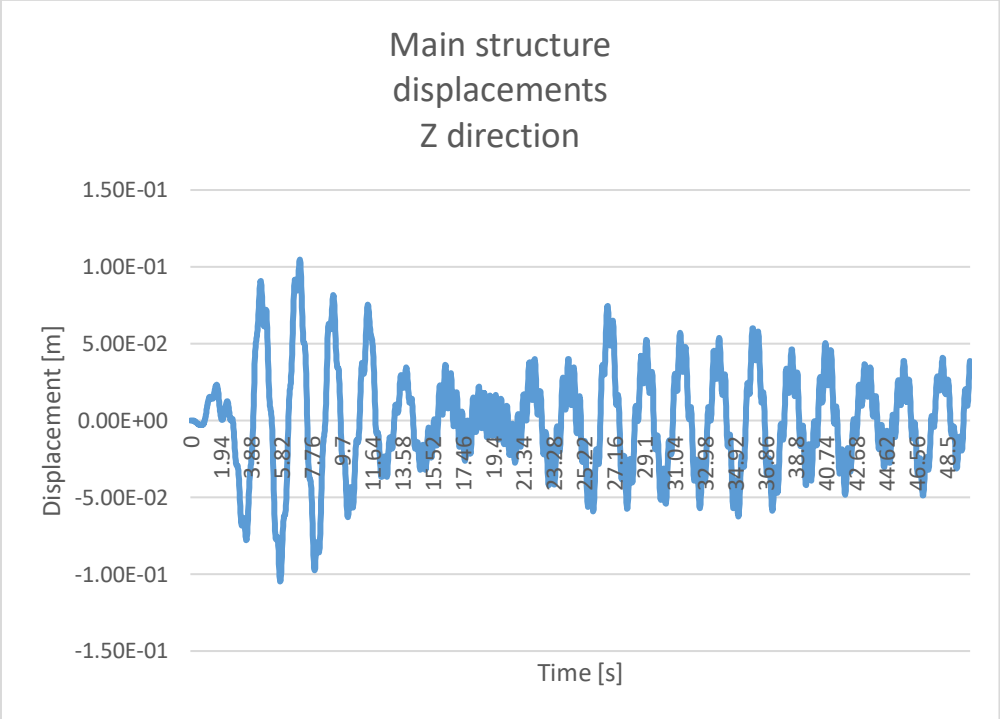

Figure 6.39: Main structure displacements in East-West direction for no variation

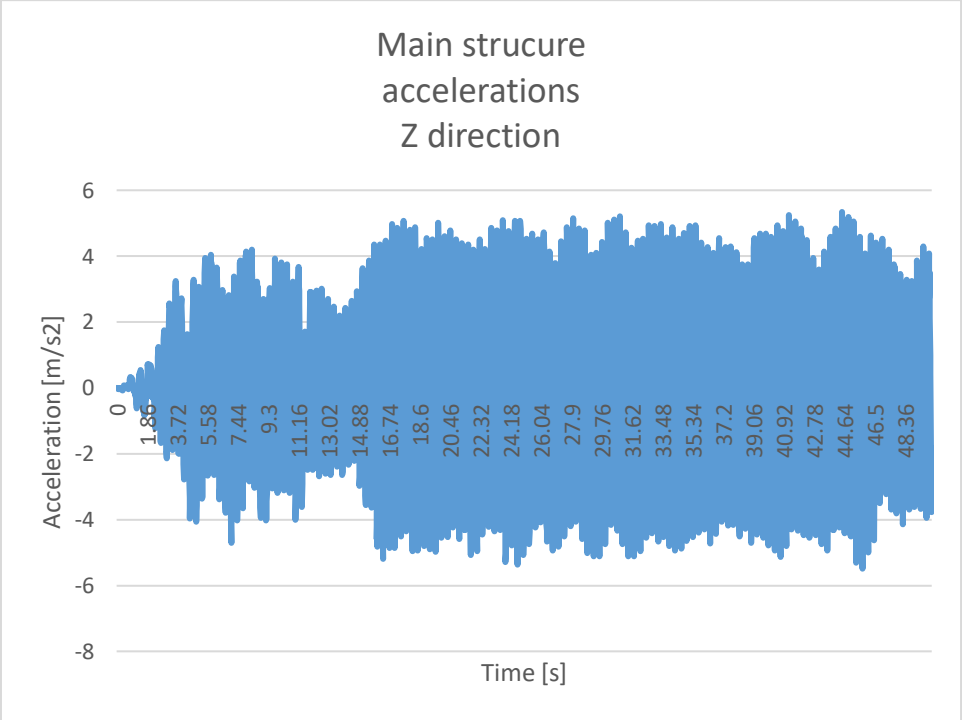

Figure 6.40: Main structure accelerations in East-West direction for no variation

The largest vertical displacement experienced by the main structure is $0.008m$ downward. Horizontally, the nodal displacement is $0.104m$ in both the *North-South* and the *East-West* direction.

6.2.2 Analysis with Variation in Horizontal Stiffness, Vertical Stiffness and Buckling Load Capacity

The following analysis reports the behavior of the structure with the included variations of the stiffness in both directions, as well as the critical buckling load. Their values are computed at each time step according the Equations (3.1), (3.7) and (3.8) reported in Chapter 3. To avoid unnecessary data clutter, a single bearing's response is reported from the analysis. The bearing of choice is **D2_180**, and the obtained results are as follows:

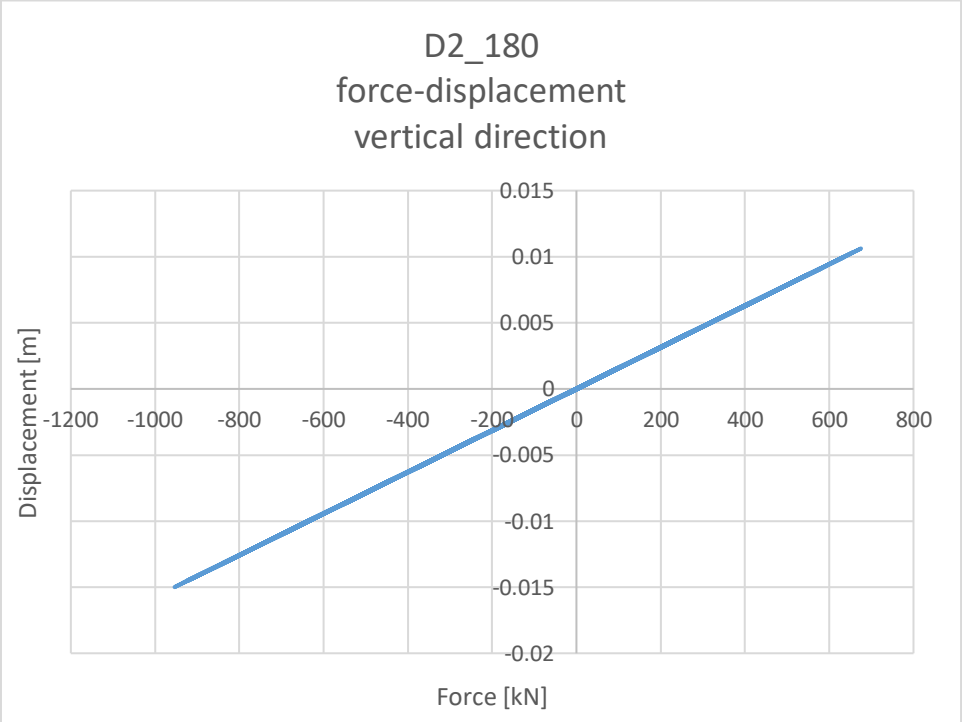

Figure 6.41: D2_180 force-displacement curve in vertical direction for variation in Kv, Kh and Pcr

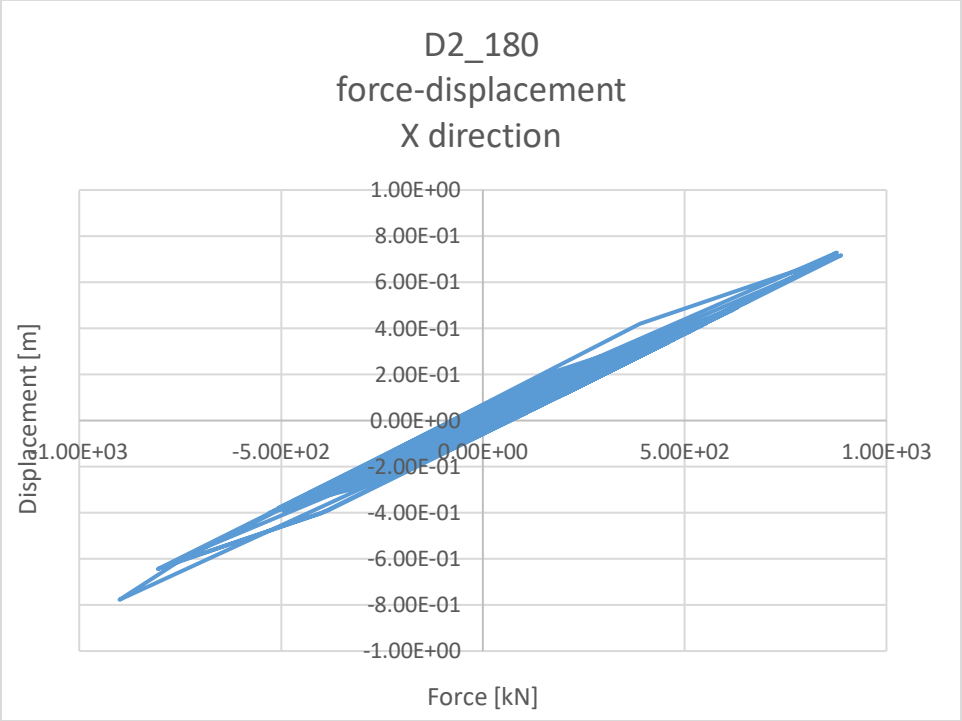

Figure 6.42: D2_180 force-displacement curve in North-South direction for variation in Kv, Kh and Pcr

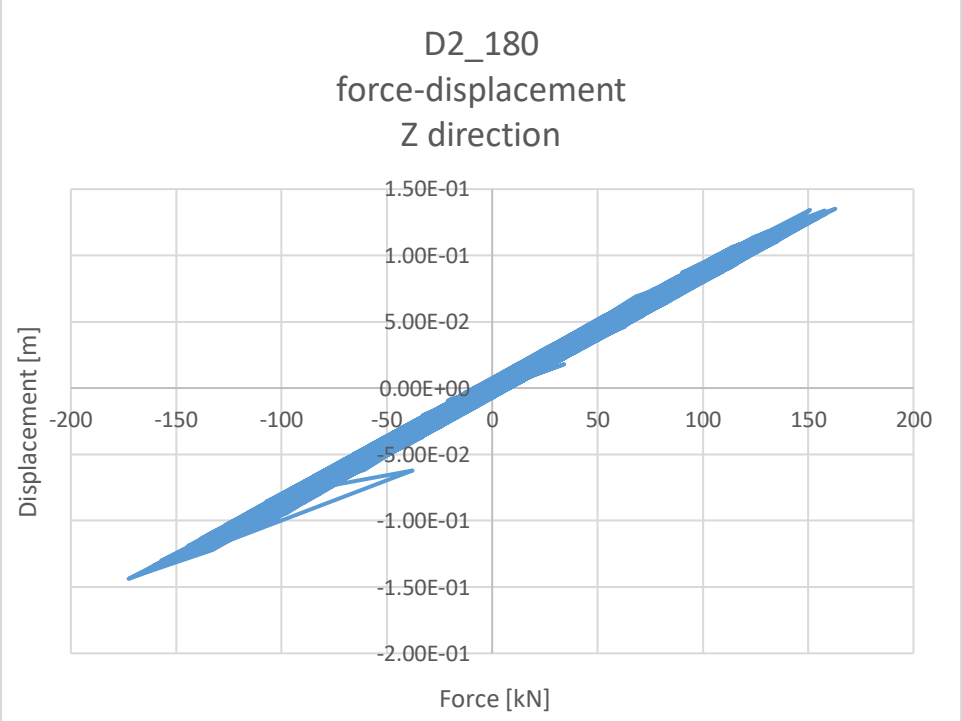

Figure 6.43: D2_180 force-displacement curve in East-West direction for variation in Kv, Kh and Pcr

As expected, in the vertical direction the largest recorded displacement is

downward, with a value of $0.015m$, corresponding to an axial force of $953kN$. In the horizontal plane, the bearing behavior clearly again portrays the bi-linear shape. The largest recorded displacement is in the *North-South* direction with a value of $0.77m$, caused by a horizontal force of $900kN$. In the *East-West* direction the displacement is $0.144m$ with a maximum force of $172kN$.

The impact of the lowered horizontal stiffness and critical load can be seen by the increase in the maximum lateral displacement in comparison to the one obtained through the analysis with stationary parameters.

Interestingly, the vertical displacement is quite close, and even slightly smaller than the one recorded in the analysis with no variations, which can be seen as a result of good vertical stiffness, considering the thickness chosen for the bearing's rubber layers.

The recorded nodal displacements and accelerations for the telescope pier are as follows:

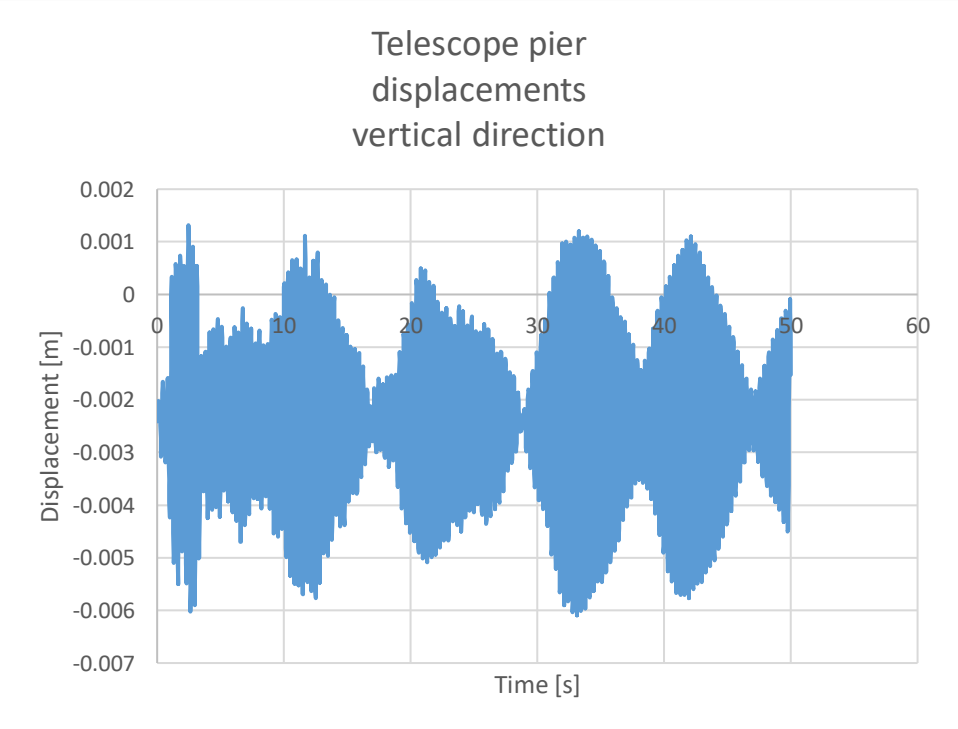

Figure 6.44: Telescope pier displacements in vertical direction for variation in Kv, Kh and Pcr.

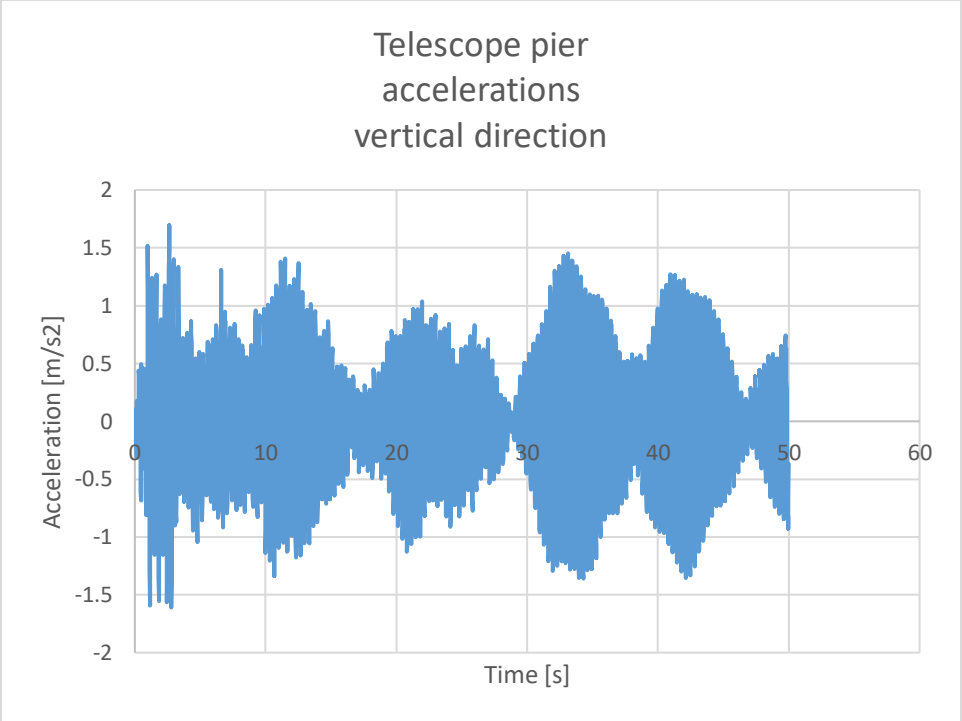

Figure 6.45: Telescope pier accelerations in vertical direction for variation in Kv, Kh and Pcr.

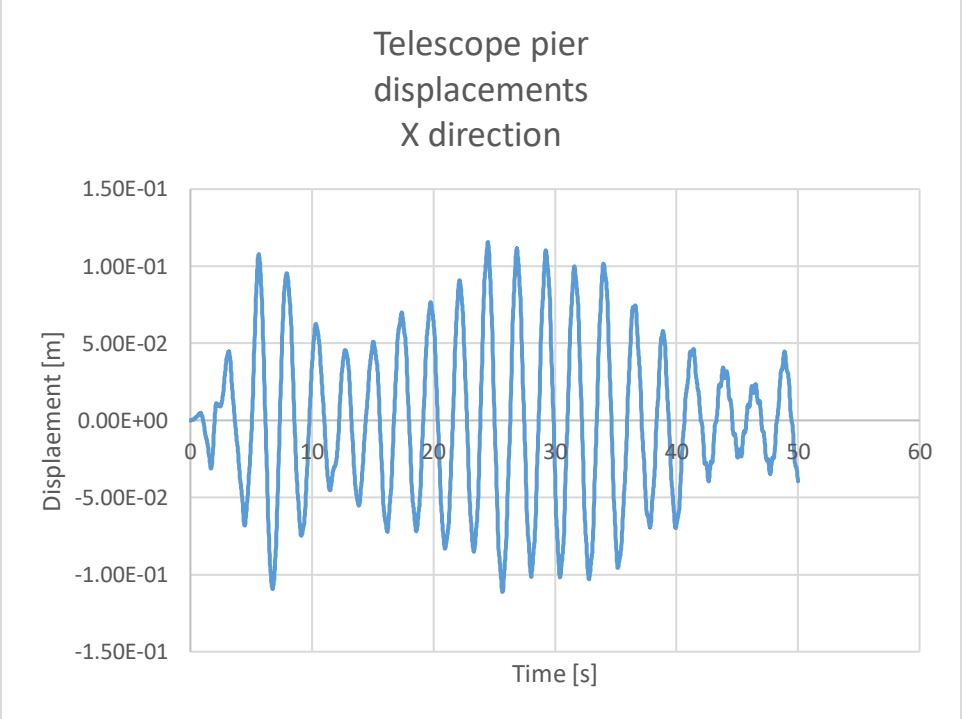

Figure 6.46: Telescope pier displacements in North-South direction for variation in Kv, Kh and Pcr.

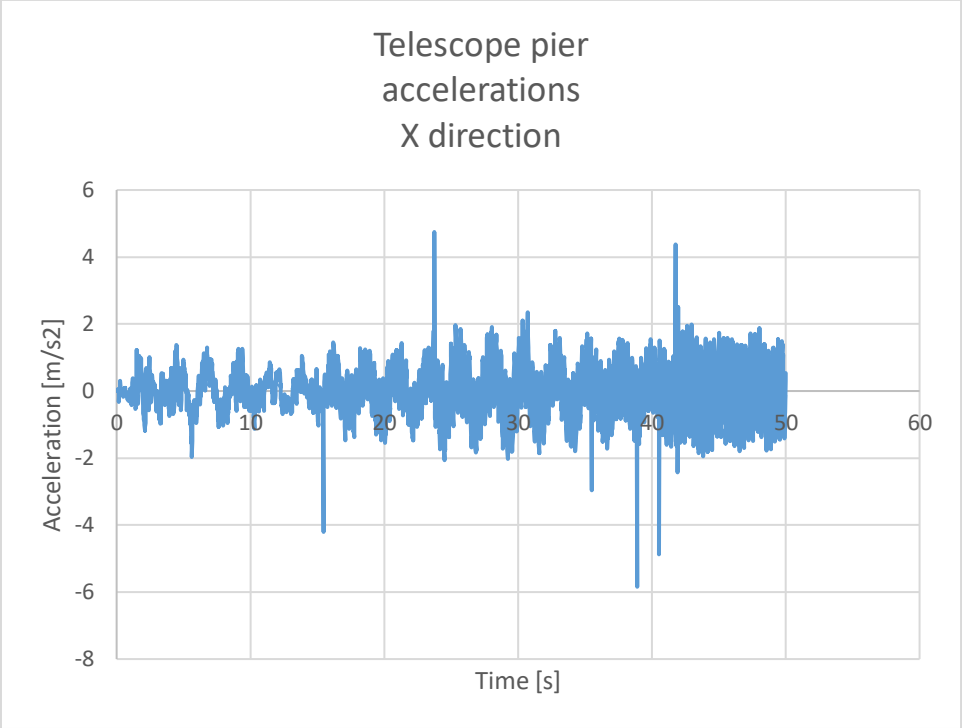

Figure 6.47: Telescope pier accelerations in North-South direction for variation in Kv, Kh and Pcr.

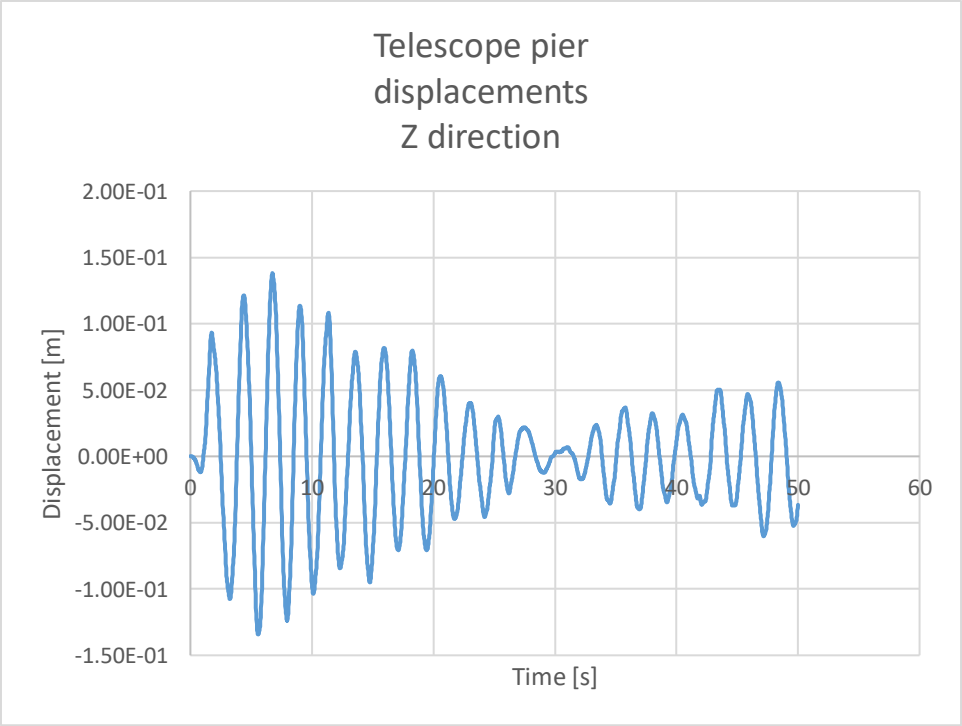

Figure 6.48: Telescope pier displacements in East-West direction for variation in Kv, Kh and Pcr.

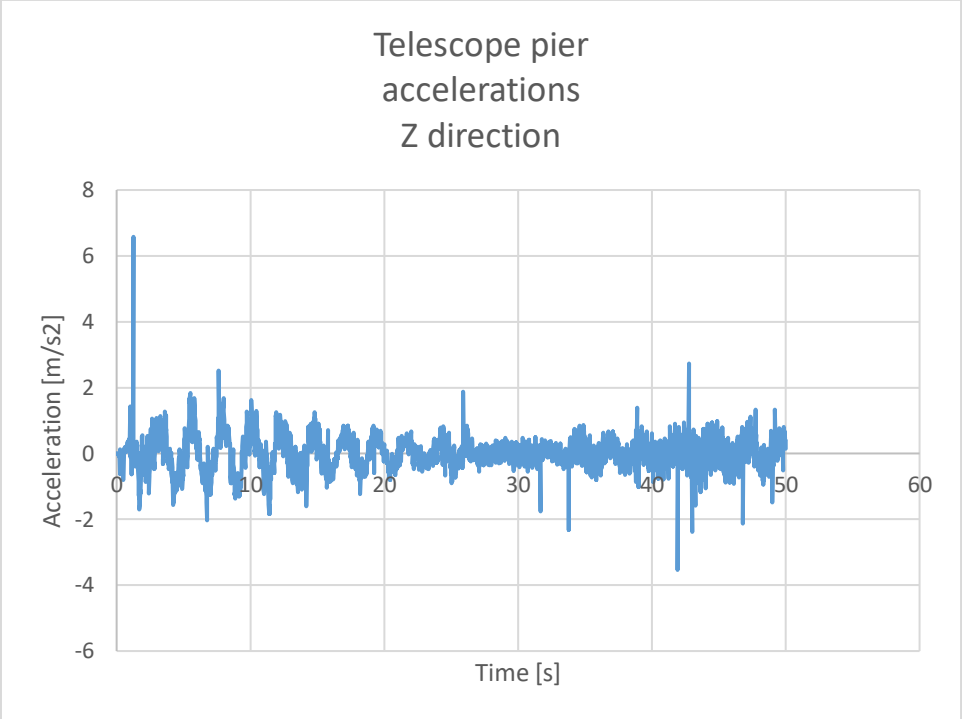

Figure 6.49: Telescope pier accelerations in East-West direction for variation in Kv, Kh and Pcr.

The largest displacement for the telescope pier in the vertical direction is $0.006m$, recorded at $33.12s$. A maximum lateral displacement of $0.136m$ is recorded in the *East-West* direction, whereas the one in the *North-South* direction is $0.110m$.

The time history for the main structure recorded:

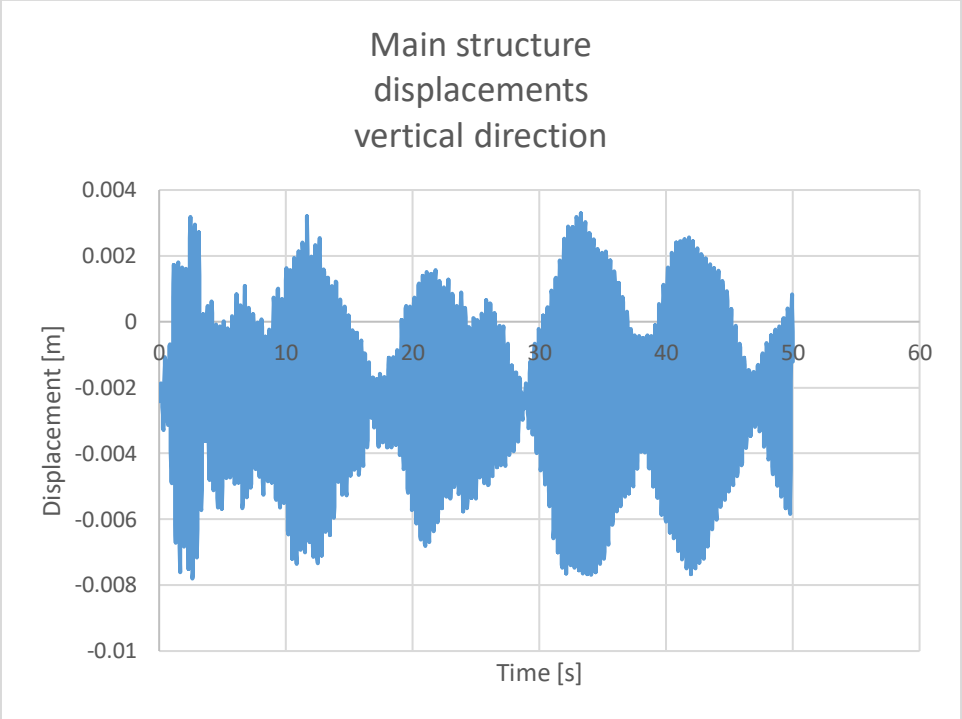

Figure 6.50: Main structure displacements in vertical direction for variation in Kv, Kh and Pcr.

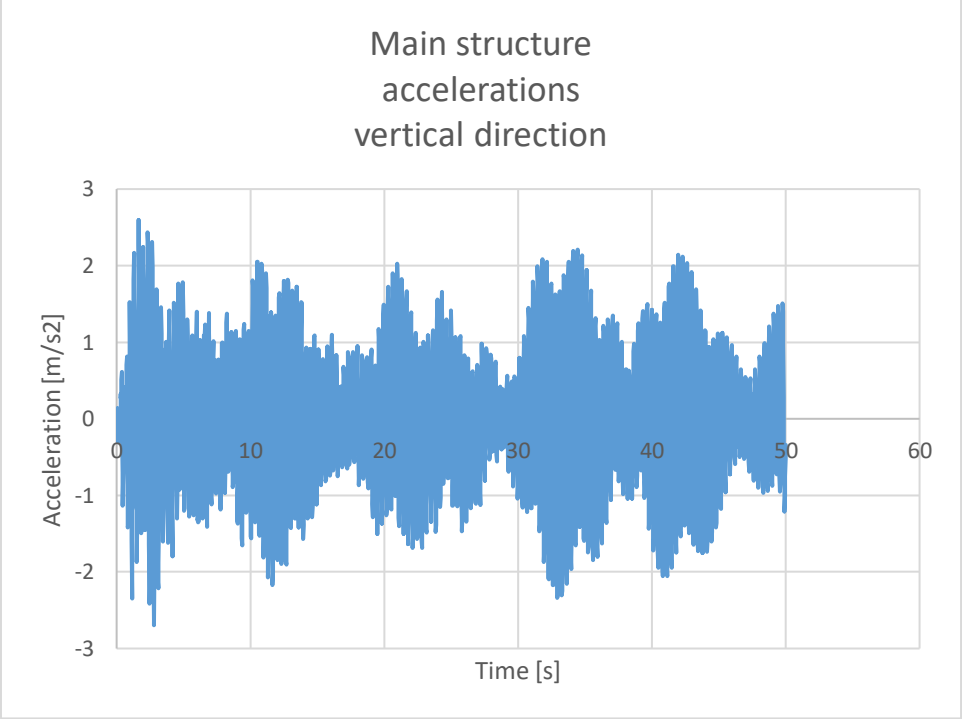

Figure 6.51: Main structure accelerations in vertical direction for variation in Kv, Kh and Pcr.

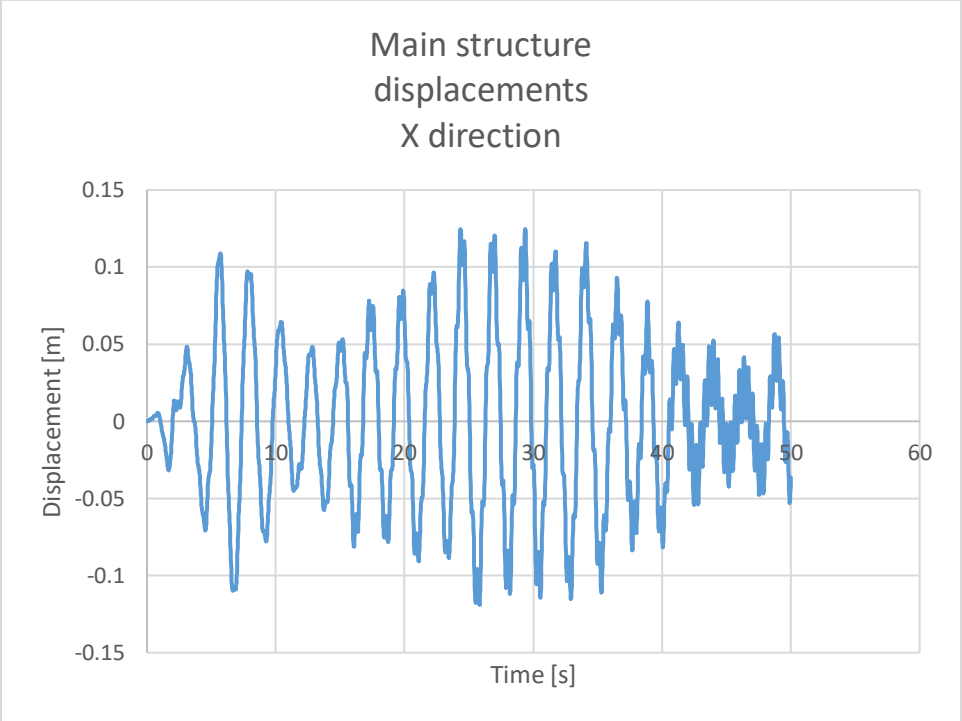

Figure 6.52: Main structure displacements in North-South direction for variation in Kv, Kh and Pcr.

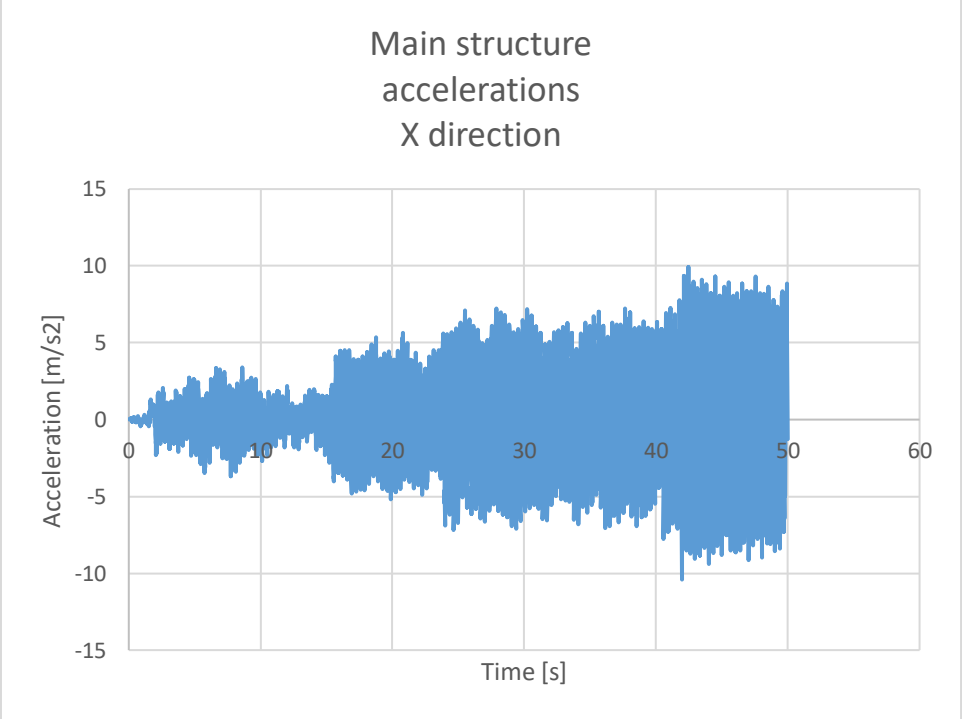

Figure 6.53: Main structure accelerations in North-South direction for variation in Kv, Kh and Pcr.

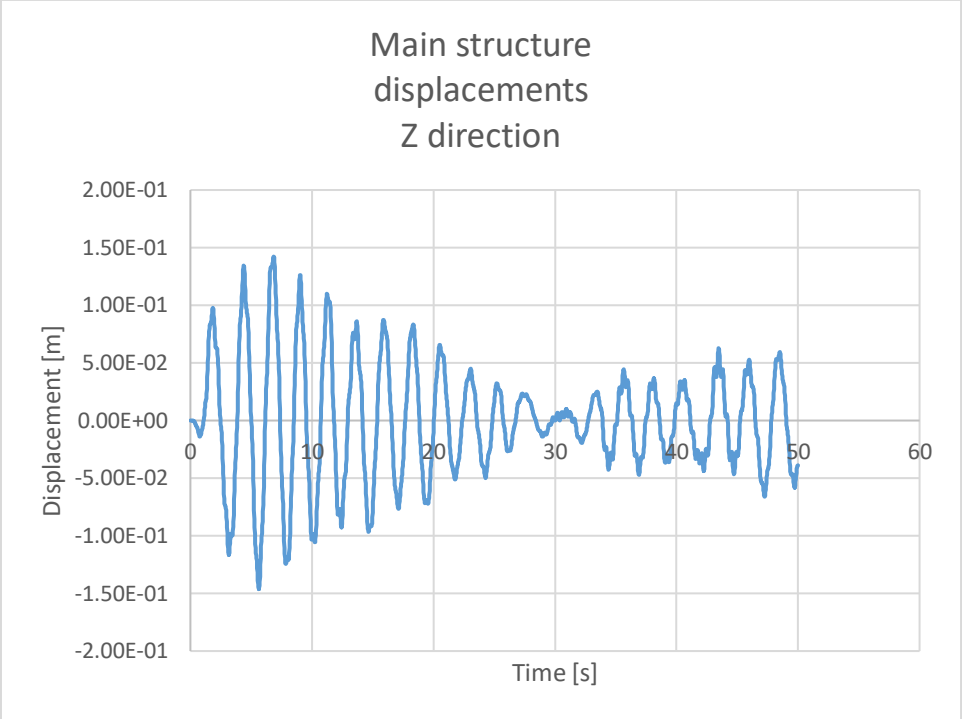

Figure 6.54: Main structure displacements in East-West direction for variation in Kv, Kh and Pcr.

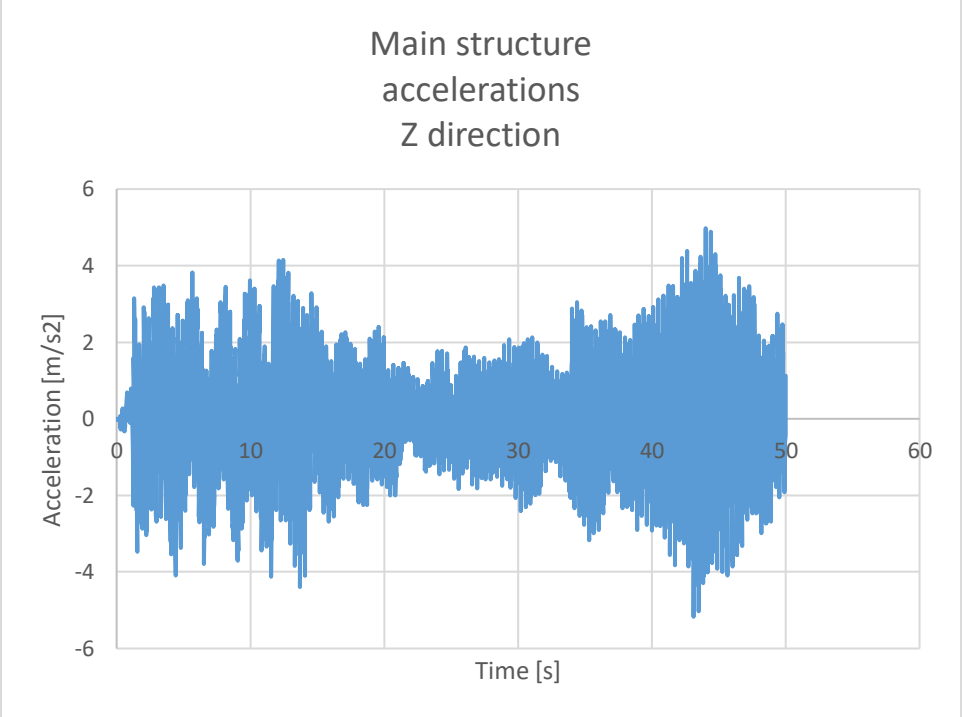

Figure 6.55: Main structure accelerations in East-West direction for variation in Kv, Kh and Pcr.

The main structure experiences a maximum vertical displacement in

compression at the beginning of the simulation, with a value of $0.007m$. The largest lateral displacement is again in the *East-West* direction with a value of $0.146m$, whereas the displacement in the *North-South* direction is $0.119m$.

6.3 Summary of the Obtained Results

According to the force-displacement curve in the vertical direction of the bearings for both the case with no variation in parameters and the case with variation in stiffness and buckling capacity, it can be concluded that the vertical behavior of the bearings is elastic, and can be modelled as such.
As for the horizontal behavior, the curves resemble that of the ideal bi-linear behavior, with small deviations noticeable for directions tangent with respect to the bearings' location in the azimuth ring.

It is important to note that in the analysis with variable stiffness and buckling capacity, which is the closest representation of the real situation, the point mass representing the main structure with the vibration-sensitive instruments exhibits a vertical period of $0.32s$ and a horizontal period of about $2.4s$, which are very good values inside the required long range intervals for both directions. In correlation to this, the same analysis shows that the bearing **D2_180** is subjected to the maximum vertical and horizontal forces in different time intervals. The largest vertical force of $-953kN$ occurs at $49.56s$, when the horizontal force is $277kN$. The reverse check finds the largest horizontal force of $900kN$ at $38.92s$, which corresponds to a vertical force of $-201kN$. This proves the fundamental theory of the alternative design approach to be true, since the vertical and horizontal periods are within the long range and the maximum vertical and horizontal loads indeed occur at different time steps, thus ensuring that the safety has not been compromised by following this approach.

As for the stability criteria defined by EN15129, it can be considered satisfied since the maximum axial force of $953kN$ is quite smaller than half of the critical buckling load which is $\frac{P_{cr}}{2} = 2523.5kN$.

The largest lateral displacements of the bearings are within permissible limits, however they clearly surpass the design values obtained with respect to the European Standards. This can be regarded as a clear indication of the complexity of predicting the behavior of a 3D isolation system, and shows that such task requires a serious and detailed approach.

Chapter 7

Conclusions

A design for a base isolation system using elastomeric bearings has been proposed in in accordance with the European Standards for earthquake engineering. However, notable deviations have been made with respect to the practices defined within these standards. Mainly, a shape factor with a quite low value is assumed ($S = 3.33$) in order to stay true to the scope of this thesis, which is a design that will provide sufficient isolation in both the horizontal and the vertical direction. To reach this value for the shape factor, the thickness of the rubber layers has been assumed to be large, with the intention to arrive at a lower stiffness in the vertical direction of the bearings. An additional deviation from the European Standards has been made by relying on a hypothesis that allows a relief from the strict requirements of the standards at a rational reduction of their safety. This hypothesis states that since the values of the isolation periods in vertical and horizontal direction are so far apart, the maximum earthquake-induced loads in vertical and horizontal direction are not expected to occur simultaneously and can be considered separately. Following this logic, the earthquake contributions in the two directions have been individually added to the self-weight of the structure to create two independent values for the design axial load. The design procedure can then be executed using only one of those values, however the following procedure according to the European Standards must be satisfied.

To thoroughly test the seismic isolation system that is discussed, it is implemented in a structure of immense importance and size, with large sensitivity to vibrations in all directions. The structure in question is the European – Extremely Large Telescope (E-ELT) funded by the European Southern Observatory (ESO) and expected to be the largest telescope in the world to date. The complex design of the structure has been simplified to ease the design process and its elements have been superimposed to two point

masses, further known as *telescope pier* and *main structure*. The equipment in the building is supported by two concentric azimuth rings, whose interface with the foundations has been chosen for the location of the elastomeric bearings.

The mathematical and numerical model of the bearing behavior have been adopted by Kelly et al. [2015], with certain modifications in an attempt to better present the realistic situation. These modifications refer to the manner in which the isotropic formulation considers the restoring forces. They are computed as the sum of a hysteretic and a viscoelastic component, where the latter is dependent on the viscous damping coefficient and the horizontal stiffness. The hysteretic component depends on the characteristic strength, which governs the hysteresis cycles and thus the energy dissipation. A problem arises due to the fact that the effective damping governs both the hysteretic component through the characteristic strength and the damping coefficient, which means that by using this model the damping effect is considered twice. For a case of high damping rubber bearings such as the ones considered in this thesis, the response in highly hysteretic, so the component that is eliminated in order to avoid the double damping effect is the viscous damping coefficient.

In the implementing of the elastomeric bearings, due attention has been paid to the effect of the imposed high thickness of the rubber layers, that is required in order to achieve sufficiently low stiffness and to provide isolation in both the vertical and horizontal direction. This thickness leads to a large overall height of the bearing, which in turn assures that the lateral displacements during the ground motions cause a shear strain considerably smaller than 100%. Since the parameters of the hysteresis cycle are typically computed at 100% shear strain, they need to be re-evaluated in order to give a more accurate representation of the actual bearing behavior. To this aim, a value for the characteristic bearing strength needs to be established that will provide the energy dissipated per cycle that is in correspondence with the elastic strain energy defined by the effective damping, which is in fact established for the design lateral displacement. Pecchillo [2019] proposed an iterative process that begins by recognizing the actual lateral displacement and defines values for the characteristic strength until one is reached that presents the real effective damping. The lateral displacements increase, and with it also the elastic strain energy and the energy dissipated per each cycle, which leads to a decrease in the effective damping value initially assumed as 10%.

After making this adjustment, the bearings have been implemented in the open framework OpenSees (Open System for Earthquake Engineering Simulation) through *ElastomericX* element objects. These objects are composed of two nodes with 12 DOFs, connected by six springs that represent the mechanical behavior in each direction. A dynamic analysis has been performed in OpenSees, using ground motions recorded in the three principal directions during the El Centro (1940) earthquake, which has been chosen due to the similarity in its response spectrum in the horizontal direction and the one for

the El Cerro Armazones, the location of the E-ELT. Two different analyses are performed, in particular the difference being the manner in which OpenSees considers the buckling load capacity and the stiffness in both directions. In the first analysis, these parameters have been defined as constant, with their values being the initial elastic ones. In the second analysis, these parameters vary and are computed at each new time step of the analysis, where the time step has been set to $0.02s$ in a simulation that lasts a total of $50s$. The force-displacements curves of the several examined bearing devices have shown that the vertical behavior of the bearings develops in a perfect elastic fashion. The behavior in the horizontal plane clearly resembles the idealized bi-linear behavior, with minor deviations over the duration of the simulation.

The periods in the vertical and horizontal directions of the main structure which is sensitive to vibrations are well within the desired specters that represent the long range, specified in order to avoid the dangerous modes of the structure.

The more sophisticated of the two analyses that includes the variation in stiffness and buckling capacity has shown that the most severe earthquake-induced loads in the vertical and horizontal directions occur at completely different time steps. This decoupling of the maximum forces in the two directions, along with the fact that both periods are within the long range, can justify the hypothesis of the alternative approach used for the design of the bearings.

The OpenSees analysis has also shown that the maximum axial load experienced by the bearings is significantly smaller than half of the design critical buckling load, satisfying the main stability criteria defined in the European Standards.

However, although within reasonable limits, the lateral displacements of the bearings in the OpenSees analysis have been recorded to be well over the ones defined in the design process.

It can be concluded that predicting the behavior of a 3D seismic isolation system is a severely complicated task that requires a very detailed approach, accompanied by a sophisticated structural analysis software.

Bibliography

Ian G Buckle. Passive control of structures for seismic loads. *Bulletin of the New Zealand Society for Earthquake Engineering*, 33(3):209–221, 2000.

Ian G Buckle and Ronald L Mayes. Seismic isolation: history, application, and performance-a world view. *Earthquake spectra*, 6.2:161–201, 1990.

Michalakis C Constantinou, Tsu T Soong, and Gary F Dargush. Passive energy dissipation systems for structural design and retrofit. 1998.

Michalakis C Constantinou, AS Whittaker, Y Kalpakidis, DM Fenz, and Gordon P Warn. Performance of seismic isolation hardware under service and seismic loading. 2006.

Giulia Pecchilo. 3D Seismic Base Isolation of Large Structure using Elastomeric Bearings. 2019

EN1337-3:2005. Structural bearings-part 3: Elastomeric bearings. *Brussels: European Committee for Standardization*.

UNI EN15129:2018. Anti seismic devices. *Brussels: European Committee for Standardization*.

EN1998-1:2004. Eurocode 8: Design of structures for earthquake resistance- part 1: general rules, seismic actions and rules for buildings. *Brussels: European Committee for Standardization*.

European Southern Observatory ESO. The E-ELT construction proposal, 2011. URL https://www.eso.org/public/archives/books/pdf/book_0046.pdf. Accessed: 03.2019.

Takafumi Fujita. Seismic isolation of civil buildings in japan. *Progress in Structural Engineering and Materials*, 1(3):295–300, 1998.

Alan Neville Gent. Elastic stability of rubber compression springs. *Journal of Mechanical Engineering Science*, 6(4):318–326, 1964.

AN Gent and PB Lindley. The compression of bonded rubber blocks. *Proceedings of the Institution of Mechanical Engineers*, 173(1):111–122, 1959.

Damian N Grant, Gregory L Fenves, and Ferdinando Auricchio. Modelling and analysis of high-damping rubber bearings for the seismic protection of bridges. 2005.

Johannes Adrianus Haringx. On highly compressible helical springs and rubber rods and their application for vibration-free mountings, iii. *Philips Research Reports*, 4:206–220, 1949b.

James M Kelly. Earthquake-resistant design with rubber. 1993.

James M Kelly, Ian D Aiken, and Frederick F Tajirian. Mechanics of low shape factor elastomeric seismic isolation bearings. *Earthquake engineer- ing research center UCB/EERC-89/13*, 1989.

Trevor E Kelly. Base isolation of structures: design guidelines. *Holmes Consulting Group Ltd*, 2001.

Chan Ghee Koh and James M Kelly. A simple mechanical model for elas- tomeric bearings used in base isolation. *International journal of mechan- ical sciences*, 30(12):933–943, 1988.

Manish Kumar. ElastomericX, leadRubberX, and HDR: User elements in OpenSees for analysis of elastomeric seismic isolation bearings un- der extreme loading [computer program], 2016. URL http://opensees. berkeley.edu/wiki/index.php. Accessed: 02.2019.

Manish Kumar, Andrew S Whittaker, and Michael C Constantinou. Seismic isolation of nuclear power plants using elastomeric bearings. Technical report, MCEER, 2015.

Silvia Mazzoni, Frank McKenna, Michael H Scott, Gregory L Fenves, et al. Opensees command language manual. *Pacific Earthquake Engineering Research (PEER) Center*, 264, 2006.

Frank McKenna. Opensees: a framework for earthquake engineering simu- lation. *Computing in Science & Engineering*, 13(4):58–66, 2011.

YJ Park, YK Wen, and A H-S Ang. Random vibration of hysteretic systems under bi-directional ground motions. *Earthquake engineering & structural dynamics*, 14(4):543–557, 1986.

Michael D Symans. Seismic protective systems: seismic isolation. *Instruc- tional material complementing FEMA*, 451, 2009.

Stephen P Timoshenko and James M Gere. *Theory of elastic stability*. McGraw-Hill Book, New York, 1961.

Gordon P Warn and Keri L Ryan. A review of seismic isolation for buildings: historical development and research needs. *Buildings*, 2(3):300–325, 2012.

Gordon P Warn and Andrew Stuart Whittaker. A study of the coupled horizontal-vertical behavior of elastomeric and lead-rubber seismic isola- tion bearings. 2006.